University of Alberta

Analytical and Simulation Techniques for the Error Rate Performance of Jointly Optimal BPSK Receivers

by

Tim Victor Poon 

A thesis submitted to the Faculty of Graduate Studies and Research in partial fulfillment of the requirements for the degree of **Master of Science**.

Department of Electrical and Computer Engineering

Edmonton, Alberta

Spring 2004

Your file Votre référence
ISBN: 0-612-96539-2
Our file Notre référence
ISBN: 0-612-96539-2

Abstract

Optimal receivers are useful to ensure effective bit error rates (BERs) in communications systems, particularly in an environment of cochannel interference. This work analyzes optimal detection of a binary phase-shift keying (BPSK) signal in the presence of cochannel interference and noise. The definition of individually and jointly optimal receivers is clarified, and the decision boundaries of these receivers in two-dimensional signal space are examined. A new, exact analytical expression for the BER performance is then derived. In addition, an efficient importance sampling simulation technique is described. This new application of a two-dimensional importance sampling method allows one to efficiently simulate the case of multiple cochannel interferers for arbitrarily small probabilities of error. A thorough discussion of the effects of interferers on the jointly optimal receiver is provided.

To the memory of my grandmother

J. Lee-Poon

25 September 1923 – 26 February 2004

Acknowledgements

I would like to express thanks to my supervisor Dr. Norman C. Beaulieu for his feedback, guidance, and financial support. Indeed, I would like to thank all members of the *i*CORE Wireless Communications Laboratory for their support and friendship. In particular, I would like to thank the following individuals who assisted me in technical matters: Amir Masoud Rabiei, David J. Young, Julian Cheng, K. Sivanesan, Lei Xiao, Mohamed Oussama Damen, Pavel Loskot, and Sasan Haghani.

As of this writing, I have spent nearly eight years as a part of the University of Alberta community. These years have been one of the most rewarding and motivating periods of my life. I would like to thank all my friends and colleagues at the University of Alberta for making these years so enjoyable.

Finally, I would like to thank my parents for providing support and encouragement throughout my university career.

This thesis was financially supported through the Natural Sciences and Engineering Research Council of Canada (NSERC) and the Alberta Informatics Circle of Research Excellence (*i*CORE).

Contents

1 Introduction **1**

1.1 Background and Motivation 1

1.2 Thesis Outline and Contributions 4

2 Jointly and Individually Optimal Receivers – A Comparison **6**

2.1 Individually and Jointly Optimal BPSK Receivers 6

2.2 Individually and Jointly Optimal Decisions for a 2-User BPSK System . . . 8

2.2.1 Individually Optimal Decisions 8

2.2.2 Jointly Optimal Decisions 15

2.3 Examining the Decision Regions for Individually and Jointly Optimal Receivers 16

2.4 Simulation Results and Comparisons of Receivers 27

2.5 Summary 30

3 Performance Analysis of the Jointly Optimal BPSK Receiver **31**

3.1 Signaling Constellation of a BPSK Desired Signal Plus Interferer 32

3.2 An Analytical Expression for the Error Rate Performance of the Jointly Optimal Receiver 37

3.2.1 Error Rate Performance in Large SIR Regions 39

3.2.2 Error Rate Performance in Intermediate SIR Regions 41

3.2.3 Error Rate Performance in Small SIR Regions 42

3.3 Numerical Results and Discussion 42

3.4 Bounds to the Error Rate Performance of the Jointly Optimal Receiver . . . 49
3.5 Summary . . . 60

4 Simulating the Jointly Optimal Receiver with Importance Sampling 61
4.1 A Background to Importance Sampling . . . 61
4.2 Importance Sampling in 2-Dimensional Space . . . 66
4.3 Importance Sampling and the Jointly Optimal 2-User Receiver . . . 74
4.4 Importance Sampling Simulation Gains . . . 81
4.4.1 Comparing Monte Carlo Simulations to Importance Sampling Simulations . . . 81
4.4.2 Number of Trials for Importance Sampling and Monte Carlo Simulations . . . 87
4.5 Summary . . . 89

5 Performance of Multiple-Interferer Jointly Optimal Receivers 91
5.1 Simulating the Multiple-Interferer Jointly Optimal Receivers . . . 91
5.2 Results and Discussion . . . 97
5.3 Summary . . . 112

6 Conclusions 114

References 116

List of Figures

2.1 Block diagram of an individually optimal receiver for a BPSK signal plus a single cochannel interferer, from [1]. 14

2.2 Block diagram of a jointly optimal receiver for a BPSK signal plus a single cochannel interferer, from [2]. 15

2.3 Signal constellation for a desired signal plus interferer, from [1]. 17

2.4 Decision boundaries for an individually optimum receiver at various values of SNR, determined using (2.19e), with $\Psi = 0$ dB, and $\theta = \frac{\pi}{6}$. 18

2.5 Sample signal constellation for a BPSK signal plus one cochannel interferer, for $\Psi = 0$ dB, $\theta = \frac{\pi}{6}$, with decision boundaries for an individually optimum receiver (at 6 dB and 12 dB SNR), and a decision boundary for a jointly optimum receiver determined by (2.31a). 20

2.6 Decision boundaries for an individually optimum receiver at various values of SNR, determined using (2.19e), with $\Psi = -3$ dB, and $\theta = \frac{\pi}{4}$. 21

2.7 Individually optimal decision boundaries for a BPSK signal plus one cochannel interferer, for different values of SIR, with $\gamma = 3$ dB, and $\theta = \frac{\pi}{6}$. 22

2.8 Jointly optimal decision boundaries for a BPSK signal plus one cochannel interferer, for different values of SIR, with $\gamma = 3$ dB, and $\theta = \frac{\pi}{6}$. 23

2.9 Individually optimal decision boundaries for a BPSK signal plus one cochannel interferer, for different phases, with $\gamma = 3$ dB, and $\Psi = -2$ dB. 25

2.10 Jointly optimal decision boundaries for a BPSK signal plus one cochannel interferer, for different phases, with $\gamma = 3$ dB, and $\Psi = -2$ dB. 26

2.11 The BER performance versus SNR for individually optimum and jointly optimum receivers, with $\Psi = 0$ dB, and $\theta=\frac{\pi}{6}$. 28
2.12 The BER performance versus SIR of the individually optimal receiver and jointly optimal receiver, where the SNR is $\gamma = -3$ dB, and $\theta = \frac{\pi}{6}$. 29

3.1 Sample signal constellation for a BPSK signal plus one cochannel interferer for large SIR. The thick solid line is the decision boundary. The grey regions are trilaterals used to calculate the error performance for the upper right point, as in [3]. 34
3.2 Sample signal constellation for a BPSK signal plus one cochannel interferer for an intermediate SIR region ($\cos^2\theta < \Psi < \frac{1}{\cos^2\theta}$). The grey regions and the thick solid lines indicate trilaterals and the decision boundary, respectively. 35
3.3 Sample signal constellation for a BPSK signal plus one cochannel interferer. This case is for small SIR. Note that P_i is lower than P_j in this SIR region. 36
3.4 Trilateral decision regions for a signal point, from [3] and [4]. 38
3.5 The 5 trilateral regions used in (3.7)-(3.11). A high SIR example is used here. These trilaterals were found using techniques similar to those described in [3] and [4]. The drawing is for illustration purposes; it is not to scale. (a) Regions 1-3 are referenced to the upper right constellation point. (b) Regions 4-5 are referenced to the lower right constellation point. Note that region 6 is geometrically identical to region 1. 40
3.6 Bit-error performance of optimal receiver obtained using (3.9) with (3.12). The simulation points for 9 dB SNR are from [1]. 44
3.7 Bit-error performance of optimal receiver obtained using (3.9) with (3.12), for low values of SNR. 45
3.8 The BER performance versus SNR and SIR, of the jointly optimal receiver, for $\theta = \pi/12$. 47

3.9 The BER performance versus SNR and SIR, of the jointly optimal receiver, for $\theta = \pi/6$. 48
3.10 Lower and upper BER bounds for a jointly optimal receiver for a BPSK signal plus one cochannel interferer, with $\Psi = 1$ dB, and $\theta = \pi/12$, along with the exact analytical result. 52
3.11 Lower and upper BER bounds for a jointly optimal receiver for a BPSK signal plus one cochannel interferer, with $\Psi = 1$ dB, and $\theta = 5\pi/12$, along with the exact analytical result. 53
3.12 Lower and upper BER bounds for a jointly optimal receiver for a BPSK signal plus one cochannel interferer, with $\Psi = -3$ dB, and $\theta = 5\pi/12$, along with the exact analytical result. 54
3.13 Lower and upper BER bounds for a jointly optimal receiver for a BPSK signal plus one cochannel interferer, with $\Psi = 6$ dB, and $\theta = 5\pi/12$, along with the exact analytical result. 55
3.14 Lower and upper BER bounds of the jointly optimal BPSK receiver with one interferer, with θ uniformly distributed over $[0, 2\pi)$, $\gamma = 9$ dB, along with the exact analytical result. 56
3.15 Lower bound and composite upper bound of the BER of the jointly optimal BPSK receiver with one interferer, with θ uniformly distributed over $[0, 2\pi)$, $\gamma = 9$ dB, along with the exact analytical result. 58
3.16 Lower bound and composite upper bound of the BER of the jointly optimal BPSK receiver with one interferer, with θ uniformly distributed over $[0, 2\pi)$, $\Psi = 3$ dB, along with the exact analytical result. 59

4.1 Block diagram of baseband communications system, from [5]. 63
4.2 Three-dimensional representation of the jointly Gaussian PDF (versus x and y, from (4.12)), with σ=1. 66
4.3 Scatterplot of 2-dimensional Gaussian noise simulation (with N=1500, and $\sigma = 1$), centered at the origin. 70

4.4 Slice of 2-dimensional joint Gaussian PDF, from (4.12), and the biased PDF from (4.27), with y=0, σ=1, and R=1. 71
4.5 Scatterplot of biased noise simulation, using the PDF in (4.27), centered at the origin, with N=1500, and R=1. 72
4.6 Scatterplot simulation points of 2-dimensional biased Gaussian noise for 2 points centered at A and B, with a straight line decision boundary, with N=350, and $R = d$. 73
4.7 Constellation points and decision boundary calculation (dotted line) for a jointly optimal BPSK receiver for 2 users. The value of R (in this case, $d_{(1,0)}$) is also shown. 75
4.8 The BER performance versus SIR of a jointly optimal receiver for a BPSK signal plus one interferer, determined by analysis and IS simulations, with θ=π/6. 77
4.9 Error rate performance versus θ and SIR, of the jointly optimal receiver for a BPSK signal plus one interferer, with γ = 6 dB. 79
4.10 Error rate performance versus θ and SNR, of the jointly optimal receiver for a BPSK signal plus one interferer, with SIR of Ψ = 6 dB. 80
4.11 Number of Monte Carlo samples versus SNR for $N = \frac{100}{P_e}$, with $\theta = \frac{\pi}{6}$. . . 83
4.12 Number of Monte Carlo samples versus SIR for $N = \frac{100}{P_e}$, with $\theta = \frac{\pi}{6}$. . . . 84
4.13 Sample savings gain versus SNR for a similar variance σ as that in Fig. 4.11, with $\theta = \frac{\pi}{6}$. 85
4.14 Sample savings gain versus SIR for a similar variance σ as that in Fig. 4.12, with $\theta = \frac{\pi}{6}$. 86

5.1 Scatterplot of BPSK signal plus 2 interferers and AWGN, with SNR=20 dB, Ψ_1=3 dB, Ψ_2=0 dB, $\theta_1 = \pi/6$, and $\theta_2 = 2\pi/3$. 94
5.2 Scatterplot of BPSK signal plus 3 interferers and AWGN, with SNR=20 dB, Ψ_1=3 dB, Ψ_2=0 dB, Ψ_3=$-$15 dB, $\theta_1 = \pi/6$, $\theta_2 = 2\pi/3$, and $\theta = 3\pi/2$. . 95

5.3 The BER performance of a jointly optimal receiver versus SIR_1, for a BPSK signal plus two interferers, with SIR_1=SIR_2, and θ uniformly distributed over [0,2π). 98

5.4 The BER performance of a jointly optimal receiver versus SIR_1, for a BPSK receiver with three interferers, with $SIR_1 = SIR_2 = SIR_3$, and θ a uniformly distributed random variable on [0,2π). 100

5.5 The BER performance of a jointly optimal BPSK receiver versus SIR_i (i = 1,2,3), in the presence of one, two, or three interferers, with $SIR_1 = SIR_2 = SIR_3$, and θ_i uniformly distributed over [0,2π). 102

5.6 The BER performance of a jointly optimal BPSK receiver versus total SIR, in the presence of one, two, three, or six interferers, with all interferer SIR_i equal, an SNR of 12 dB, and θ_i uniformly distributed over [0,2π). 104

5.7 The BER performance of a jointly optimal BPSK receiver versus SNR, in the presence of one, two, three, and six interferers, with all interferer SIR_i = 12 dB, and θ_i uniformly distributed over [0,2π). 106

5.8 The BER performance of a jointly optimal BPSK receiver versus SNR, in the presence of one, two, three, and six interferers, with the net interferer energy constant (i.e. the total SIR is 10 dB), and θ_i uniformly distributed over [0,2π). 108

5.9 The BER performance of a jointly optimal BPSK receiver versus SNR, in the presence of one, two, three, and six interferers, with the SNR between 0 and 14 dB, the net interferer energy constant (i.e. the total SIR is 10 dB), and θ_i uniformly distributed over [0,2π). 109

5.10 The BER performance of a jointly optimal BPSK receiver versus SIR_1, with two and three interferers, where SIR_2 = 10 dB + SIR_1. In the case of three interferers, $SIR_3 = SIR_1 - 20$ dB. 111

Acronyms

Acronyms	Definition
AWGN	additive white Gaussian noise
BER	bit error rate
BPSK	binary phase shift keying
CDMA	code-division multiple-access
IS	importance sampling (simulation)
MAP	maximum *a posteriori*
MC	Monte Carlo (simulation)
ML	maximum-likelihood
PDF	probability density function
PSK	phase shift keying
QPSK	quadrature phase shift keying
SIR	signal-to-interference ratio
SNR	signal-to-noise ratio

List of Symbols

Symbol	Definition
A_c	carrier amplitude
A_0	carrier amplitude of desired signal
A_i	carrier amplitude of interferer i (i = 1, 2, 3...)
b_0	transmitted bit of desired signal
b_i	transmitted bit of interferer i (i = 1, 2, 3...)
$\hat{b}_0$	bit decision of desired signal
$\hat{b}_i$	bit decision of interferer i (i = 1, 2, 3...)
d	decision distance from constellation point to decision boundary
E(x)	expectation of x
erfc(x)	complementary error function
E_b	energy per bit
$f(x)$	PDF of x
$f(x,y)$	joint PDF of x and y
f_c	carrier frequency
$I_\vartheta(y), I_\vartheta(x,y)$	error counter function
k	bias for importance sampling noise trials
$k_{(i,j)}$	bias for importance sampling noise trials for constellation point (i, j)
$L(b)$	likelihood function of b
l_a, l_b, l_c	trilateral side lengths in two-dimensional signal space
$m(t)$	random binary signal

$n(t)$	noise signal
N	number of simulation trials
N_{IS}	number of importance sampling simulation trials
N_{MC}	number of Monte Carlo simulation trials
N_0	noise power spectral density
$P[\cdot]$	probability function
P_e	average probability of bit error
$\hat{P}_e$	estimator of the average probability of bit error
$P_{e,LB}$	lower bound to the average probability of bit error
$P_{e,UB}$	upper bound to the average probability of bit error
P_i, P_j	decision boundary intersection points
$Q(\cdot)$	Q-function, the area under the tail of the Gaussian PDF
R	radius parameter to bias IS noise trials
$s_0(t)$	deterministic signal for the desired user
$s_i(t)$	deterministic signal for the interferer i (i = 1, 2, 3...)
t	time (variable)
t_D	time to compute the decision in the receiver system
t_G	generation time for a Monte Carlo random noise trial
t_{G2}	generation time for an importance sampling random noise trial
T	symbol duration
T_{IS}	importance sampling simulation time
T_{MC}	Monte Carlo simulation time
$v(t)$	received signal plus interference plus noise
v_i	projection of $v(t)$ along signal $s_i(t)$ (i = 0, 1, 2...)
$W(y), W(x,y)$	weighting function for importance sampling
$y(t)$	received signal (including interference), without noise
β_a, β_b	trilateral angles in two-dimensional signal space
γ, γ_s	output signal-to-noise ratio
$\gamma_{samples}$	sample savings gain; i.e. the ratio of MC trials to IS trials

η_a, η_b, η_c	trilateral angles in two-dimensional signal space
θ	phase difference between BPSK signals
θ_i	phase difference between signals 0 and i (i = 1, 2, 3...)
ϑ	error region
$\Lambda(\cdot)$	maximum likelihood ratio function
$\xi_a, \xi_b, \xi_c, \xi_d, \xi_e$	trilateral angles in two-dimensional signal space
ρ	correlation coefficient between $s_0(t)$ and $s_1(t)$
σ^2	variance of the noise
σ^2_{IS}	variance of the importance sampling estimator
σ^2_{MC}	variance of the Monte Carlo estimator
$\phi'_i(t)$	deterministic signal for user i
$\phi_0(t), \phi_1(t)$	orthonormal basis functions in two-dimensional signal space
Φ_a, Φ_b, Φ_c	trilateral angles in two-dimensional signal space
Ψ	signal-to-interference ratio
ω_c	carrier angular frequency
ω_0	carrier angular frequency of desired signal
ω_i	carrier angular frequency of interferer i (i = 1, 2, 3...)

Chapter 1

Introduction

1.1 Background and Motivation

The wireless communications industry has been a dominant force over the past century. From broadcast radio stations to cellular telephones to wireless Internet, there are more wireless applications than ever before.

Nonetheless, the high growth of wireless communications poses challenges and issues for today's society. As wireless communications becomes more ubiquitous, there are increasing demands for higher bandwidth, greater amounts of data, and lower costs. These demands exist in spite of a limited supply of radiofrequency spectrum. Indeed, there exists only a finite amount of radiofrequency spectrum, and the increasing number of users who want wireless devices is causing the system to be strained. As more radio bandwidth is used in the world, it is becoming increasingly difficult to provide reliable wireless communications. The excessive number of wireless channel users causes them to interfere with one another, eroding the quality of all users.

It is thus important to assess the nature of signals in the presence of interference. In particular, it is useful to analyze the effects of *cochannel* interference, where the desired and interfering users are transmitted with identical carrier frequencies. Cochannel interference is essentially a fact of life in the wireless industry. There is a limited number of chan-

nels and an increasing number of users. Therefore, proper characterization of cochannel interference is needed.

One performance metric for wireless communications is the level of bit error rate (BER). The BER represents the proportion of the total transmitted signal bits that are received incorrectly. For effective communications, it is therefore desirable to attain as low a BER as possible. However, the BER of a communications system is limited by the external environment – if there are more interferers present, the BER increases. As well, there may be other undesired disturbances within the frequency band of interest. Additive noise is one such disturbance. Additive white Gaussian noise (AWGN) can affect a signal and distort the information carried by the signal over a specific frequency band. The BER of a communications system is also limited by the relative amount of AWGN present.

As a result of the negative consequences of interference and noise, it is desirable to design a commmunications receiver that reaches a minimum BER under certain conditions. In general, this is synonymous to designing an *optimal* receiver.

This work discusses the performance of various types of optimal receivers. Reference [1] serves as the motivation for this work. In [1], Kwan and Leung derive an optimal receiver structure for a binary phase-shift keying (BPSK) signal in the presence of one interferer and AWGN. This receiver is "individually optimal", i.e. it achieves the minimum bit error rate for the desired bit in this system [2].

As BPSK is used throughout this work, it is relevant to define binary phase-shift keying. Suppose that one has a random binary signal $m(t)$ that consists of symbols 1 and 0. In particular, symbol 1 is represented by a constant level of $+1$ and symbol 0 is represented by a constant -1, each of which lasts for a time duration T. To facilitate the transmission of these symbols over a communications channel, one can employ a basic modulation scheme known as phase shift keying. Specifically, the information in $m(t)$ is multiplied by a sinusoidal carrier wave $A_c s(t) = A_c \cos(2\pi f_c t)$, where A_c is the carrier amplitude, f_c is the carrier frequency, and t is time. One can also denote the carrier wave with an angular

frequency ω_c, which would yield a binary phase-shift keying signal of

$$y(t) = m(t)A_c s(t) = \begin{cases} A_c s(t) = \sqrt{\frac{2}{T}} A_c \cos(\omega_c t) & \text{for symbol 1} \\ -A_c s(t) = -\sqrt{\frac{2}{T}} A_c \cos(\omega_c t) & \text{for symbol 0.} \end{cases} \tag{1.1}$$

The $\sqrt{\frac{2}{T}}$ term in (1.1) is used to ensure that the signal $s(t)$ is normalized. Essentially, the signals in (1.1) are different only by a relative phase shift of 180 degrees (π radians) – hence the term "phase-shift keying".

There are generally two main techniques for determining the BER performance of an arbitrary communications system. One method is to determine exact analytical results (such as those in [3] and [4]) that can mathematically show the error rate performance of the system. Another method is to perform a random simulation of the communications system. This simulation can be done using unique importance sampling techniques (such as those in [5]), or they can be completed using traditional Monte Carlo simulation methods.

Literature is available on the subject of error rate performance of cochannel interference systems. Reference [6] developed a method to determine exact error probabilities for a BPSK signal corrupted with Gaussian noise and cochannel interference. While this method does consider traditional coherent detection and quasi-coherent detection, no attempt is made to determine an "optimal" detection for the system. In [7], error probabilities for intersymbol and cochannel interference are calculated. The approach in [7] uses numerical quadratures of Laplace inversion integrals. Reference [8] introduces an infinite series to determine the error probability of the system. This approach introduces significant computational savings for error performance analysis. This series representation is used in [9] to perform a precise analysis of cochannel interference in quadrature phase-shift keying (QPSK) systems. Reference [10] investigates the BER of non-coherent frequency shift-keying in the presence of interferers. Note that none of [6] – [10] examine an optimal detection for the communications system.

Multiuser detection theory [2] is a useful approach to examine the case of a desired signal in the presence of other interfering users. Because of the system complexity, multiuser detection theory has generally focused on approximate analytical results. Maximum-

likelihood multiuser receivers are studied in [11] and [12]. Reference [13] investigates improved receiver designs for cochannel interference and noise. Optimal detection is examined for signals in various noise environments in [14] and [15]. Reference [16] examines a type of maximum *a posteriori* (MAP) receiver to improve system performance in code-division multiple-access (CDMA) channels. In [17], a multiuser detector is examined using a successive cancellation technique. While the field of multiuser detection is useful in examining cochannel interference, the results in [11] – [17] are either sub-optimal or not specific to the case of BPSK signals.

This thesis analyzes the error rate performance of a jointly optimal receiver for BPSK signals in the presence of cochannel interferers and noise. One clarifies the definition of "optimality" in this work, and analyzes how the receiver in [1] is optimal. An exact analytical expression for the error rate performance is then derived. In addition, an interesting application of importance sampling simulation is used as an efficient method for simulating this system. Thus, this thesis examines the performance using both analytical and simulation techniques.

1.2 Thesis Outline and Contributions

This thesis is organized as follows. Chapter 2 provides a thorough description of the difference between "jointly optimal" and "individually optimal" multiuser receivers. This clarification is essential to the analysis of [1]. Indeed, through this clarification, one learns that the receiver structure in [1] is not a new result. Even so, the analysis of the two-dimensional decision boundaries in Chapter 2 provides good background for later analysis and simulation.

Chapter 3 provides a new and exact analytical expression for the BER of a jointly optimal BPSK receiver. This result is achieved through the use of Craig's method in [3], and is a result of the fact that the decision regions of this receiver are polygonal. Through this analytical result, one makes useful observations in the joint detection of a BPSK signal plus one cochannel interferer.

An importance sampling simulation technique is introduced in Chapter 4. Through importance sampling, one is able to quickly simulate the performance of the jointly optimal receiver. This technique is an interesting and new application of the results of [18], which provides a useful method of simulating in two-dimensional signal space. One discovers that very low BER values can be simulated, which is a significant improvement over traditional Monte Carlo simulation processes. Chapter 5 extends this importance sampling technique to the case of a BPSK signal with multiple interferers. Indeed, the usefulness of the technique in [18] is reinforced in this chapter, as one is able to effectively simulate more than one interferer using this technique. Various observations are then made for the case of a BPSK signal in the presence of multiple interferers. To the best of the author's knowledge, these observations are new in the literature.

Chapter 6 concludes the thesis with a summary of contributions.

Chapter 2

Jointly and Individually Optimal Receivers – A Comparison

To properly analyze and simulate "optimal receivers", it is useful to properly define an *individually optimum* receiver and a receiver that is *jointly optimum.* This Chapter compares and contrasts the individually optimum and jointly optimum receivers for BPSK signals in the presence of a cochannel interferer plus noise. The decision boundaries of each receiver in two-dimensional space are shown, and simulation results are discussed. By using this foundation in individually and jointly optimal receivers, one can effectively analyze and simulate this system in future chapters.

2.1 Individually and Jointly Optimal BPSK Receivers

To properly derive the optimum receiver, it is important to correctly define what one means by an *individually optimum* receiver and a receiver that is *jointly optimum.*

Verdú effectively distinguishes the differences between receivers that are jointly optimal and individually optimal in [2]. The definitions below follow Verdú's discussion closely.

Consider a desired BPSK signal $A_0 b_0 s_0(t)$ transmitted over an AWGN channel. This transmission is in the presence of a second interfering BPSK signal, $A_1 b_1 s_1(t)$. In this

notation, A_i is the amplitude of the signal from user i, while b_i is the bit transmitted (either -1 or $+1$) by user i. The deterministic signal assigned to the ith user is denoted as $s_i(t)$.

If one assumes that the desired and interfering signals are cochannel and synchronous, the received signal can then be written as

$$\begin{aligned} v(t) &= A_0 b_0 s_0(t) + A_1 b_1 s_1(t) + n(t), \ 0 \le t \le T \\ &= A_0 b_0 \sqrt{\frac{2}{T}} \cos(\omega t) + A_1 b_1 \sqrt{\frac{2}{T}} \cos(\omega t + \theta) + n(t), \ 0 \le t \le T, \end{aligned} \tag{2.1}$$

where $n(t)$ is white Gaussian noise with two-sided power spectral density $N_0/2$, T is the bit duration, ω is the angular frequency, and θ is the phase difference between signals 0 and 1.

To minimize the bit error rate (BER) of the receiver, one should use a maximum *a posteriori* (MAP) receiver. Receivers that use the MAP decision rule will select the hypothesis with the highest a posteriori probability. If one was to recover user 0 from (2.1), the minimum BER decision is obtained by selecting the appropriate bit $b_0 \in \{-1, +1\}$ that maximizes the *a posteriori* probability

$$P[b_0 | v(t), \ 0 \le t \le T]. \tag{2.2}$$

Since the received signal is a function of both b_0 and b_1, this is equivalent to maximizing the probability

$$\begin{aligned} P[b_0 | v(t), \ 0 \le t \le T] &= P[((b_0), (b_1 = -1)) | v(t), \ 0 \le t \le T] \\ &\quad + P[((b_0), (b_1 = +1)) | v(t), \ 0 \le t \le T]. \end{aligned} \tag{2.3}$$

If we maximize this a posteriori probability, one obtains an *individually optimum* receiver.

Determining the *jointly optimum* receiver provides a solution to a different problem – selecting the pair of bits (b_0, b_1) that maximizes the joint a posteriori probability

$$P[(b_0, b_1) | v(t), \ 0 \le t \le T]. \tag{2.4}$$

At first glance, the jointly optimum and individually optimum probabilities seem to be similar. Verdú [2] elaborates that these probabilities do not necessarily have to be equal

because of the fact that b_0 and b_1 are not independent when conditioned on the observed waveform $v(t)$. Using these definitions, one can then proceed to derive the individually optimal receiver structure.

2.2 Individually and Jointly Optimal Decisions for a 2-User BPSK System

2.2.1 Individually Optimal Decisions

References [1], [2], [19] all perform some type of individually optimum receiver derivation for two-user antipodal systems. Much of the derivation below originates from these works.

It is known that a detector based on the MAP criterion makes the same decisions as one based on a maximum-likelihood (ML) criterion if the a priori probabilities are equal. Assuming that user 0 in (2.1) is the desired signal (and user 1 is the interferer), the likelihood ratio is

$$\Lambda(v_{ML}(t)) = \frac{f(v(t)|+A_0 s_0(t))}{f(v(t)|-A_0 s_0(t))}, \tag{2.5}$$

where $f(v(t)|+A_0 s_0(t))$ is the probability density function (PDF) of $v(t)$ given that $+A_0 s_0(t)$ is sent. As a result, it is desired to precisely derive the likelihood function for an individually optimum detector.

To determine the individually optimum decision for a BPSK signal in the presence of a cochannel interferer plus noise, one can examine the characteristics of multiuser detection systems. As explained above, a MAP decision rule for user 0 selects the hypothesis with the highest a posteriori probability, i.e. the bit $b_0 \in \{-1,+1\}$ that maximizes

$$\begin{aligned} P[b_0|v(t),\ 0 \le t \le T] \ &= \ P[((b_0),(b_1=-1))|v(t),\ 0 \le t \le T] \\ &\quad +P[((b_0),(b_1=+1))|v(t),\ 0 \le t \le T]. \end{aligned} \tag{2.6}$$

It is thus important to obtain a likelihood function for each of the probability summands in (2.6). Consider an arbitrary n-dimensional received signal $\mathbf{r} = [r_1\ r_2\ \ldots\ r_n] = \mathbf{x}+\mathbf{n}$,

where $\mathbf{x} = [x_1\ x_2 \ldots x_n]$ is the signal sent, and $\mathbf{n} = [n_1\ n_2 \ldots n_n]$ is n-dimensional AWGN. The conditional probability density [20] is

$$\begin{aligned} f(\mathbf{r}|\mathbf{x}) &= f(\mathbf{r}-\mathbf{x}) \\ &= \prod_{k=1}^{n} f(r_k|x_k), \end{aligned} \tag{2.7}$$

where

$$f(r_k|x_k) = \frac{1}{\sqrt{\pi N_0}} \exp\left[-\frac{(r_k - x_k)^2}{N_0}\right]. \tag{2.8}$$

Note that the $(r_k - x_k)^2$ term is simply a metric for the distance between r_k and x_k, $\|r_k - x_k\|^2$. This PDF essentially states that the received signal minus the transmitted deterministic components is Gaussian.

Note that one can also use a distance metric for (2.1). Since the distance is simply the received signal minus the deterministic component of the signal, the distance can be written as

$$\|\mathbf{v} - A_0 b_0 \mathbf{s_0} - A_1 b_1 \mathbf{s_1}\|^2 = \int_0^T \left[v(t) - (A_0 b_0 s_0(t) + A_1 b_1 s_1(t))\right]^2 dt. \tag{2.9}$$

Therefore, disregarding the $\frac{1}{\sqrt{\pi N_0}}$ term from (2.8) (this term does not depend on the pair of bits (b_0, b_1) for maximization), the likelihood function becomes

$$L[v(t), 0 \le t \le T | (b_0, b_1)] = \exp\left\{-\frac{1}{N_0}\int_0^T [v(t) - A_0 b_0 s_0(t) - A_1 b_1 s_1(t)]^2 dt\right\}. \tag{2.10}$$

The individually optimum decision for user 0 is equivalent to maximizing the probability given in (2.6). Assuming equiprobable bits $b_1 \in \{-1, +1\}$, this is equivalent to maximizing the likelihood function sum of

$$\begin{aligned} L(b_0) &= L_{b_1=+1}(b_0) + L_{b_1=-1}(b_0) \\ &= \exp\left\{-\frac{1}{N_0}\int_0^T [v(t) - A_0 b_0 s_0(t) - A_1 s_1(t)]^2 dt\right\} \\ &\quad + \exp\left\{-\frac{1}{N_0}\int_0^T [v(t) - A_0 b_0 s_0(t) + A_1 s_1(t)]^2 dt\right\}. \end{aligned} \tag{2.11}$$

One can then expand this sum algebraically using some manipulations. Consider the

first summand. One has

$$\begin{aligned} L_{b_1=+1}(b_0) &= \exp\left\{-\frac{1}{N_0}\int_0^T [v(t)-A_0b_0s_0(t)-A_1s_1(t)]^2dt\right\} \\ &= \exp\left\{-\frac{1}{N_0}\left[\int_0^T v^2(t)dt+\int_0^T A_0^2b_0^2s_0^2(t)dt+\int_0^T A_1^2s_1^2(t)dt\right.\right. \\ &\quad -2\int_0^T v(t)A_0b_0s_0(t)dt-2\int_0^T v(t)A_1s_1(t)dt \\ &\quad \left.\left.+2\int_0^T A_0A_1b_0s_0(t)s_1(t)dt\right]\right\}. \end{aligned} \tag{2.12}$$

Let $s_0(t)$ and $s_1(t)$ be normalized, i.e.

$$\int_0^T s_i^2(t)dt = 1. \tag{2.13}$$

One can also define the correlation coefficient ρ between $s_0(t)$ and $s_1(t)$ as

$$\rho = \int_0^T s_0(t)s_1(t)dt. \tag{2.14}$$

Define

$$v_i = \int_0^T v(t)s_i(t)dt \tag{2.15}$$

as the projection of $v(t)$ along signal $s_i(t)$. Since $b_0 \in \{-1,+1\}$, $b_0^2 = 1$, and (2.12) can be written as

$$\begin{aligned} L_{b_1=+1}(b_0) &= \exp\left\{-\frac{1}{N_0}\left[\int_0^T v^2(t)dt+A_0^2+A_1^2-2A_0v_0b_0-2A_1v_1+2A_0A_1\rho b_0\right]\right\} \\ &= \exp\left(-\frac{1}{N_0}\int_0^T v^2(t)dt\right)\exp\left(-\frac{A_0^2+A_1^2}{N_0}\right)\cdot \\ &\quad \cdot\exp\left(-\frac{2}{N_0}\left(-A_0v_0b_0-A_1v_1+A_0A_1\rho b_0\right)\right) \\ &= \kappa(t)\exp\left(-\frac{2}{N_0}\left(-A_0v_0b_0-A_1v_1+A_0A_1\rho b_0\right)\right), \end{aligned} \tag{2.16}$$

where $\kappa(t)$ is a function that is independent of the b_0 term.

Similar algebra would yield the second summand in (2.11) as

$$L_{b_1=-1}(b_0) = \kappa(t)\exp\left(-\frac{2}{N_0}\left(-A_0v_0b_0+A_1v_1-A_0A_1\rho b_0\right)\right). \tag{2.17}$$

To determine the decision bit b_0, one can do a simple likelihood ratio test. One can compare the likelihood functions for each bit b_0 to see which one is larger. The likelihood function with the larger value will be associated with the decision bit, as in

$$L(b_0 = +1) \underset{b_0=-1}{\overset{b_0=+1}{\gtrless}} L(b_0 = -1). \tag{2.18}$$

We can manipulate (2.18) and use (2.16) and (2.17) to obtain the likelihood ratio

$$\frac{L(b_0 = +1)}{L(b_0 = -1)} \underset{b_0=-1}{\overset{b_0=+1}{\gtrless}} 1, \tag{2.19a}$$

$$\frac{\kappa(t)\exp\left(-\frac{2}{N_0}\left(-A_0v_0 - A_1v_1 + A_0A_1\rho\right)\right) + \kappa(t)\exp\left(-\frac{2}{N_0}\left(-A_0v_0 + A_1v_1 - A_0A_1\rho\right)\right)}{\kappa(t)\exp\left(-\frac{2}{N_0}\left(+A_0v_0 - A_1v_1 - A_0A_1\rho\right)\right) + \kappa(t)\exp\left(-\frac{2}{N_0}\left(+A_0v_0 + A_1v_1 + A_0A_1\rho\right)\right)} \underset{b_0=-1}{\overset{b_0=+1}{\gtrless}} 1, \tag{2.19b}$$

$$\frac{\exp\left(-\frac{2}{N_0}\left(-A_0v_0 - A_1v_1 + A_0A_1\rho\right)\right) + \exp\left(-\frac{2}{N_0}\left(-A_0v_0 + A_1v_1 - A_0A_1\rho\right)\right)}{\exp\left(-\frac{2}{N_0}\left(+A_0v_0 - A_1v_1 - A_0A_1\rho\right)\right) + \exp\left(-\frac{2}{N_0}\left(+A_0v_0 + A_1v_1 + A_0A_1\rho\right)\right)} \underset{b_0=-1}{\overset{b_0=+1}{\gtrless}} 1, \tag{2.19c}$$

$$\frac{\exp\left(\frac{2A_0v_0}{N_0}\right)}{\exp\left(-\frac{2A_0v_0}{N_0}\right)} \cdot \frac{\exp\left(-\frac{2}{N_0}\left(-A_1v_1 + A_0A_1\rho\right)\right) + \exp\left(-\frac{2}{N_0}\left(+A_1v_1 - A_0A_1\rho\right)\right)}{\exp\left(-\frac{2}{N_0}\left(-A_1v_1 - A_0A_1\rho\right)\right) + \exp\left(-\frac{2}{N_0}\left(+A_1v_1 + A_0A_1\rho\right)\right)} \underset{b_0=-1}{\overset{b_0=+1}{\gtrless}} 1, \tag{2.19d}$$

$$\exp\left(\frac{4A_0v_0}{N_0}\right) \cdot \frac{\cosh\left(\frac{2}{N_0}\left(A_1v_1 - A_0A_1\rho\right)\right)}{\cosh\left(\frac{2}{N_0}\left(+A_1v_1 + A_0A_1\rho\right)\right)} \underset{b_0=-1}{\overset{b_0=+1}{\gtrless}} 1, \tag{2.19e}$$

since $\cosh(x) = \frac{e^x + e^{-x}}{2}$.

Eqn. (2.19e) is the likelihood ratio test result that determines the individually optimum decision. One key note regarding this optimum decision is that it is dependent on the noise term N_0. This fact will be significant when determining the decision boundaries of this receiver in orthonormal space.

Verdú [2] denotes the maximum likelihood decision in a different form. One can show

that the result in (2.19e) is equivalent to Verdú's notation:

$$\exp\left(\frac{4A_0v_0}{N_0}\right)\cdot\frac{\cosh\left(\frac{2}{N_0}\left(A_1v_1-A_0A_1\rho\right)\right)}{\cosh\left(\frac{2}{N_0}\left(+A_1v_1+A_0A_1\rho\right)\right)}\underset{b_0=-1}{\overset{b_0=+1}{\gtrless}}1, \tag{2.20a}$$

$$\exp\left(\frac{4A_0v_0}{N_0}\right)\underset{b_0=-1}{\overset{b_0=+1}{\lessgtr}}\frac{\cosh\left(\frac{2}{N_0}\left(A_1v_1+A_0A_1\rho\right)\right)}{\cosh\left(\frac{2}{N_0}\left(A_1v_1-A_0A_1\rho\right)\right)}, \tag{2.20b}$$

$$\frac{4A_0v_0}{N_0}\underset{b_0=-1}{\overset{b_0=+1}{\lessgtr}}\ln\left[\frac{\cosh\left(\frac{2}{N_0}\left(A_1v_1+A_0A_1\rho\right)\right)}{\cosh\left(\frac{2}{N_0}\left(A_1v_1-A_0A_1\rho\right)\right)}\right], \tag{2.20c}$$

$$v_0\underset{b_0=-1}{\overset{b_0=+1}{\lessgtr}}\frac{N_0}{4A_0}\ln\left[\frac{\cosh\left(\frac{2}{N_0}\left(A_1v_1+A_0A_1\rho\right)\right)}{\cosh\left(\frac{2}{N_0}\left(A_1v_1-A_0A_1\rho\right)\right)}\right], \tag{2.20d}$$

$$v_0-\frac{N_0}{4A_0}\ln\left[\frac{\cosh\left(\frac{2}{N_0}\left(A_1v_1+A_0A_1\rho\right)\right)}{\cosh\left(\frac{2}{N_0}\left(A_1v_1-A_0A_1\rho\right)\right)}\right]\underset{b_0=-1}{\overset{b_0=+1}{\gtrless}}0. \tag{2.20e}$$

Eqn. (2.20e) matches the result of [2] for the optimum decision bit $\hat{b}_0$ of

$$\hat{b}_0=\operatorname{sgn}\left(v_0-\frac{\sigma^2}{2A_0}\ln\left[\frac{\cosh\left(\frac{1}{\sigma^2}\left(A_1v_1+A_0A_1\rho\right)\right)}{\cosh\left(\frac{1}{\sigma^2}\left(A_1v_1-A_0A_1\rho\right)\right)}\right]\right), \tag{2.21}$$

where sgn(t) is the sign function.

One can expand the result from (2.21) by noting that the correlation coefficient ρ can be found using (2.14). One can recall the system model for a BPSK signal plus interferer as

$$v(t)=b_0A_0\sqrt{\frac{2}{T}}\cos(\omega_0t)+b_1A_1\sqrt{\frac{2}{T}}\cos(\omega_1t+\theta)+n(t). \tag{2.22}$$

Assuming that the frequency of the desired signal and the cochannel interferer are the same (i.e. $\omega=\omega_0=\omega_1$), the variable ρ can be found through simple trigonometric manipula-

tions as

$$\begin{aligned}
\rho &= \int_0^T s_0(t)s_1(t)dt \\
&= \int_0^T \sqrt{\frac{2}{T}}\cos(\omega t)\sqrt{\frac{2}{T}}\cos(\omega t+\theta)dt \\
&= \frac{2}{T}\cdot\frac{1}{2}\int_0^T \left[\cos\theta+\cos(\frac{4\pi}{T}t+\theta)\right]dt \\
&= \frac{1}{T}\int_0^T \cos\theta dt+0 \\
&= \cos\theta. \qquad (2.23)
\end{aligned}$$

Using this value for ρ, (2.20e) becomes

$$v_0-\frac{N_0}{4A_0}\ln\left[\frac{\cosh\left(\frac{2}{N_0}\left(A_1v_1+A_0A_1\cos\theta\right)\right)}{\cosh\left(\frac{2}{N_0}\left(A_1v_1-A_0A_1\cos\theta\right)\right)}\right]\underset{b_0=-1}{\overset{b_0=+1}{\gtrless}}0, \qquad (2.24)$$

where θ is the phase difference between $s_0(t)$ and $s_1(t)$.

As a result of the derived individually optimum decision statistic in (2.24), it is useful to examine other derivations of the individually optimum receiver in the literature. In 1995, reference [19] described an individually optimum decision with the likelihood ratio function

$$\Lambda(\mathbf{r}|\Psi,\theta)=\exp(4\gamma r_1)\frac{\cosh\left(\frac{2\gamma}{\sqrt{\Psi}}((r_1-1)\cos\theta+r_2\sin\theta)\right)}{\cosh\left(\frac{2\gamma}{\sqrt{\Psi}}((r_1+1)\cos\theta+r_2\sin\theta)\right)} \qquad (2.25)$$

where γ is the signal-to-noise ratio (SNR) (in the system model from (2.1), $\gamma=\frac{A_0^2}{N_0}$), and Ψ is the signal-to-interference ratio (SIR, $\Psi=\frac{A_0^2}{A_1^2}$). The quantities r_1 and r_2 are simply components of the received signal (denoted as $v(t)$ in the system model in (2.1)) along a pair of orthonormal signals. It is apparent that (2.19e) and (2.25) are similar in form.

In 2002, reference [1] introduced an optimal detection scheme for a BPSK signal in the presence of a cochannel interferer plus noise. The likelihood decision ratio was denoted as

$$\Lambda(\mathbf{v})=\exp\left(\frac{4}{N_0}Z\right)\frac{\cosh\left(\frac{2}{N_0}(Y-y)\right)}{\cosh\left(\frac{2}{N_0}(Y+y)\right)}, \qquad (2.26)$$

where

$$Y = \int_0^T v(t) A_1 \sqrt{\frac{2}{T}} \cos(\omega_1 t + \theta) dt \tag{2.27}$$

$$Z = \int_0^T v(t) A_0 \sqrt{\frac{2}{T}} \cos(\omega_0 t) dt \tag{2.28}$$

$$y = \frac{\sin(\omega_1 - \omega_0)T}{(\omega_1 - \omega_0)T} A_0 A_1 \cos\theta - \frac{1 - \cos(\omega_1 - \omega_0)T}{(\omega_1 - \omega_0)T} A_0 A_1 \sin\theta. \tag{2.29}$$

Reference [1] also shows a schematic diagram of this receiver, shown in Fig. 2.1. One point of note is that implementing this decision metric may be difficult, due to the hyperbolic cosine terms. Indeed, the diagram in [1] simply shows a "Likelihood ratio calculation and Decision Device".

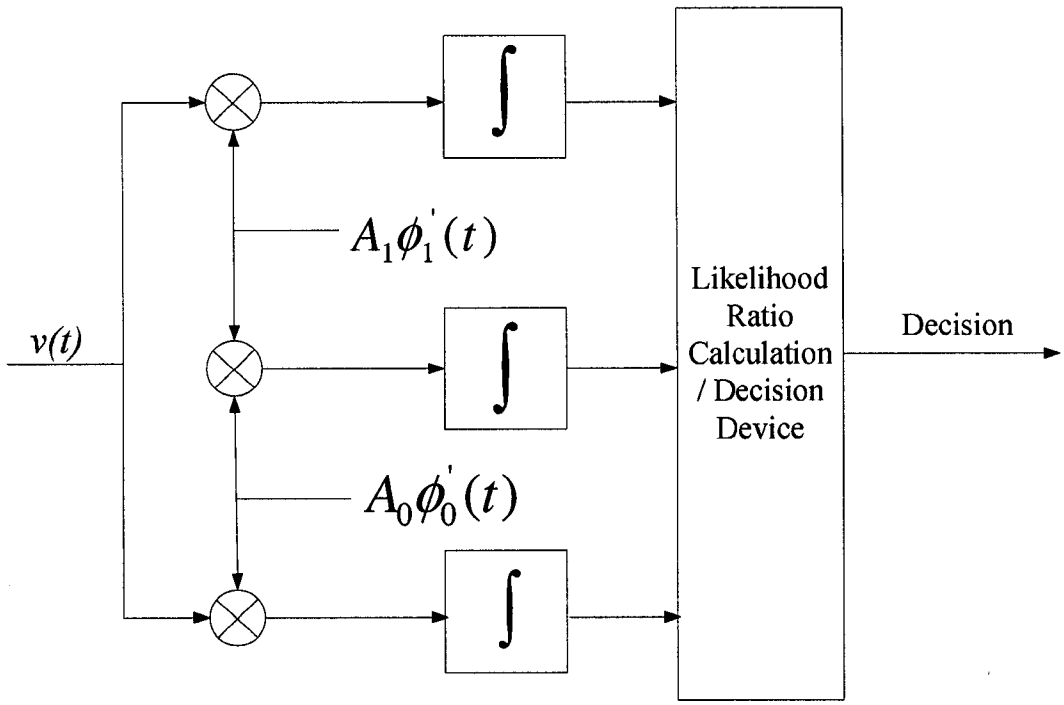

Fig. 2.1. Block diagram of an individually optimal receiver for a BPSK signal plus a single cochannel interferer, from [1].

Note that the structure of (2.26) is very similar to (2.19e) and (2.25). Thus, one sees that the individually optimum receiver derived in [1] is not a new result. Nonetheless, the

derivation of this receiver is important when comparing the performance of this receiver with a jointly optimum one.

2.2.2 Jointly Optimal Decisions

A jointly optimum receiver needs to maximize the likelihood function from (2.10). After some manipulations, this is equivalent to choosing the pair of bits that maximizes

$$L_{joint}(b_0, b_1) = b_0 A_0 \nu_0 + b_1 A_1 \nu_1 - b_0 b_1 A_0 A_1 \cos\theta. \tag{2.30}$$

Verdú [2] shows that the jointly optimal decisions $(\hat{b}_0, \hat{b}_1)$ are

$$\hat{b}_0 = \operatorname{sgn}\left(A_0\nu_0 + \frac{1}{2}|A_1\nu_1 - A_0A_1\cos\theta| - \frac{1}{2}|A_1\nu_1 + A_0A_1\cos\theta|\right), \tag{2.31a}$$

$$\hat{b}_1 = \operatorname{sgn}\left(A_1\nu_1 + \frac{1}{2}|A_0\nu_0 - A_0A_1\cos\theta| - \frac{1}{2}|A_0\nu_0 + A_0A_1\cos\theta|\right). \tag{2.31b}$$

A diagram for the jointly optimal receiver can be found in [2], and is shown in Fig. 2.2.

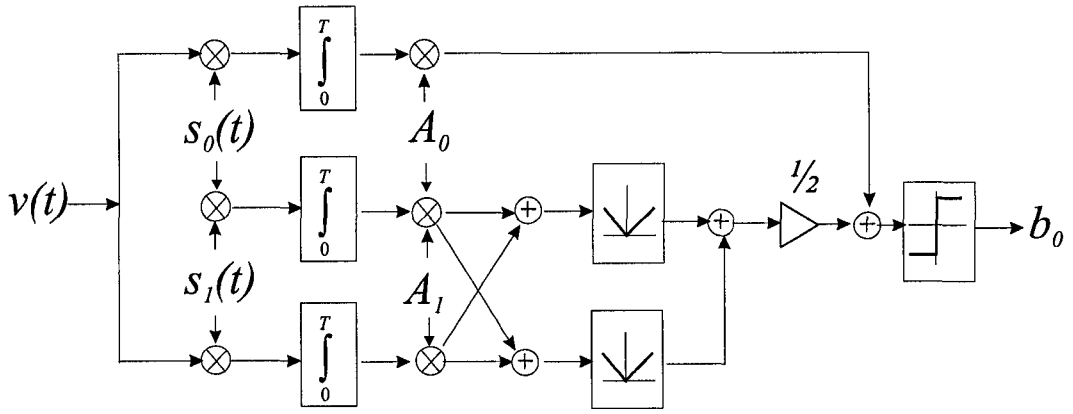

Fig. 2.2. Block diagram of a jointly optimal receiver for a BPSK signal plus a single cochannel interferer, from [2].

When examining (2.21), (2.31a), and (2.31b), there are a couple of notes. Firstly, the jointly optimal case is *independent* of the variance of the Gaussian noise. This is a sharp contrast to the decision for an individually optimum receiver. The individually optimum decision has its decision boundaries *changing depending on the noise variance*. This does not occur in the joint case, which does not have a noise factor.

Secondly, further mathematical manipulations [2] can show that as the noise decreases (i.e. $N_0 \to 0$), the joint decision for b_0 approaches that for the individual case. With this knowledge, the comparisons between the decision regions for the two receivers can be shown.

2.3 Examining the Decision Regions for Individually and Jointly Optimal Receivers

Fig. 2.3 shows a sample signal constellation diagram of the system, which originally was shown in [1].[1] The received signal $v(t)$ is projected along 2 orthnormal axes determined by the Gram-Schmidt procedure [21] as

$$\phi_0(t) = \phi_0'(t) = \sqrt{\frac{2}{T}}\cos(\omega_0 t) \tag{2.32a}$$

$$\phi_1(t) = -\frac{\cos\theta}{\sin\theta}\phi_0'(t) + \frac{1}{\sin\theta}\phi_1'(t) = -\sqrt{\frac{2}{T}}\sin(\omega_0 t) \tag{2.32b}$$

where $\phi_0'(t) = \sqrt{\frac{2}{T}}\cos(\omega_0 t)$ and $\phi_1'(t) = \sqrt{\frac{2}{T}}\cos(\omega_0 t + \theta)$. Consider the received signal without noise, $y(t) = v(t) - n(t)$. There are four possible received signal combinations, $\pm A_0\phi_0'(t) \pm A_1\phi_1'(t)$, given by

$$y_1(t) = \left(A_0 + A_1\cos\theta\right)\phi_0(t) + \left(A_1\sin\theta\right)\phi_1(t) \tag{2.33a}$$

$$y_2(t) = \left(A_0 - A_1\cos\theta\right)\phi_0(t) - \left(A_1\sin\theta\right)\phi_1(t) \tag{2.33b}$$

$$y_3(t) = -\left(A_0 - A_1\cos\theta\right)\phi_0(t) + \left(A_1\sin\theta\right)\phi_1(t) \tag{2.33c}$$

$$y_4(t) = -\left(A_0 + A_1\cos\theta\right)\phi_0(t) - \left(A_1\sin\theta\right)\phi_1(t). \tag{2.33d}$$

The resulting signal constellation is similar to that shown in Fig. 2.3. If one wished to *jointly* detect the correct constellation point on this diagram, one would have the decision boundaries shown in Fig. 2.3. Note that because the decision metric from (2.31a) does not

[1]Note that the authors of [1] show decision boundaries as straight lines, even though an individually optimum receiver is derived in [1].

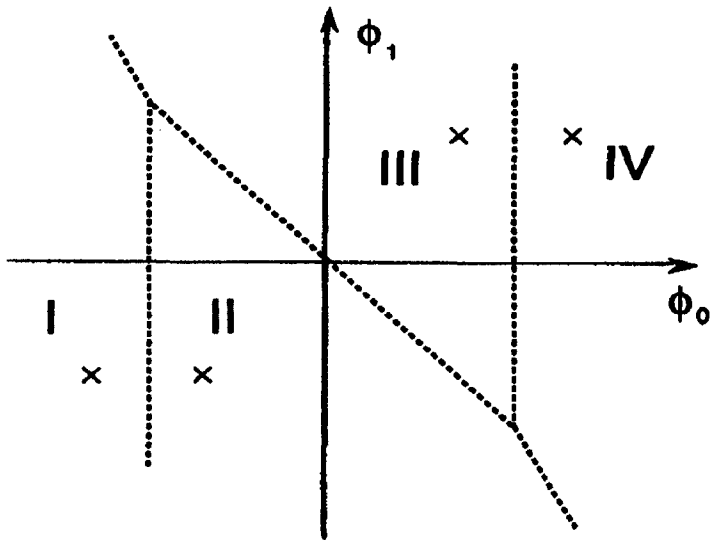

Fig. 2.3. Signal constellation for a desired signal plus interferer, from [1].

have a dependency on the noise variance N_0, the decision boundaries are independent of N_0.

However, in an individually optimum detection case, one does not simply draw the decision boundaries based on straight lines which divide the constellation points. Since (2.19e) is the decision metric, one sees that the decision is a function of N_0.

One can observe this difference with a few examples. The following example figures are structured in a manner similar to those given in [19] and [22]. Consider a scenario where the signal-to-interference ratio (SIR), $\Psi = \frac{A_0^2}{A_1^2} = 1$, or 0 dB SIR. For purposes of illustration, let θ be known, and equal to $\theta = \frac{\pi}{6}$. Fig. 2.4 illustrates the varying decision boundary for an individually optimum receiver when the signal-to-noise ratio (SNR, $\gamma = \frac{A_0^2}{N_0}$) changes.

Note that the decision boundary for the individually optimum receiver varies significantly when the noise component is large. One point of note is that the decision boundary is not equidistant from the various points of the signal constellation. An explanation of this fact is that one must consider the two *joint PDFs*, which are formed from the individual PDFs when the interferer bits b_1 are -1 or $+1$. In effect, averaging the PDFs for the two constellation points ($b_0 = -1$ and $b_0 = +1$) over b_1 bends the decision boundaries.

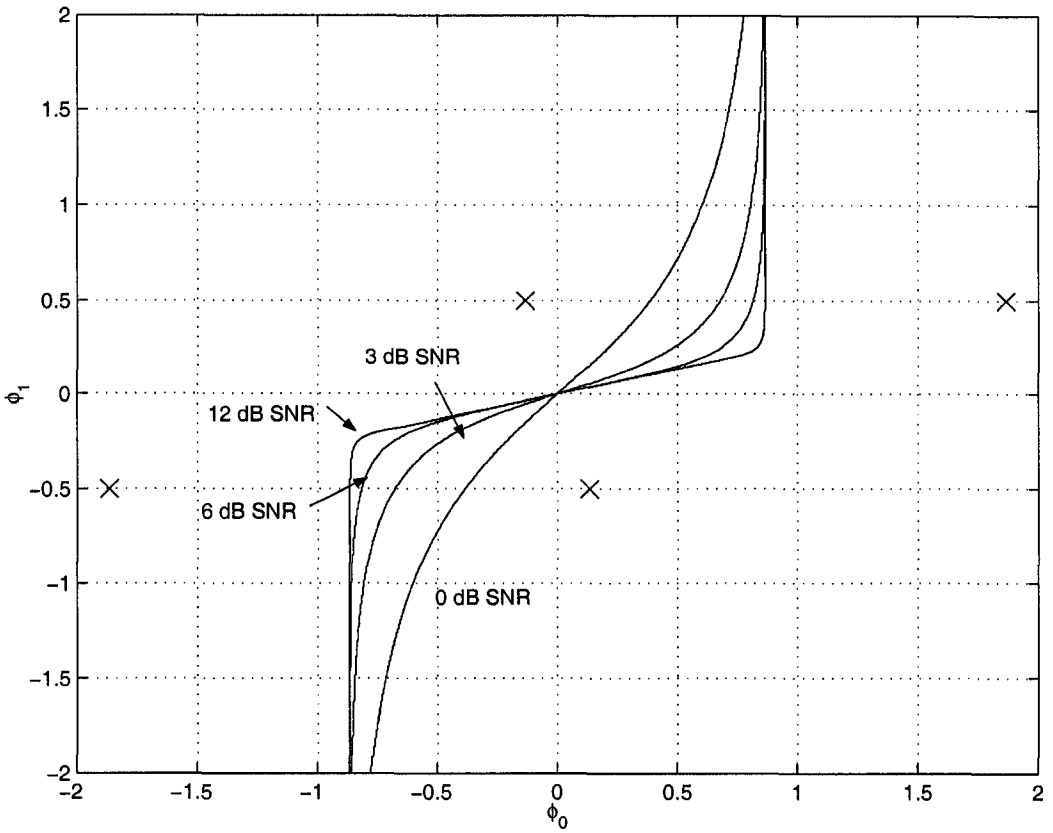

Fig. 2.4. Decision boundaries for an individually optimum receiver at various values of SNR, determined using (2.19e), with $\Psi = 0$ dB, and $\theta = \frac{\pi}{6}$.

One can compare this to the jointly optimum decision, where the decision regions are made based on the PDFs for each of the four constellation points (b_0, b_1). Since the decision statistic from (2.31a) does not depend on N_0, the decision boundary is formed by straight lines.

Fig. 2.5 compares a jointly optimal decision boundary with those for individually optimum decisions, using the same parameters as Fig. 2.4. Note that as the signal-to-noise ratio increases, the individually optimum receiver boundary approaches that of the jointly optimum case. This is to be expected, since the decision statistic (2.19e) asymptotically approaches (2.31a) as the noise variance N_0 decreases.

Another interesting example for the decision boundaries of the individually optimum receiver occurs when $\Psi = -3$ dB, and $\theta = \frac{\pi}{4}$. For these values, the jointly optimal decision boundaries are composed of perpendicular line segments. In contrast, the individually optimal decision boundaries, as shown in Fig. 2.6, are curved. In particular, note that as the SNR decreases to small values, the minimum distance to the decision boundary is no longer halfway between constellation points. Recognizing this fact will be very useful when simulating jointly optimal receivers in future chapters.

Using the decision metrics given in (2.19e) and (2.31a), one can further examine the decision boundaries for the individually optimum receiver by changing different parameters.

Consider the case where the SNR and θ are fixed, and one varies the SIR. Fig. 2.7 is one such example ($\theta = \frac{\pi}{6}$, $\gamma = 3$ dB). Note that when the interferer increases in amplitude relative to the desired signal (i.e. a smaller SIR), the decision boundary becomes increasingly curved. When the SIR is large, the decision boundary is very similar to that of a matched filter receiver. A smaller SIR results in a decision boundary with more distinct corners, as seen in Fig. 2.7. The jointly optimum case is shown in Fig. 2.8. In Fig. 2.8, a decrease in SIR causes a significant change in the decision boundary, but since the receiver uses a jointly optimal scheme, the decision boundaries are straight lines. These straight boundaries would become useful in the analysis of Chapter 3.

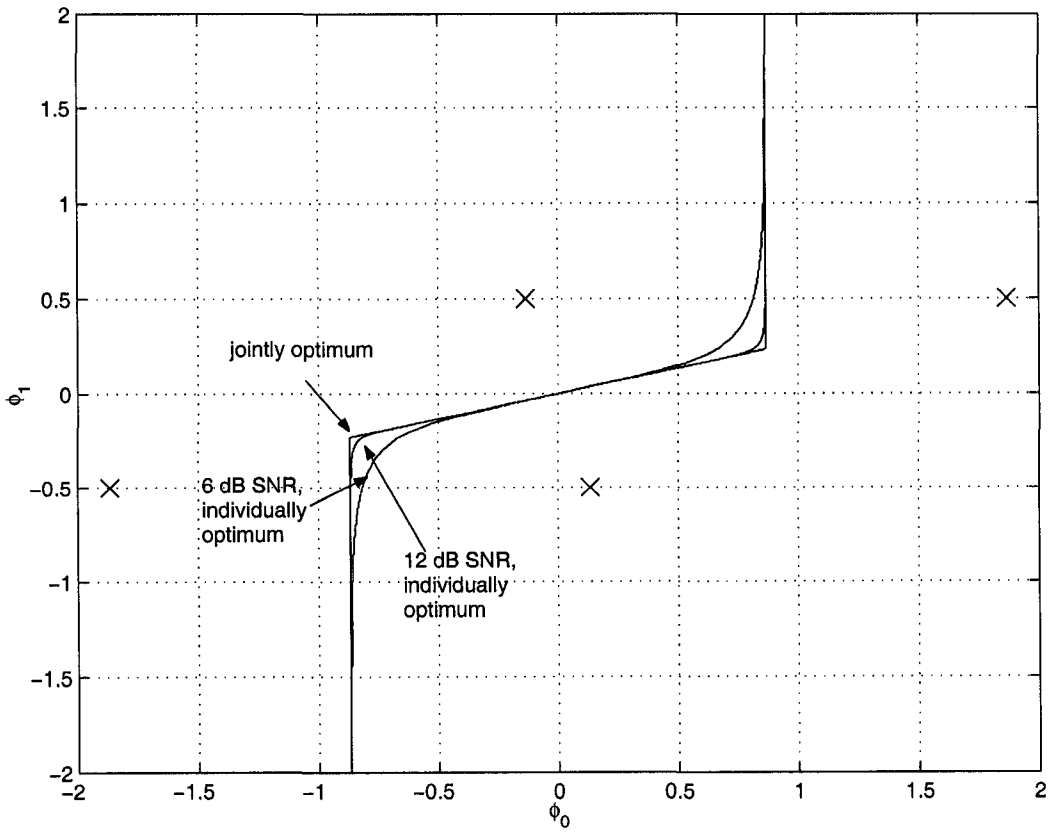

Fig. 2.5. Sample signal constellation for a BPSK signal plus one cochannel interferer, for $\Psi = 0$ dB, $\theta = \frac{\pi}{6}$, with decision boundaries for an individually optimum receiver (at 6 dB and 12 dB SNR), and a decision boundary for a jointly optimum receiver determined by (2.31a).

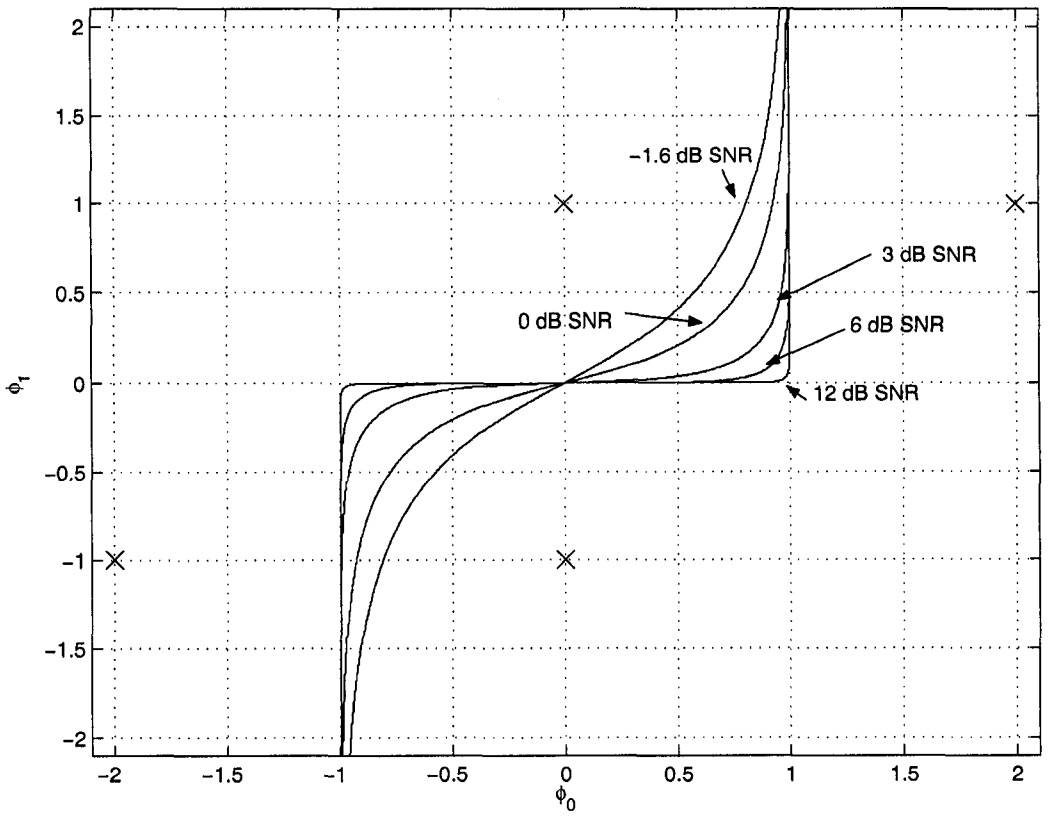

Fig. 2.6. Decision boundaries for an individually optimum receiver at various values of SNR, determined using (2.19e), with $\Psi = -3$ dB, and $\theta = \frac{\pi}{4}$.

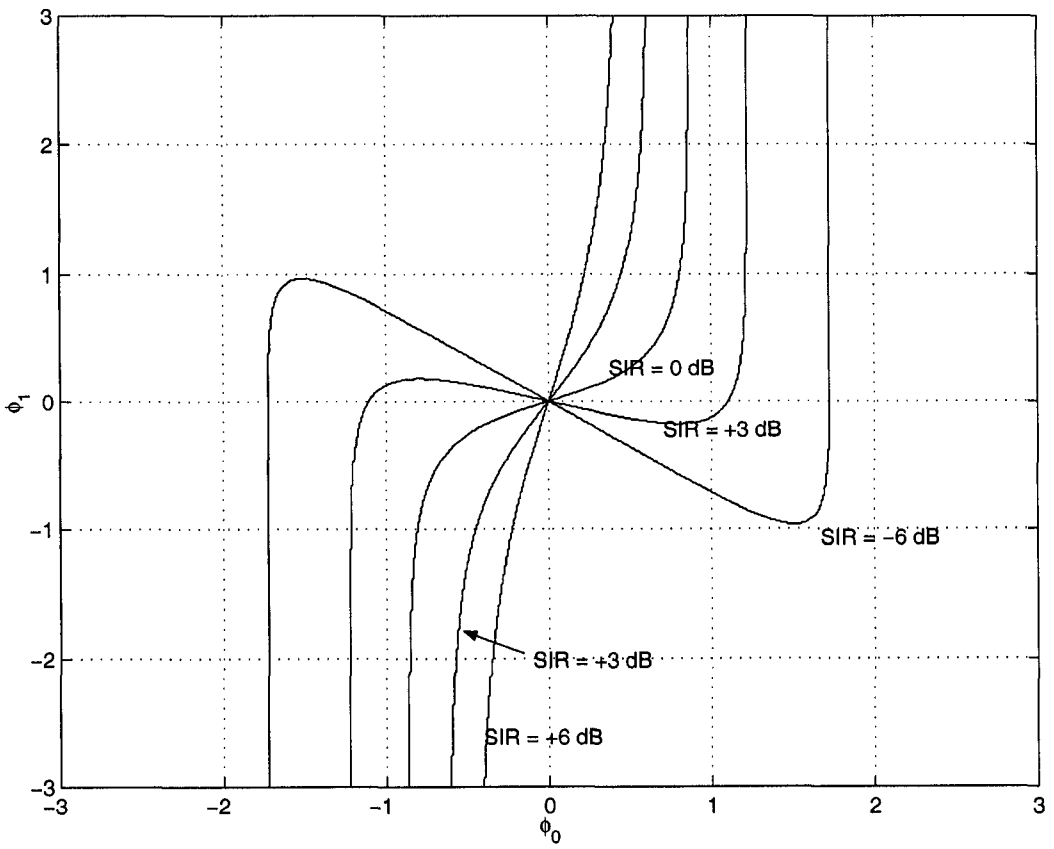

Fig. 2.7. Individually optimal decision boundaries for a BPSK signal plus one cochannel interferer, for different values of SIR, with $\gamma = 3$ dB, and $\theta = \frac{\pi}{6}$.

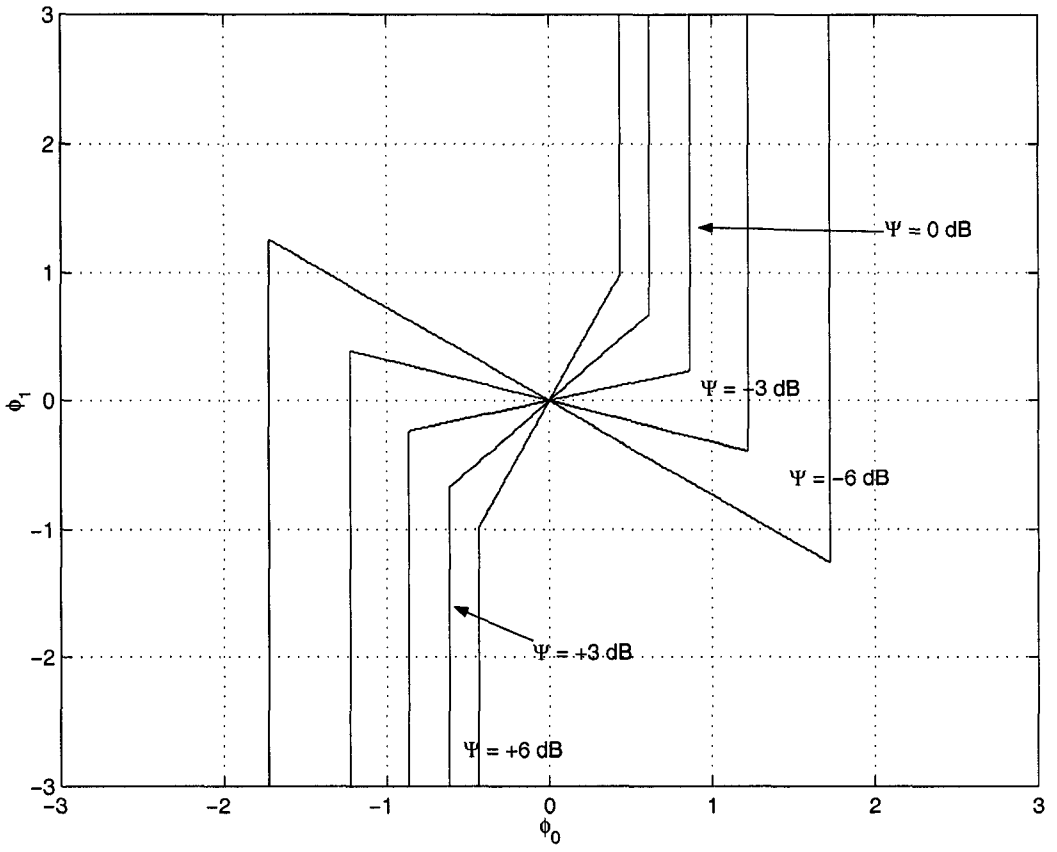

Fig. 2.8. Jointly optimal decision boundaries for a BPSK signal plus one cochannel interferer, for different values of SIR, with $\gamma = 3$ dB, and $\theta = \frac{\pi}{6}$.

Fig. 2.9 shows the effects of known phase difference on the individually optimum decision, with $\gamma = 3$ dB, and $\Psi = -2$ dB. A phase difference of $\theta = \frac{\pi}{2}$ results in a straight vertical line for the individually optimum decision. As the phase difference becomes less than $\frac{\pi}{2}$ and approaches $\theta = 0$, the decision regions become significantly more curved. This is also seen in the jointly optimum case shown in Fig. 2.10.

By examining the actual decision boundaries on a pair of orthonormal axes $\phi_0(t)$ and $\phi_1(t)$, one can clearly see that there are differences in the decision boundaries between jointly optimal and individually optimal receivers. This is largely because the noise variance N_0 affects the joint PDFs used in the individually optimal case. One can also see that the use of Fig. 2.3 in [1] is misleading, since it is a diagram for jointly optimal decisions, despite the fact that [1] discusses only individually optimal receivers.

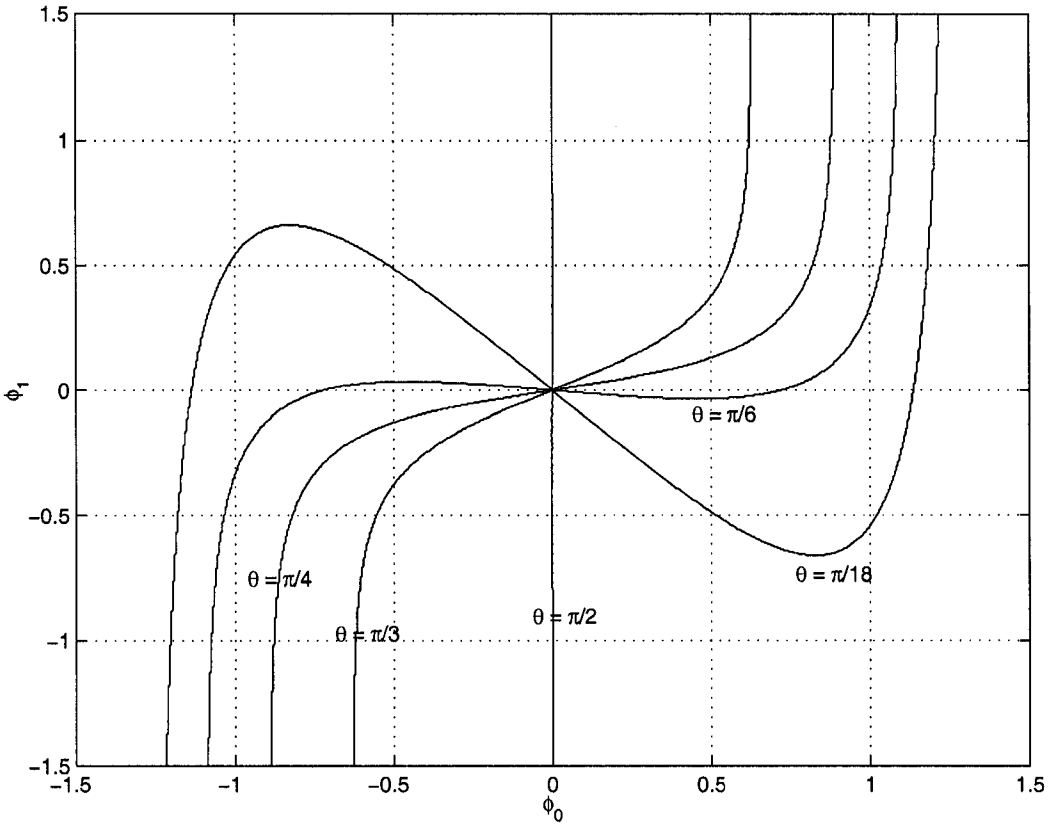

Fig. 2.9. Individually optimal decision boundaries for a BPSK signal plus one cochannel interferer, for different phases, with $\gamma = 3$ dB, and $\Psi = -2$ dB.

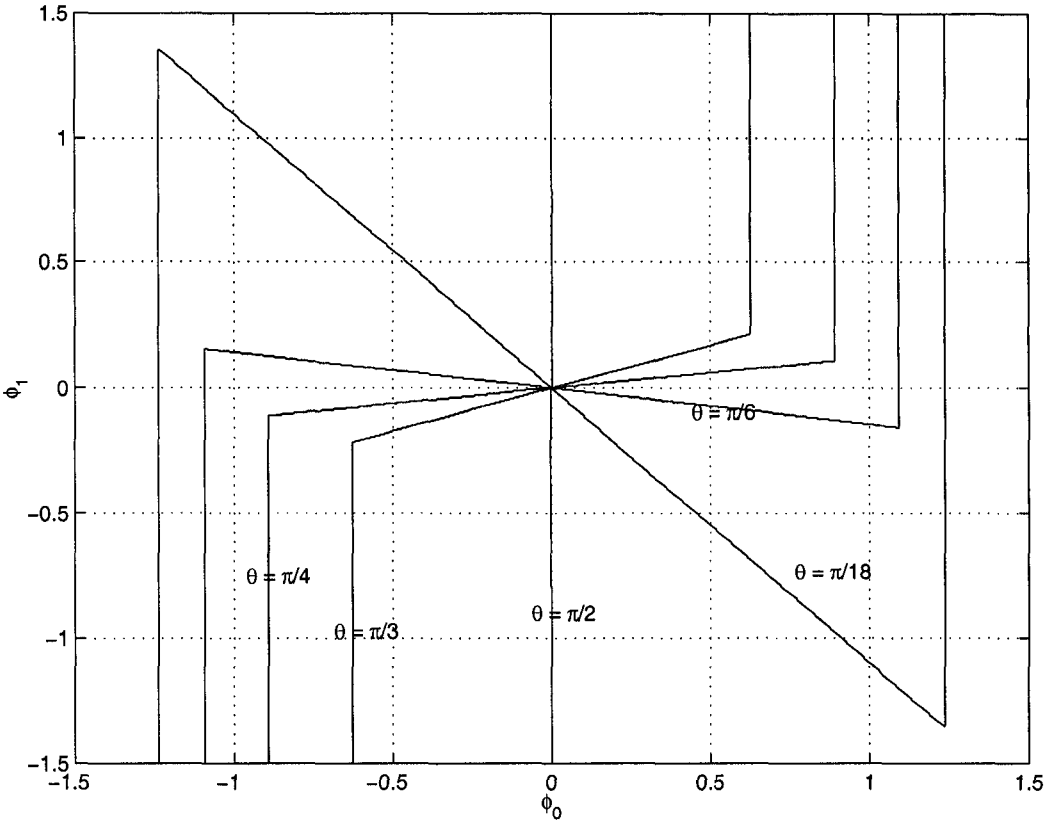

Fig. 2.10. Jointly optimal decision boundaries for a BPSK signal plus one cochannel interferer, for different phases, with $\gamma = 3$ dB, and $\Psi = -2$ dB.

2.4 Simulation Results and Comparisons of Receivers

Having the knowledge of the effects of SNR on an individually optimal receiver, one can obtain simulation results comparing the individually optimal receiver with a jointly optimal one.

From the decision boundary plots in Figs. 2.4-2.10, one can see that as the SNR increases, the difference between an individually optimal decision boundary and one for jointly optimal decisions is negligible. As a result, one can focus on the differences at low regions of SNR. Indeed, simulation results for the two types of receivers show that even at SNR levels of γ = 0 to 3 dB, the performance improvement in the individually optimal case is negligibly small.

Some BER performance results for the two types of receiver are shown in Fig. 2.11. Note that above 2 dB SNR, the two receiver structures have similar error performance. That is, for SNR values larger than 2 dB, there is little difference in performance between jointly optimal receivers and individually optimal receivers. However, the results show that for SNR values less than 0 dB, there is a small improvement in performance for individually optimum receivers.

To see an individually optimal receiver performance that is significantly different from a jointly optimal one, one has to have an even lower SNR. Fig. 2.12 shows the performance curves for various SIR simulations for $\theta = \frac{\pi}{6}$, and $\gamma = -3$ dB. Obviously, $\gamma = -3$ dB is not a useful case. The purpose of the plot is to show that the individually optimal receiver does perform better than the jointly optimal one. However, the region where this occurs is at a very small SNR. Note that in Fig. 2.12, one can see a difference in performance for a range of SIR values between -5 dB and +10 dB. However, for small and large values of SIR, the difference in performance between the two receivers is small.

The performance results of individually optimal and jointly optimal receivers are significant for practical receiver design. Since the performance of these two types of receivers are almost indistinguishable at relatively high SNR, performance analysis of jointly optimal receivers is usually sufficient. Indeed, future chapters derive an exact analysis of BER

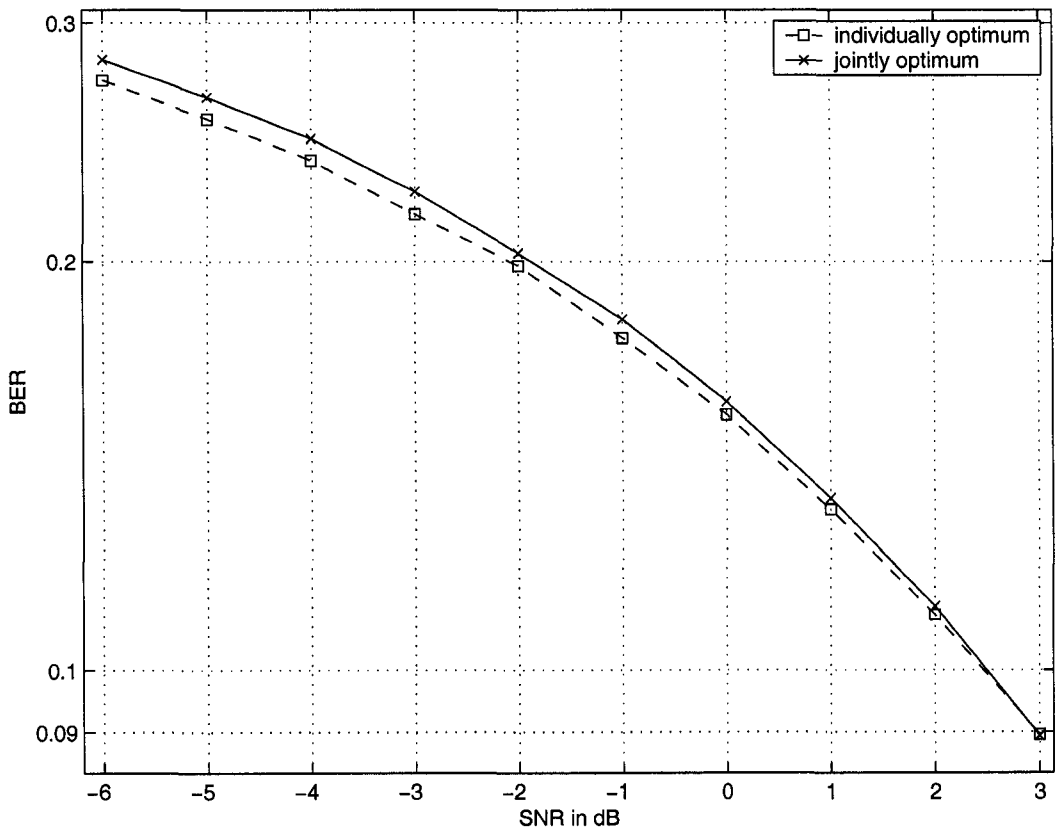

Fig. 2.11. The BER performance versus SNR for individually optimum and jointly optimum receivers, with $\Psi = 0$ dB, and $\theta=\frac{\pi}{6}$.

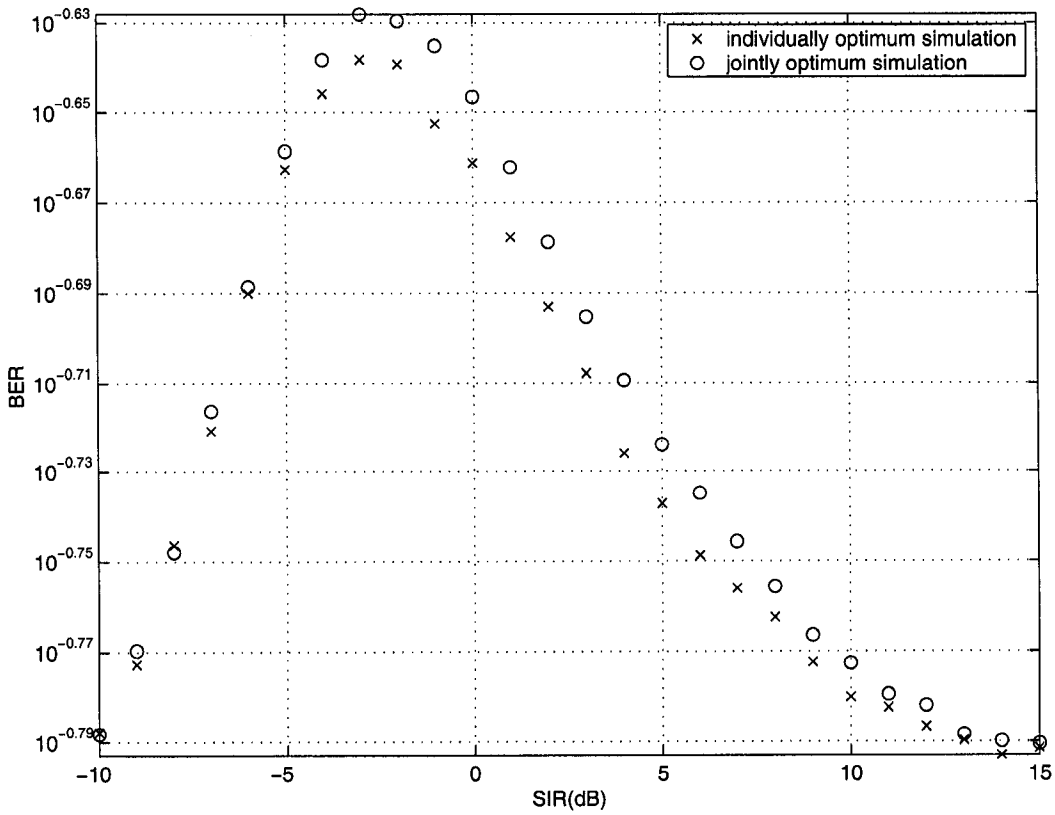

Fig. 2.12. The BER performance versus SIR of the individually optimal receiver and jointly optimal receiver, where the SNR is $\gamma = -3$ dB, and $\theta = \frac{\pi}{6}$.

performance of a jointly optimal receiver using Craig's method [3]. This methodology could not be performed under an individually optimal case, where the decision boundaries are not composed of straight line segments. Having this knowledge, future performance analysis can be completed on the jointly optimal case.

2.5 Summary

The individually optimal receiver in [1] is a useful result. The receiver has been derived to be optimal, and the performance of the receiver has been shown to be good in regions of low and high SIR.

Distinguishing between individually optimal and jointly optimal receivers is important. Individually optimal receivers have a decision region that is a curved line in orthonormal space. Jointly optimal receivers, on the other hand, have decision boundaries that are composed of straight line segments (even though the receiver is sub-optimal for an individual user). Jointly optimal receiver structures are easier to implement and their straight-line decision boundaries facilitate performance analysis. Using these straight line segments, one can obtain an exact analytical result for the error performance in future chapters.

The work in this chapter has been presented in [23], and is an important result, clarifying results in past works. While the work in [1] implies the use of a jointly optimal receiver, the results in [1] indicate that a minimum-BER individually optimal receiver is used. Furthermore, the work in this chapter also reinforces that for most levels of SNR, there is indistinguishable difference in BER between individually and jointly optimal receivers. These results justify the analysis of jointly optimal receivers in future chapters.

Chapter 3

Performance Analysis of the Jointly Optimal BPSK Receiver

Using the jointly optimal receiver described in Chapter 2, one now develops a powerful way to analyze the error rate performance of this system. In this Chapter, bounds to the error rate performance are developed, and a new, exact, analytical expression for the BER is found.

The receivers in [1] and [24] have been shown to perform better than a matched filter receiver for a BPSK signal in the presence of a cochannel interferer. In particular, when the interferer amplitude is large relative to that of the desired signal, the BER is significantly smaller than that of a matched filter receiver.

The performance assessment results in [1] and [24] were obtained using simulation. However, simulation may take a significant amount of time. It is thus valuable to obtain an analytical solution for the error rate performance of the jointly optimal BPSK receiver that follows the main assumptions in [25].

3.1 Signaling Constellation of a BPSK Desired Signal Plus Interferer

In [1] and [24], a BPSK signal with amplitude A_0 is transmitted over an AWGN channel and corrupted by an interferer signal with amplitude A_1. The received signal is given by

$$v(t) = b_0 A_0 \sqrt{\frac{2}{T}} \cos(\omega_0 t) + b_1 A_1 \sqrt{\frac{2}{T}} \cos(\omega_1 t + \theta) + n(t) \tag{3.1}$$

where ω_0 and ω_1 are the angular carrier frequencies of the desired and interferer signals, respectively, $n(t)$ is an AWGN process with two-sided power spectral density $N_0/2$, and T is the bit period of the desired and interferer signals. The carrier phase of the interferer signal, θ, has uniform distribution in [0, 2π). The binary random variable (RV) b_0 (b_1) assumes value $+1$ if the desired (interferer) bit is "1" and -1 if it is "0".

The receiver design used in [1] and [24] assumes knowledge of the carrier frequencies, the carrier phases, the amplitudes, and the symbol timings of the desired and interferer signals.

Let

$$\phi_0'(t) = \sqrt{\frac{2}{T}} \cos(\omega_0 t) \tag{3.2a}$$

$$\phi_1'(t) = \sqrt{\frac{2}{T}} \cos(\omega_1 t + \theta). \tag{3.2b}$$

Furthermore, following [1], let $\omega_0 = \omega_1$. One can then project $v(t)$ on a pair of orthonormal basis functions determined by the Gram-Schmidt procedure as

$$\phi_0(t) = \phi_0'(t) = \sqrt{\frac{2}{T}} \cos(\omega_0 t) \tag{3.3a}$$

$$\phi_1(t) = -\frac{\cos\theta}{\sin\theta}\phi_0'(t) + \frac{1}{\sin\theta}\phi_1'(t) = -\sqrt{\frac{2}{T}} \sin(\omega_0 t). \tag{3.3b}$$

Now consider the received signal without noise, $y(t) = v(t) - n(t)$. There are four possible received signal combinations, $\pm A_0\phi_0'(t) \pm A_1\phi_1'(t)$, given by

$$y_1(t) = (A_0 + A_1 \cos\theta)\,\phi_0(t) + (A_1 \sin\theta)\phi_1(t) \tag{3.4a}$$

$$y_2(t) = \left(A_0 - A_1\cos\theta\right)\phi_0(t) - (A_1\sin\theta)\phi_1(t) \tag{3.4b}$$

$$y_3(t) = -\left(A_0 - A_1\cos\theta\right)\phi_0(t) + (A_1\sin\theta)\phi_1(t) \tag{3.4c}$$

$$y_4(t) = -\left(A_0 + A_1\cos\theta\right)\phi_0(t) - (A_1\sin\theta)\phi_1(t). \tag{3.4d}$$

Note that the locations of the signal points depend on the parameters A_0, A_1, and θ. As a result, the constellation points are dependent on the signal-to-interference ratio (SIR), defined as $\Psi = \frac{A_0^2}{A_1^2}$. Since the signaling constellation is dependent on A_0, A_1, and θ, the decision boundaries for the receiver will also depend on these parameters.

Examining the four-point signal constellation, we distinguish three classes of cases, shown in Figs. 3.1-3.3. Fig. 3.1 shows a sample signal constellation where the SIR is large. The resulting signal constellation has a large $\phi_0(t)$ component and a small $\phi_1(t)$ component, due to the larger value of A_0. Note that the decision boundaries depend on the phase and the SIR. Through trigonometric manipulation, the two intersection points of these decision boundaries, P_i and P_j, can be found at

$$P_i = \left(A_1\cos\theta, \frac{(A_0 - A_1\cos\theta)}{\tan\theta}\right) \tag{3.5a}$$

$$P_j = \left(-A_1\cos\theta, -\frac{(A_0 - A_1\cos\theta)}{\tan\theta}\right). \tag{3.5b}$$

Note that the P_i component along the $\phi_1(t)$ axis is greater than the $\phi_1(t)$ component of the highest constellation point (i.e. $\frac{A_0 - A_1\cos\theta}{\tan\theta} > A_1\sin\theta$).

If, however, point P_i moves below the highest constellation point, one has the situation of Fig. 3.2. Fig. 3.2 depicts the signal constellation for an intermediate SIR level, where $A_1\sin\theta > \frac{A_0 - A_1\cos\theta}{\tan\theta}$ which occurs when $\frac{A_0^2}{A_1^2} = \Psi < \frac{1}{\cos^2\theta}$. Any SIR greater than this threshold level corresponds to the case of Fig. 3.1.

Fig. 3.3 shows an additional signal constellation scenario, which is the case if the constellation decision boundary begins to "twist". That is, this case occurs when $\frac{A_0 - A_1\cos\theta}{\tan\theta} < -\frac{A_0 - A_1\cos\theta}{\tan\theta}$. This occurs when $\frac{A_0^2}{A_1^2} = \Psi < \cos^2\theta$. If $\cos^2\theta < \Psi < \frac{1}{\cos^2\theta}$, one obtains the case of Fig. 3.2.

It is seen that the threshold regions are dependent on the phase difference between the desired and the interferer signals and that there are three distinct cases. By determining

these three cases and their corresponding decision regions, one can derive an analytical expression for the BER of this jointly optimal receiver.

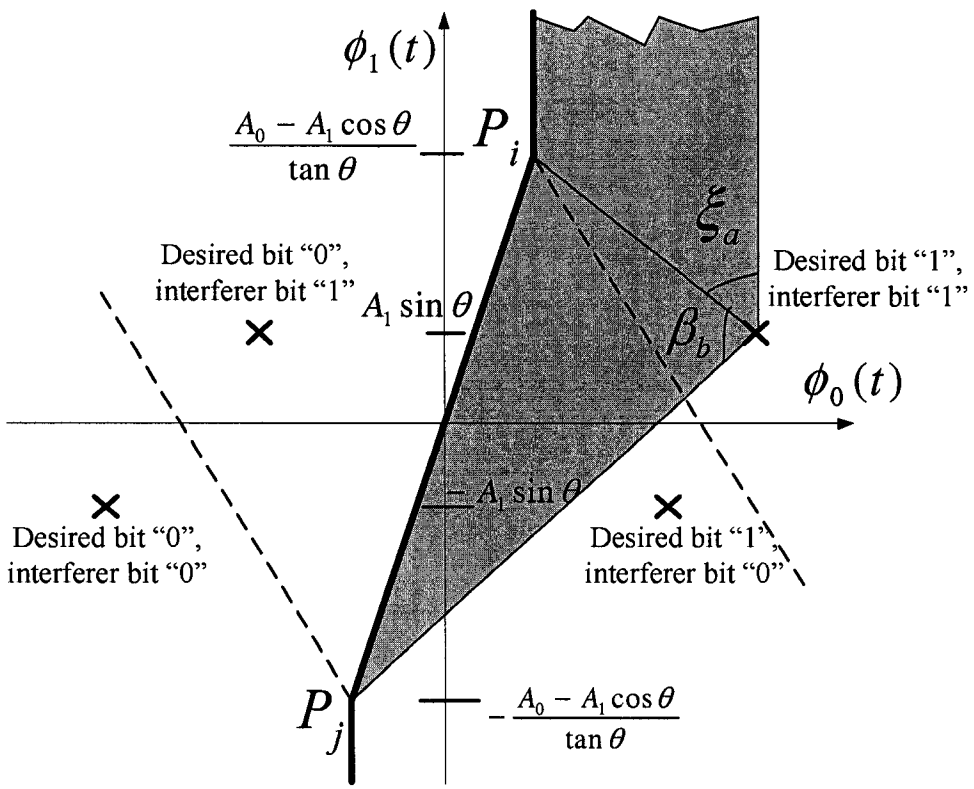

Fig. 3.1. Sample signal constellation for a BPSK signal plus one cochannel interferer for large SIR. The thick solid line is the decision boundary. The grey regions are trilaterals used to calculate the error performance for the upper right point, as in [3].

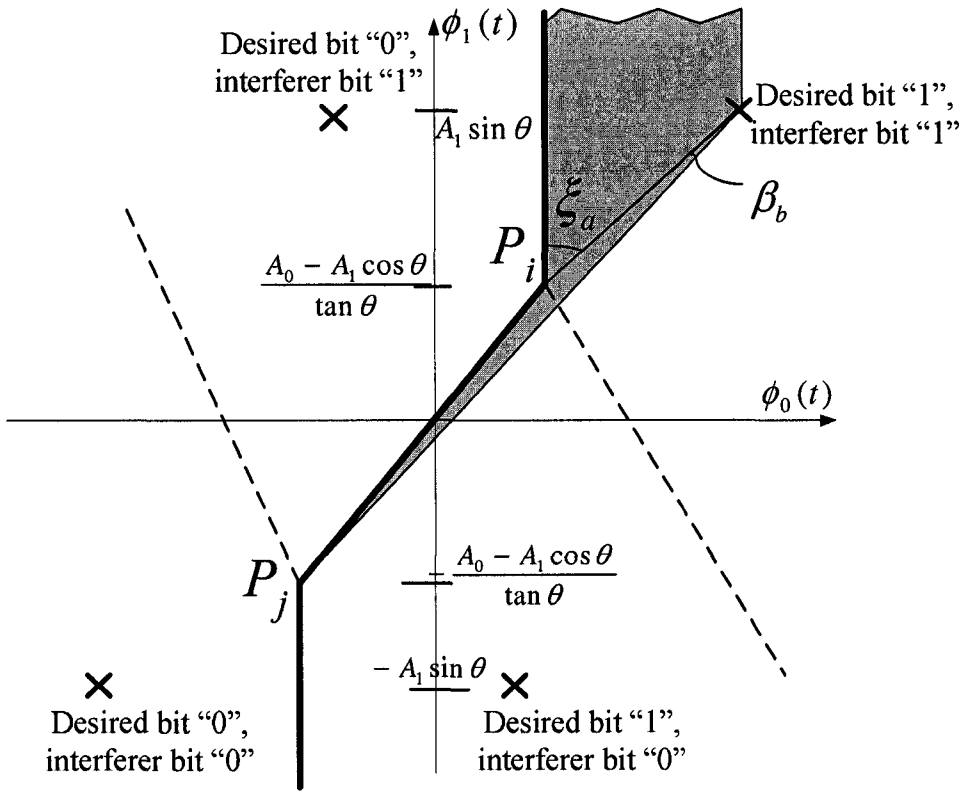

Fig. 3.2. Sample signal constellation for a BPSK signal plus one cochannel interferer for an intermediate SIR region ($\cos^2\theta < \Psi < \frac{1}{\cos^2\theta}$). The grey regions and the thick solid lines indicate trilaterals and the decision boundary, respectively.

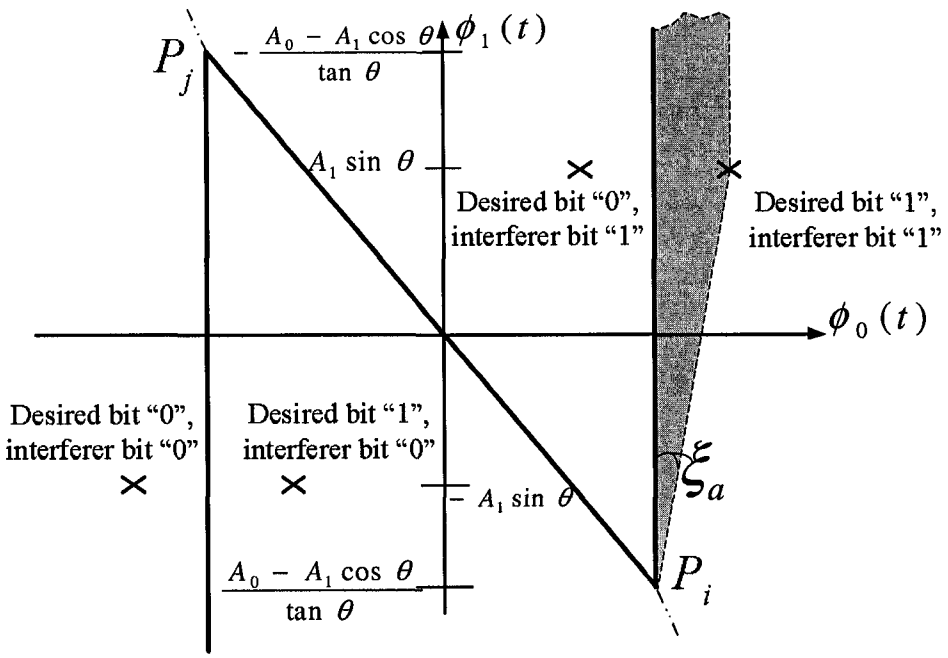

Fig. 3.3. Sample signal constellation for a BPSK signal plus one cochannel interferer. This case is for small SIR. Note that P_i is lower than P_j in this SIR region.

3.2 An Analytical Expression for the Error Rate Performance of the Jointly Optimal Receiver

The Craig representation [3] for determining the error rate performance of 2-dimensional signal constellations can be used with the signal constellation derived in Section 3.1. This approach is not straightforward. Typically, in single-user receiver structures for four-point signal constellations, one divides the signal space into four distinct decision regions. However, when used to recover only the desired signals, the jointly optimal receiver has only two decision regions, as shown in Figs. 3.1-3.3.

As shown in [3], [4], [26], the BER is the weighted sum of basic probability expressions given by

$$P_e(\gamma_s) = \frac{1}{2\pi}\int_0^{\eta} \exp\left[-\frac{\alpha E_s \sin^2\psi}{N_0 \sin^2(\zeta+\psi)}\right] d\zeta \tag{3.6}$$

where the signal-to-noise ratio (SNR) is $\gamma_s = \frac{E_s}{N_0} = \frac{A_0^2}{N_0}$ (E_s is the average symbol energy).

Using this approach, one divides the correct decision region for a given point into trilaterals, as in Fig. 3.4. The divisions are straight line segments originating at the constellation point and ending at the intersection of two decision boundaries. The angles η and ψ are determined by the geometry of the trilaterals shown in [3] and [4]. The square of the distance from the constellation point to the decision boundary intersection is $(x')^2 = \alpha E_s$. If $E_s = 1$, then $\alpha = (x')^2$. The parameter ζ is a dummy variable.

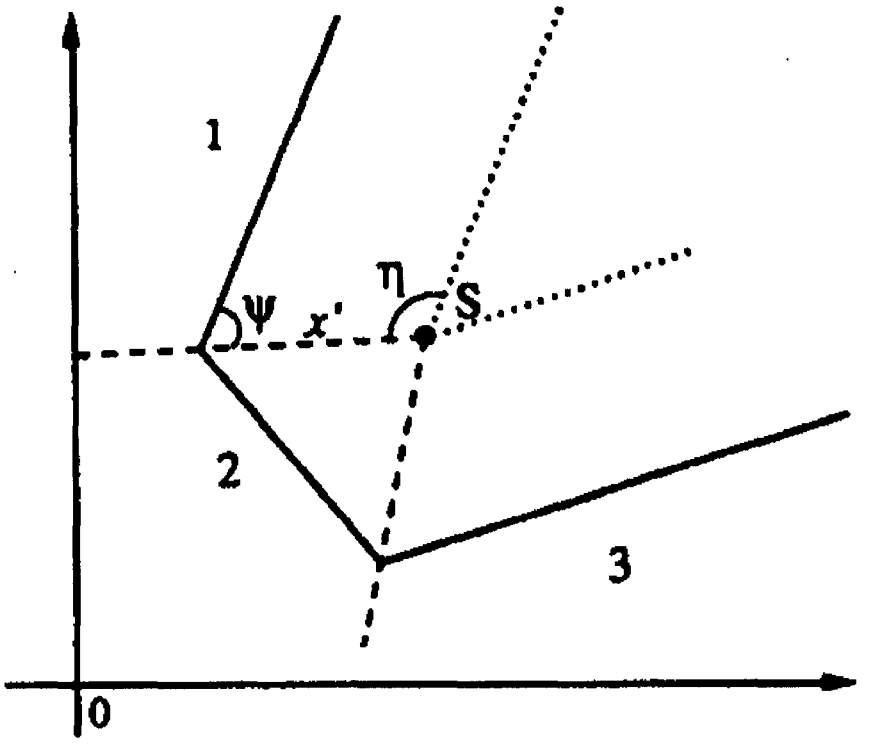

Fig. 3.4. Trilateral decision regions for a signal point, from [3] and [4].

3.2.1 Error Rate Performance in Large SIR Regions

In this case, $\Psi > \frac{1}{\cos^2\theta}$, and the constellation looks similar to Fig. 3.1. Fig. 3.5 shows the various regions used to determine the error performance of this jointly optimal detection scheme. Note that regions 1 and 6 are identical. Since each point of the constellation is equiprobable, the Craig representation as developed in (3.6) can be given in an analytical form. Through trigonometric manipulations, one can determine the angles and distances of Fig. 3.5 as

$$\kappa = \sqrt{1-\sin^2\theta} \tag{3.7a}$$

$$l_a^2 = \frac{A_0^2 + A_1^2 - 2A_0A_1\kappa}{\sin^2\theta} \tag{3.7b}$$

$$l_b^2 = \frac{A_0^2 + A_1^2 + 6A_0A_1\kappa - 8A_0A_1\kappa^3}{\sin^2\theta} \tag{3.7c}$$

$$l_c^2 = \frac{4(A_0^2 + A_1^2 - 2A_0A_1\kappa)}{\tan^2\theta} \tag{3.7d}$$

$$\beta_a = \pi - \arccos(2\cos^2\theta - 1) \tag{3.7e}$$

$$\xi_a = \arcsin\left(\frac{A_0}{l_a}\right), \quad \xi_b = \frac{\pi - \beta_a}{2} \tag{3.7f}$$

$$\xi_c = \arcsin\left(\frac{2A_1\kappa + A_0}{l_b}\right) \tag{3.7g}$$

$$\xi_d = \arcsin\left(\frac{A_0 - 2A_1\kappa}{l_a}\right) \tag{3.7h}$$

$$\xi_e = \arcsin\left(\frac{2A_1\kappa}{l_c}\right). \tag{3.7i}$$

Define six additional variables, which are the angles of the error regions as

$$\eta_a = \xi_a, \quad \Phi_a = \pi - \xi_a \tag{3.8a}$$

$$\eta_c = \xi_c, \quad \Phi_c = \pi - \xi_c \tag{3.8b}$$

$$\beta_b = \pi - \xi_a - \xi_c, \quad \Phi_b = \xi_a + \xi_e. \tag{3.8c}$$

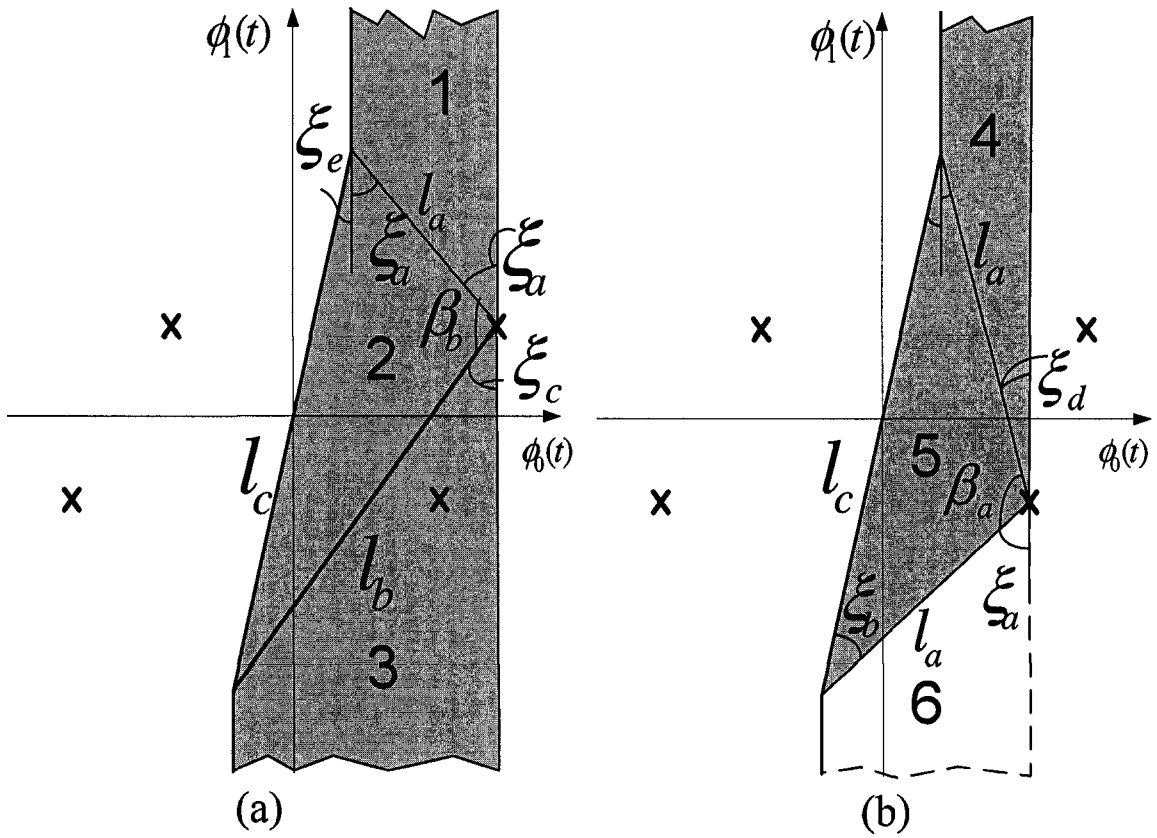

Fig. 3.5. The 5 trilateral regions used in (3.7)-(3.11). A high SIR example is used here. These trilaterals were found using techniques similar to those described in [3] and [4]. The drawing is for illustration purposes; it is not to scale. (a) Regions 1-3 are referenced to the upper right constellation point. (b) Regions 4-5 are referenced to the lower right constellation point. Note that region 6 is geometrically identical to region 1.

The average probability of bit error is

$$
\begin{aligned}
P_e(\gamma_s,\theta) &= \frac{1}{4\pi}\left[2\int_0^{\eta_a}\exp\left[\frac{-l_a^2\sin^2(\Phi_a)}{N_0\sin^2(\Phi_a+\zeta)}\right]d\zeta\right. \\
&\quad +\int_0^{\beta_a}\exp\left[\frac{-l_a^2\sin^2(\xi_b)}{N_0\sin^2(\xi_b+\zeta)}\right]d\zeta \\
&\quad +\int_0^{\eta_c}\exp\left[\frac{-l_b^2\sin^2(\Phi_c)}{N_0\sin^2(\Phi_c+\zeta)}\right]d\zeta \\
&\quad +\int_0^{\xi_d}\exp\left[\frac{-l_a^2\sin^2(\pi-\xi_d)}{N_0\sin^2(\pi-\xi_d+\zeta)}\right]d\zeta \\
&\quad \left.+\int_0^{\beta_b}\exp\left[\frac{-l_a^2\sin^2(\Phi_b)}{N_0\sin^2(\Phi_b+\zeta)}\right]d\zeta\right]. \qquad (3.9)
\end{aligned}
$$

Note that the first integral has a factor of 2 because regions 1 and 6 are identical in Fig. 3.5.

3.2.2 Error Rate Performance in Intermediate SIR Regions

If one is operating in an intermediate SIR range, $\cos^2\theta < \Psi < \frac{1}{\cos^2\theta}$, and the signal constellation looks similar to Fig. 3.2. The angles and distances needed for Craig's representation are similar to those in the large SIR case. However, because of the different orientations of the decision regions, some angles are changed. This changes the set of variables in (3.8) to

$$\eta_a = \pi - \xi_a,\ \ \Phi_a = \xi_a \qquad (3.10a)$$

$$\eta_c = \xi_c,\ \ \Phi_c = \pi - \xi_c \qquad (3.10b)$$

$$\beta_b = \xi_a - \xi_c,\ \ \Phi_b = \pi - \xi_a + \xi_e. \qquad (3.10c)$$

Note the changes in η_a and Φ_a. The values assigned to these variables are reversed from those in (3.8a). This is a result of the new orientation of the constellation points relative to the decision boundary intersection. Since the intersection point is now "below" the constellation point, the geometry changes. As a result of these changes, (3.9) can then be used to determine the probability of error in this intermediate region.

3.2.3 Error Rate Performance in Small SIR Regions

Fig. 3.3 shows a sample constellation for small SIR. This occurs when $\Psi < \cos^2\theta$. Equation (3.9) can still be used in this case, but there are different variables for the regions now given by

$$\eta_a = \pi - \xi_a, \ \Phi_a = \xi_a \tag{3.11a}$$

$$\eta_c = \pi - \xi_c, \ \Phi_c = \xi_c \tag{3.11b}$$

$$\beta_b = \pi - \xi_a - \xi_c, \ \Phi_b = \xi_a + \xi_e. \tag{3.11c}$$

Performing the integrals in small SIR regions requires care. In particular, for small SIR, an error made by "oversweeping" an area beyond the decision region is less obvious. In this case, some of the integrals in (3.9) produce negative values, indicating the oversweep. Furthermore, these negative integral values are small compared to the dominant contribution from region 1 (Figs. 3.3 and 3.5), making their inclusion harder to detect.

3.3 Numerical Results and Discussion

Using the analytical expression (3.9) with the three sets of variables in (3.8), (3.10), and (3.11), one can determine the error performance of a jointly optimal BPSK receiver in the presence of one interferer for any given θ and SIR. If θ is a uniformly distributed RV over [0,2π), the average error rate is found by taking the expected value of (3.9) over all θ, i.e.

$$P_{e,RV\,\theta} = \mathbf{E}_\theta\left[P_e(\gamma_s,\theta)\right] = \frac{1}{2\pi}\int_0^{2\pi} P_e(\gamma_s,\theta)d\theta. \tag{3.12}$$

The result is a sum of double integrals. Our use of the Craig method reduces a three-dimensional integral problem to a sum of two-dimensional integrals, where the outer integral is a simple uniform averaging over a closed definite interval. This results in a significant reduction in complexity. Fig. 3.6 shows some results for various values of SNR between 3 dB and 12 dB. Fig. 3.7 shows results for various values of SNR between -6 dB and 3 dB. While Fig. 3.7 is an extreme case, the figure is useful to show the regions of

local maxima. Note that the curve for γ_s = 12 dB is difficult to obtain by simulation in a reasonable time frame, demonstrating the usefulness and power of our analytical solution.

Note that this receiver structure has a very small BER at both small and large SIR. The theoretical curve for γ_s = 9 dB in Fig. 3.6 matches the simulation results from [1]. As in [1], both sides of this curve asymptotically approach the minimum BER in AWGN when there is no interference (at 9 dB SNR, BER = 3.2×10^{-5} in AWGN). Intuitively, this is because detecting the desired signal in a small SIR case is equivalent to detecting the interferer in a large SIR case.

Also note that for reasonably large values of SNR (e.g. 3 dB or greater), the worst performance occurs when the signal and the interferer are equally strong, i.e. 0 dB SIR. This is shown in Fig. 3.6, and enhances the results of [1], which did not have a simulation point at 0 dB and *appears* to have a maximum at approximately 0.5 dB. However, for smaller values of SNR, such as those in Fig. 3.7, the maxima are no longer at an SIR value of 0 dB. Thus, the maximum is zero only when the SNR approaches large values.

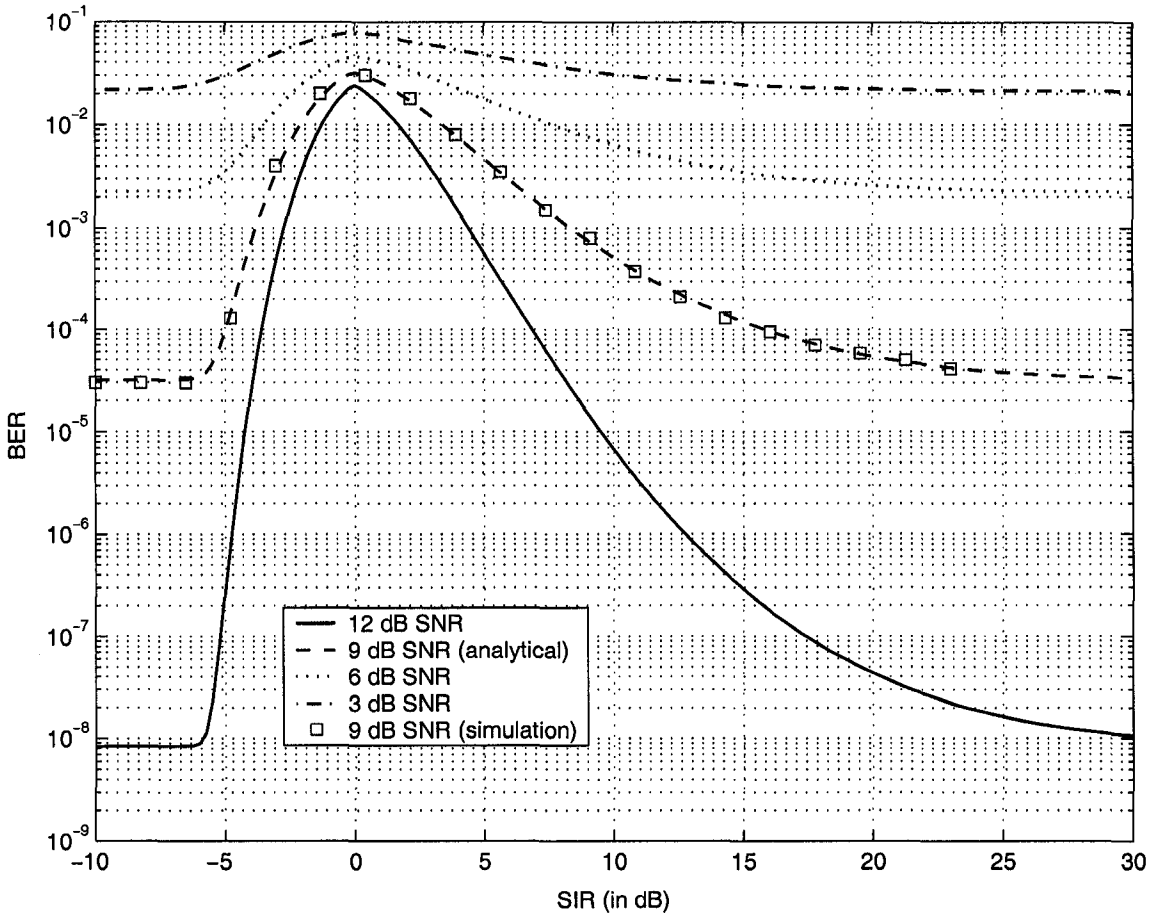

Fig. 3.6. Bit-error performance of optimal receiver obtained using (3.9) with (3.12). The simulation points for 9 dB SNR are from [1].

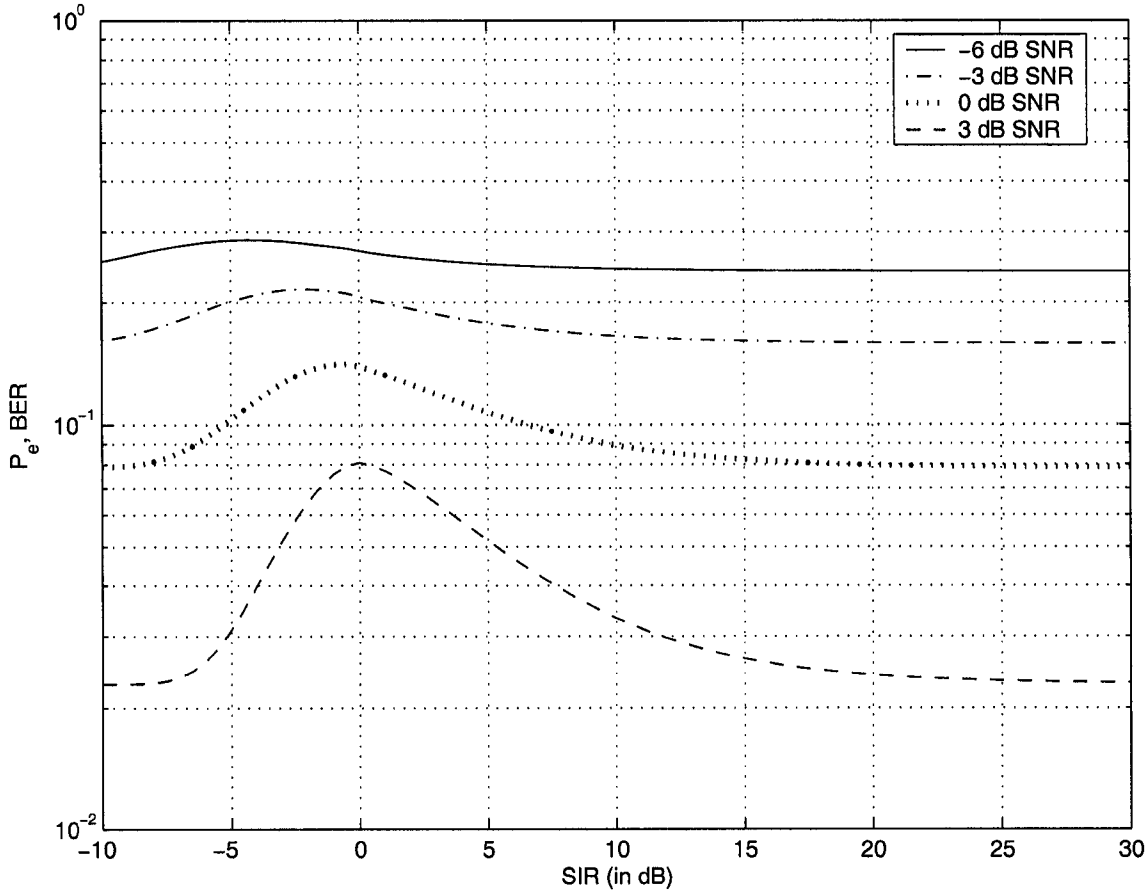

Fig. 3.7. Bit-error performance of optimal receiver obtained using (3.9) with (3.12), for low values of SNR.

The analytical result from (3.12) now allows one to examine the effects of SNR and SIR on the error performance. Figs. 3.8 and 3.9 provide good examples of the effects of SIR and SNR.

By observing Figs. 3.8 and 3.9, one can see that there is a region of SIR where the BER will remain relatively high. As one increases SNR, the BER curves usually display "waterfall"-shaped curves, particularly at very low and at very high SIR. However, in the intermediate region, the curves are much flatter, and do not display an sharp "waterfall" shape.

The exact analytical result in (3.12) is a useful result that allows one to make many observations in the jointly optimal receiver. While one had to previously compute extensive simulations to make relevant observations, this new result in (3.12) provides an effective tool in assessing the performance of the system.

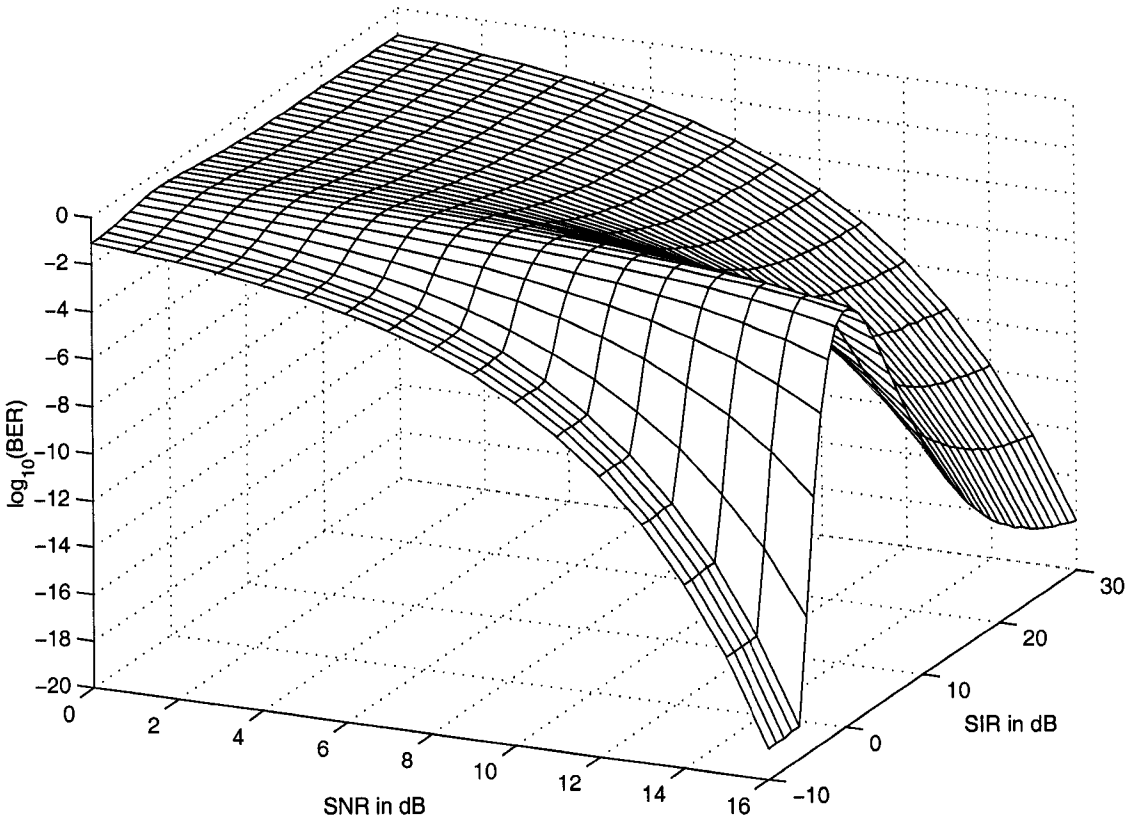

Fig. 3.8. The BER performance versus SNR and SIR, of the jointly optimal receiver, for $\theta = \pi/12$.

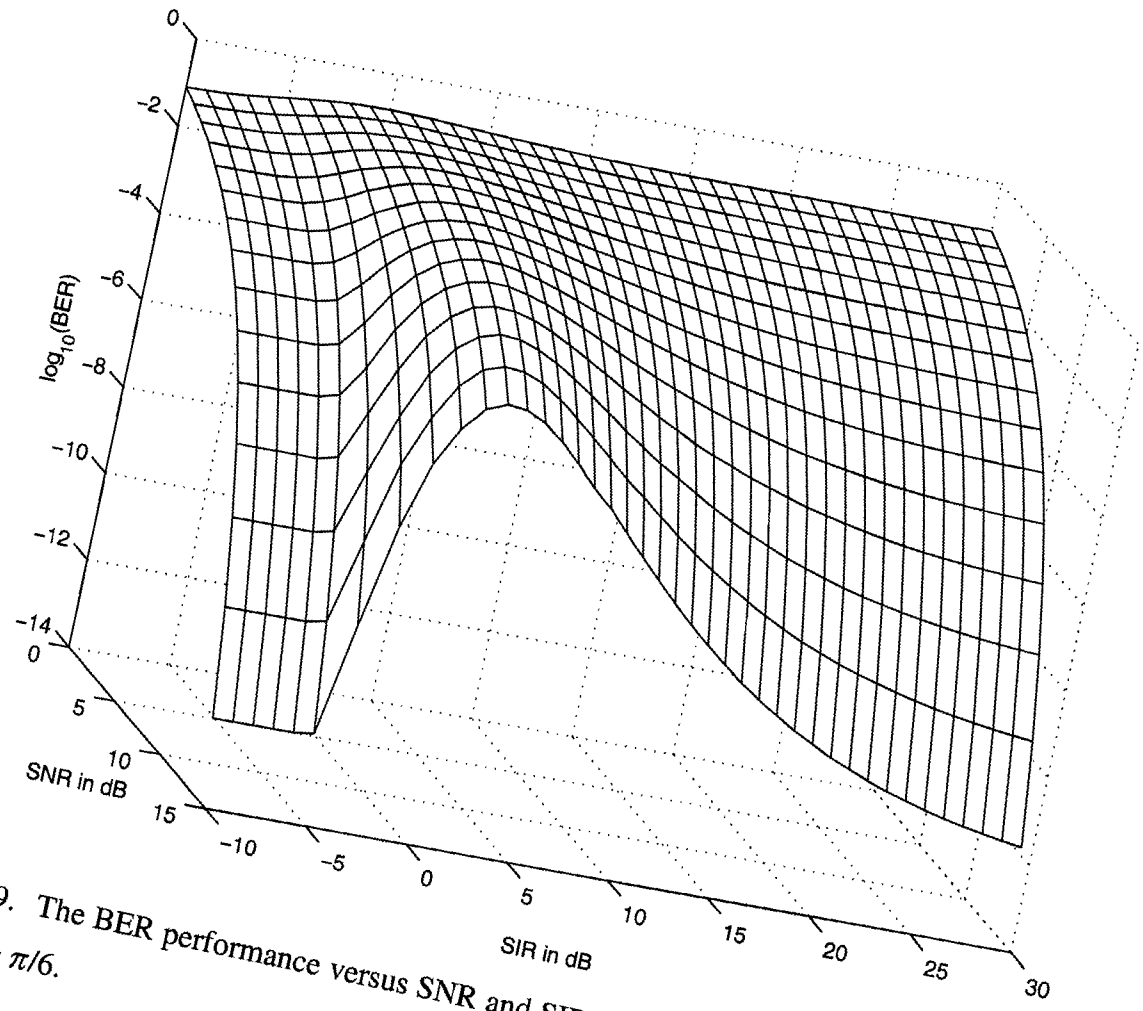

Fig. 3.9. The BER performance versus SNR and SIR, of the jointly optimal receiver, for $\theta = \pi/6$.

3.4 Bounds to the Error Rate Performance of the Jointly Optimal Receiver

The new analytical result allows one to make useful observations concerning the jointly optimal receiver. In fact, by looking at some analytical bounds to the error rate performance, one can see the power of this exact, analytical result.

Verdú [2] gives a thorough description of bounds to the jointly optimal receiver, using results from [27] and [28]. These results follow previous works by Forney [29], [30] in the investigation of error probability bounds.

In the two-user case (i.e. a desired (BPSK) signal plus one interferer), [2] shows that the b_0 error probability in the jointly optimal receiver is

$$\begin{aligned} P_{e,\,joint} &= \frac{1}{2}P[(\hat{b}_0,\hat{b}_1)=(1,0)|(b_0,b_1)=(0,0)] \\ &\quad +\frac{1}{2}P[(\hat{b}_0,\hat{b}_1)=(1,1)|(b_0,b_1)=(0,0)] \\ &\quad +\frac{1}{2}P[(\hat{b}_0,\hat{b}_1)=(1,0)|(b_0,b_1)=(0,1)] \\ &\quad +\frac{1}{2}P[(\hat{b}_0,\hat{b}_1)=(1,1)|(b_0,b_1)=(0,1)] \end{aligned} \tag{3.13}$$

where (b_0,b_1) are the input bits of the original signals, and $(\hat{b}_0,\hat{b}_1)$ are the decision bits at the output of the receiver.

One can first examine the upper bounds of this jointly optimal receiver. In [2] and [28], the two-dimensional signal space is divided into half-planes. Then, upper bounds can be evaluated so that each error probability summand in (3.13) can be upper-bounded by the probability of error of a simple binary problem. With this technique, an upper bound to the problem can be found as

$$P_{e,\,joint} \leq Q\left(\frac{A_0}{\sqrt{N_0/2}}\right)+\frac{1}{2}Q\left(\frac{\sqrt{A_0^2+A_1^2-2A_0A_1|\rho|}}{\sqrt{N_0/2}}\right) \tag{3.14}$$

where A_0 is the amplitude of the desired signal, and A_1 is the amplitude of the interferer. These signals are in the presence of an AWGN process with zero mean and double-sided

power spectral density $N_0/2$. The correlation between the desired and interfering signals is ρ. If the signals are cochannel signals and have a phase difference of θ, then $\rho = \cos\theta$. The function $Q(\cdot)$ is the Q-function (the area under the tail of a Gaussian PDF).

A lower bound to the jointly optimal receiver is also described in [2] and [29]. This lower bound is found by examining a hypothetical genie-aided receiver, which has additional side information about the transmitted bits.

As an example, suppose that a genie-aided receiver informs the receiver of the value of b_1, the interferer's bit. Since b_0, b_1, and the noise are independent, the best strategy in this genie-aided receiver is to subtract $A_1 b_1 s_1(t)$ from the received waveform $v(t)$, which gives one the single-user channel of

$$v(t) - A_1 b_1 s_1(t) = A_0 b_0 s_0(t) + \sqrt{\frac{N_0}{2}} n(t) \tag{3.15}$$

which has a minimum error probability of $Q\left(\frac{A_0}{\sqrt{N_0/2}}\right)$.

One could also have a genie-aided receiver which has information of whether bits b_0 and b_1 are equal or not, and if they are, what bits are present. This receiver then either receives full information or has to solve a binary hypothesis-testing problem. From [2], this receiver would have a probability of error of

$$P_{e,\,genie} = \frac{1}{2} Q\left(\frac{\sqrt{A_0^2 + A_1^2 - 2A_0 A_1 \rho}}{\sqrt{N_0/2}}\right). \tag{3.16}$$

Since the jointly optimal receiver has less information than these genie-aided receivers, one can thus find a minimum bound to the error rate performance P_e as

$$P_{e,\,joint} \geq \max\left\{ Q\left(\frac{A_0}{\sqrt{N_0/2}}\right), \frac{1}{2} Q\left(\frac{\sqrt{A_0^2 + A_1^2 - 2A_0 A_1 |\rho|}}{\sqrt{N_0/2}}\right)\right\}. \tag{3.17}$$

One now has enough information to compare the analytical result with these bounds to the error rate performance. By examining the effectiveness of the bounds, one can see when the exact analytical result is valuable, and when the bounds give a good approximation to the system performance.

Figs. 3.10 and 3.11 show the effects of the bounds as the SNR varies. In Fig. 3.10, where $\theta = \frac{\pi}{12}$, the lower bound is fairly tight to the exact analytical result. However, the upper bound is fairly loose, especially at SNR values less than 3 dB. In Fig. 3.11, where $\theta = \frac{5\pi}{12}$, both bounds are much more tight. This comparison shows how the value of θ can significantly affect the value of the bounds. When the desired and interferer signals are similar to one another (i.e. with a small θ), the upper bound is not tight. However, when the two signals are nearly orthogonal to one another (i.e. as θ approaches $\frac{\pi}{2}$), the bounds tighten up.

In Figs. 3.12 and 3.13, the value of θ is constant ($\theta = \frac{5\pi}{12}$), but the SIR is different in each graph. In Fig. 3.12, the SIR is -3 dB, and both the upper and lower bounds are tighter to the actual BER performance of the system. However, when the SIR increases to a level of 6 dB (in Fig. 3.13), the bounds are looser.

The bounds discussed are for a specfic correlation coefficient ρ, i.e. a specific value of θ. As previously discussed, if the signals are cochannel signals and have a phase difference of θ, then $\rho = \cos\theta$. However, it would also be useful to see these bounds with a uniformly distributed θ over the interval $[0, 2\pi)$. One can thus rewrite the bound by taking the expected value of these bounds over a uniformly distributed θ (or, alternately, over a ρ with an arcsine distribution over $[-1, 1]$ [31]), which creates an upper bound of

$$\begin{aligned} P_{e,UB1} &= \int_0^{2\pi} \frac{1}{2\pi}\left[Q\left(\frac{A_0}{\sqrt{N_0/2}}\right) + \frac{1}{2}Q\left(\frac{\sqrt{A_0^2+A_1^2-2A_0A_1|\cos\theta|}}{\sqrt{N_0/2}}\right)\right] d\theta \\ &= \int_{-1}^{1} \frac{1}{\pi\sqrt{1-\rho^2}}\left[Q\left(\frac{A_0}{\sqrt{N_0/2}}\right) + \frac{1}{2}Q\left(\frac{\sqrt{A_0^2+A_1^2-2A_0A_1|\rho|}}{\sqrt{N_0/2}}\right)\right] d\rho \\ &= Q\left(\frac{A_0}{\sqrt{N_0/2}}\right) + \int_0^1 \frac{1}{\pi\sqrt{1-\rho^2}} Q\left(\frac{\sqrt{A_0^2+A_1^2-2A_0A_1|\rho|}}{\sqrt{N_0/2}}\right) d\rho \end{aligned} \quad (3.18)$$

and a lower bound of

$$P_{e,LB} = \max\left\{Q\left(\frac{A_0}{\sqrt{N_0/2}}\right), \int_0^1 \frac{1}{\pi\sqrt{1-\rho^2}} Q\left(\frac{\sqrt{A_0^2+A_1^2-2A_0A_1|\rho|}}{\sqrt{N_0/2}}\right) d\rho\right\}. \quad (3.19)$$

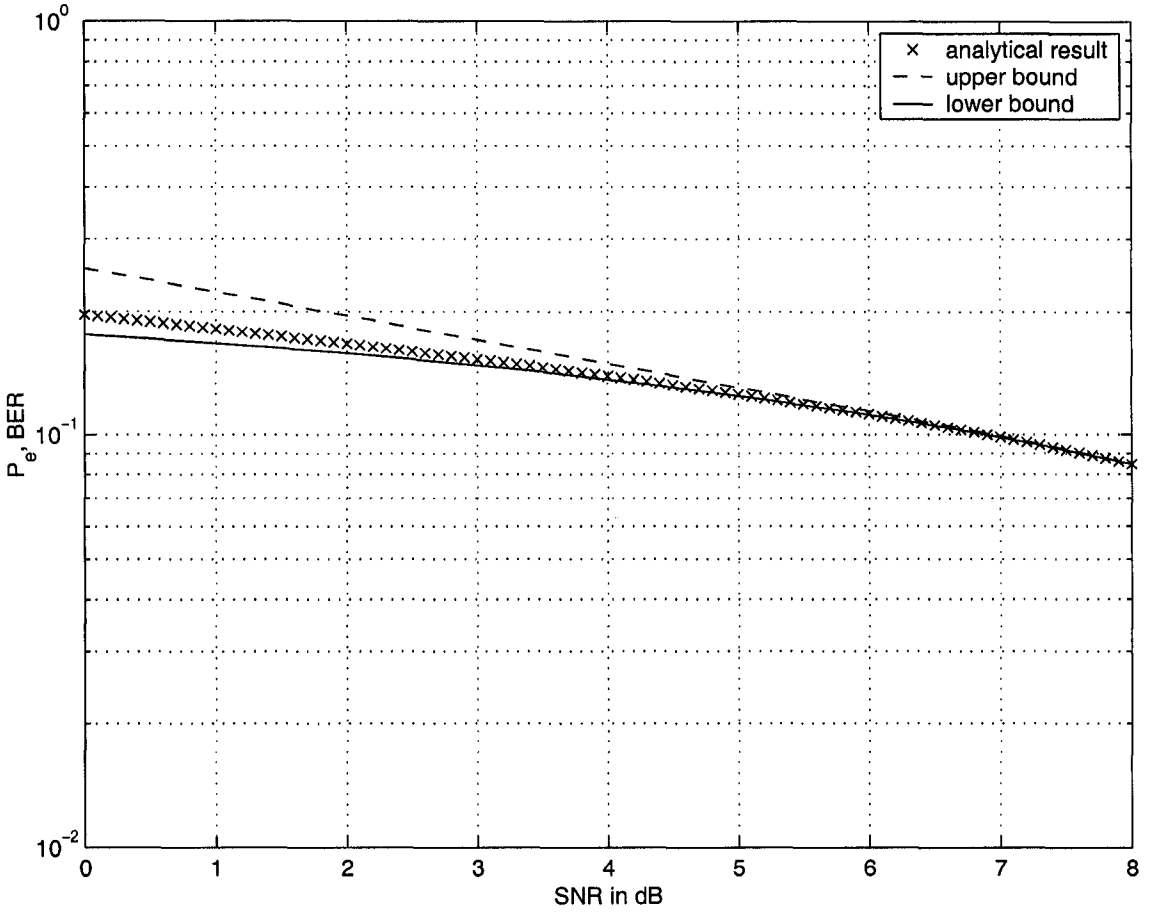

Fig. 3.10. Lower and upper BER bounds for a jointly optimal receiver for a BPSK signal plus one cochannel interferer, with Ψ = 1 dB, and $\theta = \pi/12$, along with the exact analytical result.

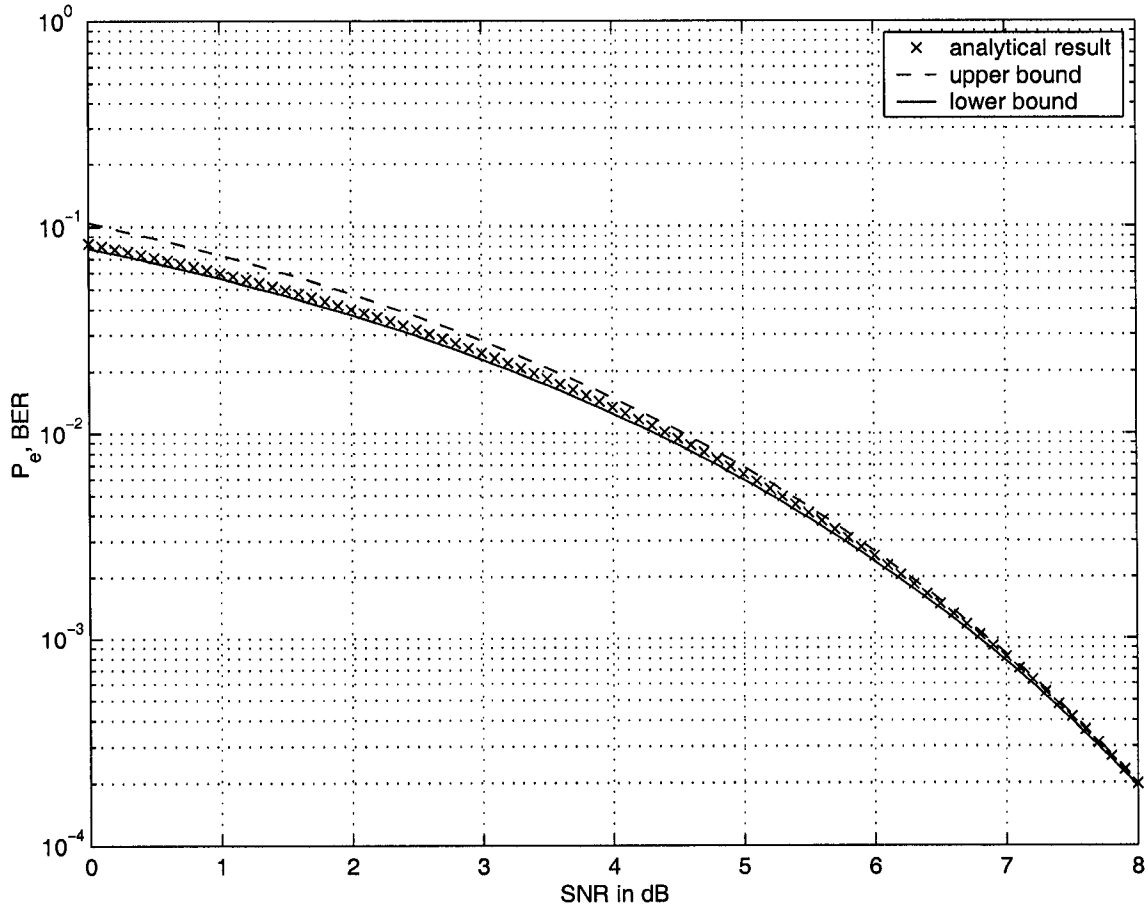

Fig. 3.11. Lower and upper BER bounds for a jointly optimal receiver for a BPSK signal plus one cochannel interferer, with Ψ = 1 dB, and $\theta = 5\pi/12$, along with the exact analytical result.

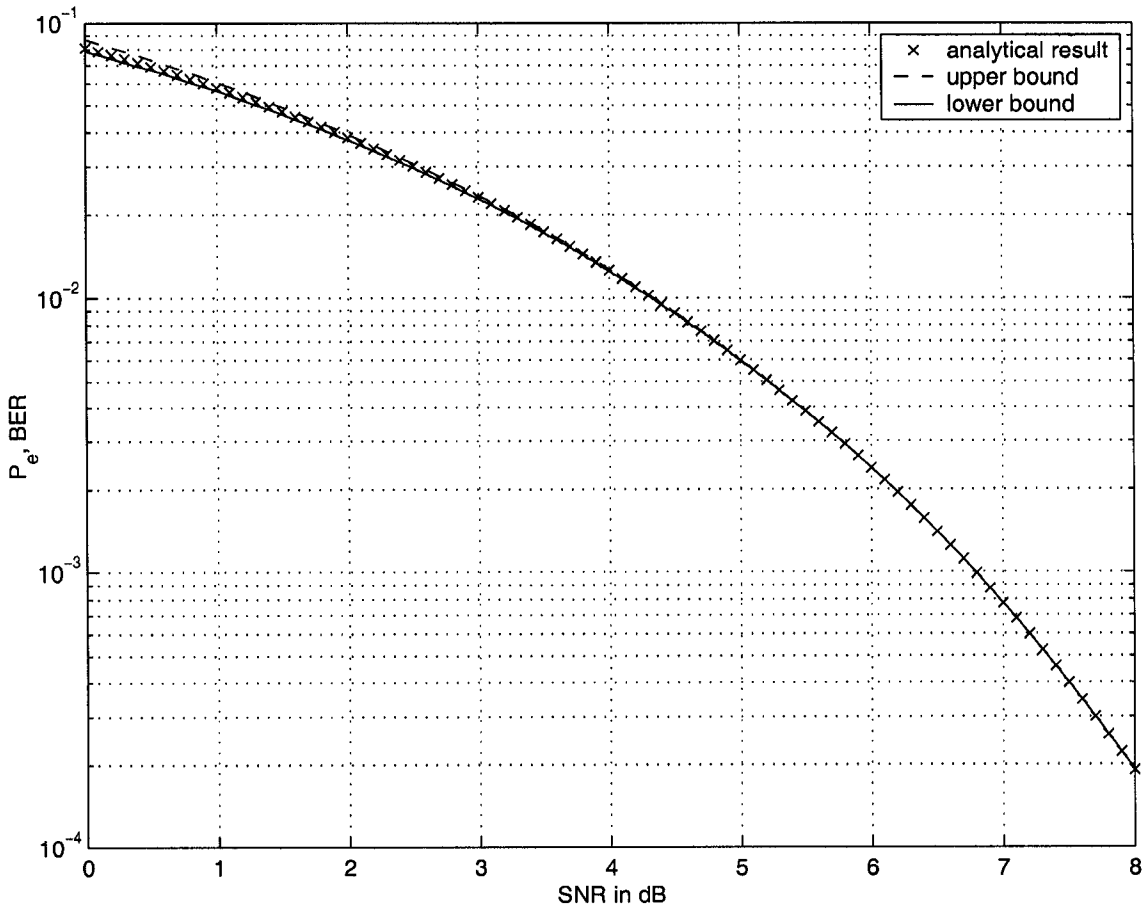

Fig. 3.12. Lower and upper BER bounds for a jointly optimal receiver for a BPSK signal plus one cochannel interferer, with $\Psi = -3$ dB, and $\theta = 5\pi/12$, along with the exact analytical result.

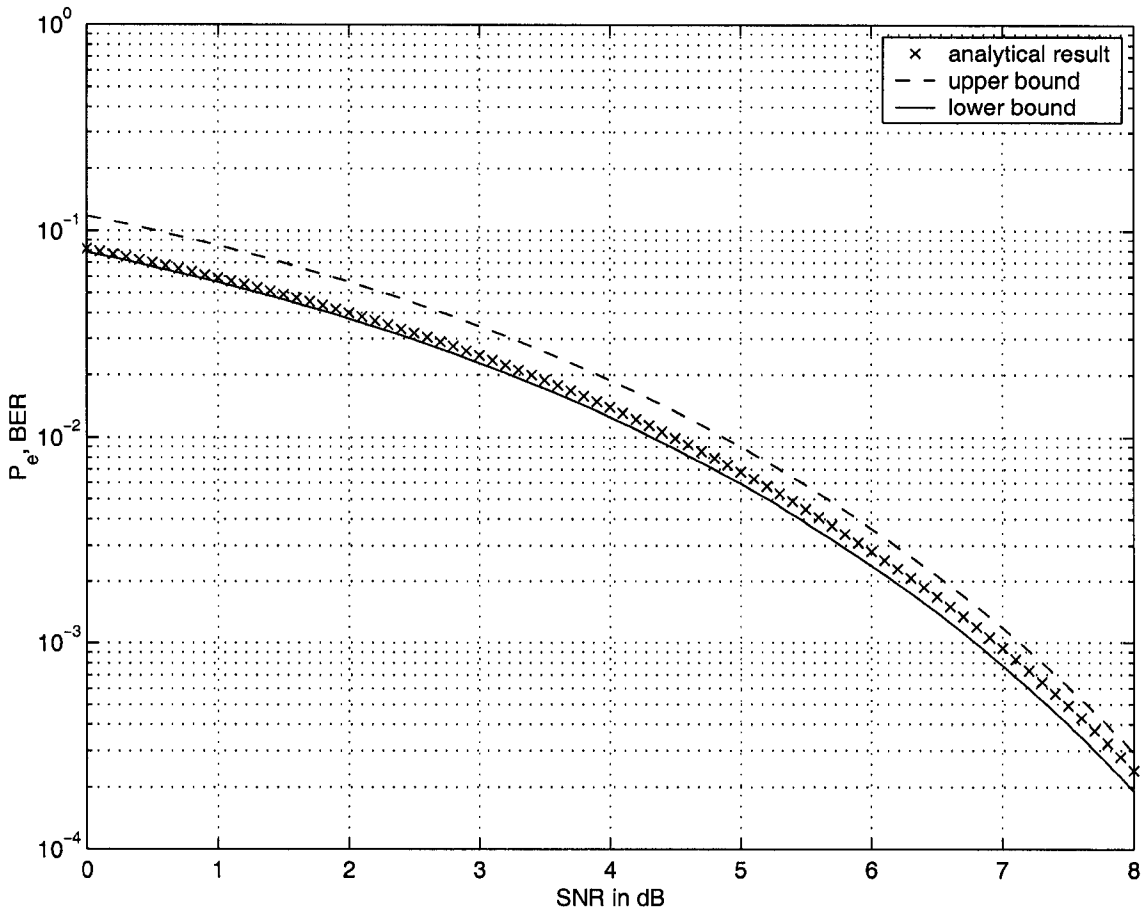

Fig. 3.13. Lower and upper BER bounds for a jointly optimal receiver for a BPSK signal plus one cochannel interferer, with Ψ = 6 dB, and $\theta = 5\pi/12$, along with the exact analytical result.

Using the bounds in (3.18) and (3.19), one can then look at the effects of the bounds with a random θ. One can see in Fig. 3.14 that with a random θ, the upper bound becomes fairly loose as the SIR increases to large levels. It can be seen from Fig. 3.14, however, that except for this high SIR region, both bounds are fairly tight.

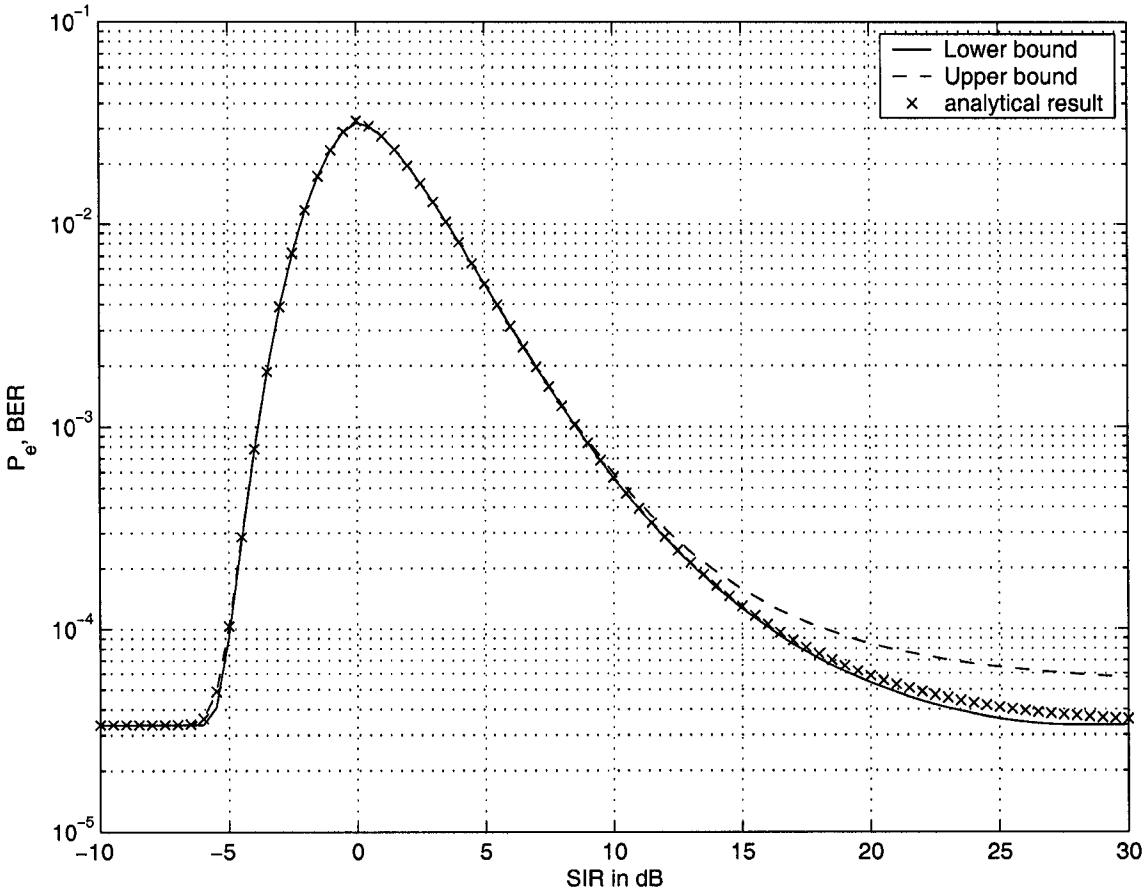

Fig. 3.14. Lower and upper BER bounds of the jointly optimal BPSK receiver with one interferer, with θ uniformly distributed over $[0, 2\pi)$, $\gamma = 9$ dB, along with the exact analytical result.

However, one can tighten the upper bound, since one knows that the jointly optimal receiver performs better than a conventional matched filter receiver. Thus, we can have another upper bound, which would be the error rate performance of a matched filter in this

system. This would create a new upper bound of

$$P_{e,UB2} = \int_0^{2\pi} \frac{1}{2\pi} \left[\frac{1}{2} Q\left(\frac{A_0 - A_1 \cos\theta}{\sqrt{N_0/2}} \right) + \frac{1}{2} Q\left(\frac{A_0 + A_1 \cos\theta}{\sqrt{N_0/2}} \right) \right] d\theta. \tag{3.20}$$

With this bound in addition to (3.18), a composite upper bound is

$$P_{e,UB} = \max\left\{ P_{e,UB1}, P_{e,UB2} \right\}. \tag{3.21}$$

The bound in (3.21) is much tighter, and does result in a more accurate upper bound for most levels of SIR, as seen in Fig. 3.15. In Fig. 3.16, one further sees how the SNR affects the tightness of the bounds. The graph shows that at most high values of SNR (i.e. greater than 6 dB), both upper and lower bounds are very tight. The bounds tend to diverge as one reaches lower values of SNR (0 to 5 dB). The upper bound is still relatively tight at these low levels of SNR, because of the additional upper bound $P_{e,UB2}$. It is stated in [2] that this particular upper bound becomes tight as the SNR approaches 0.

As a result, these 2-user bounds yield the following results:

- The lower genie bound is tight for most cases of SNR and SIR. The lower bound is slightly loose at low values of SNR, but it is still a good approximation to the derived exact analytical result.

- The original upper bound in [2] is loose for large values of SIR and small values of SNR. However, if one combines this bound with a matched filter upper bound, the upper bound is also relatively tight.

- Most importantly, both bounds are relatively tight to the derived analytical result. This gives the analytical result validity, and emphasizes the importance of the derived result. While the bounds are tight, they are not exact. This reinforces the importance of the performance analysis in this chapter.

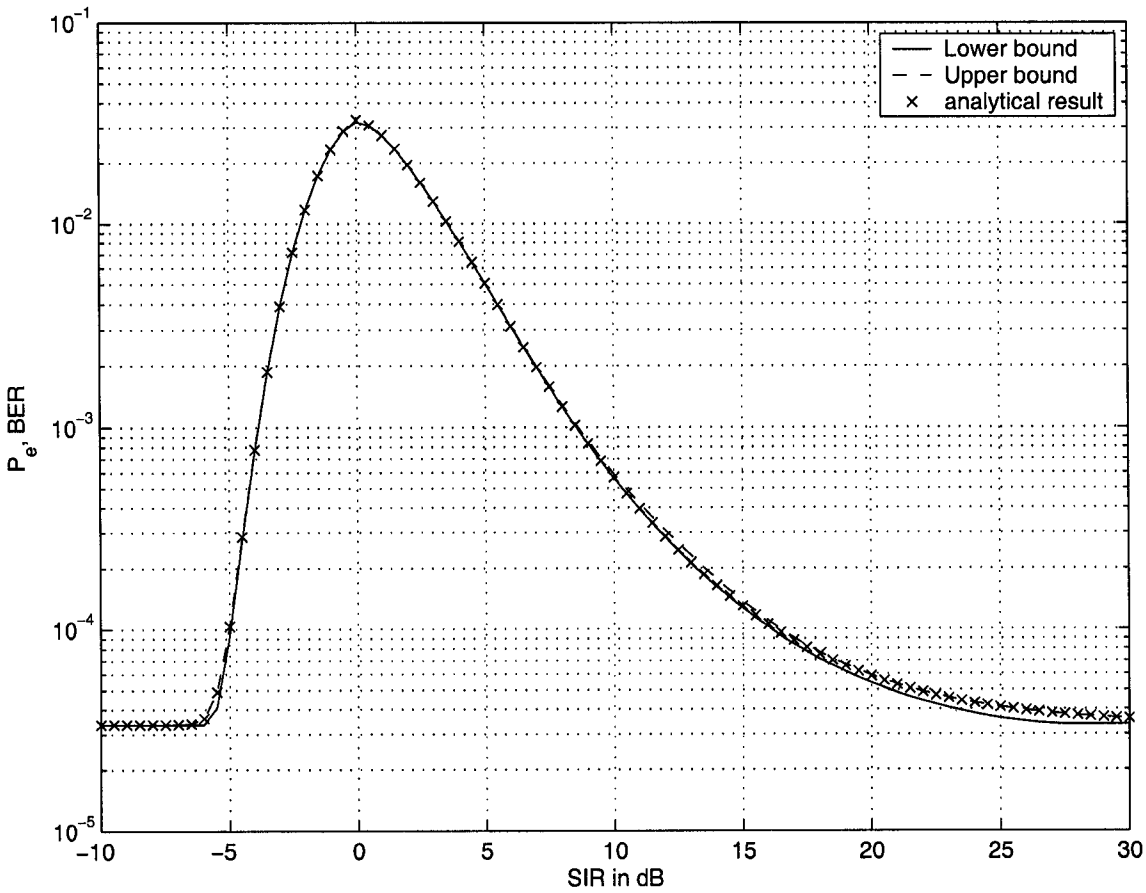

Fig. 3.15. Lower bound and composite upper bound of the BER of the jointly optimal BPSK receiver with one interferer, with θ uniformly distributed over $[0, 2\pi)$, $\gamma = 9$ dB, along with the exact analytical result.

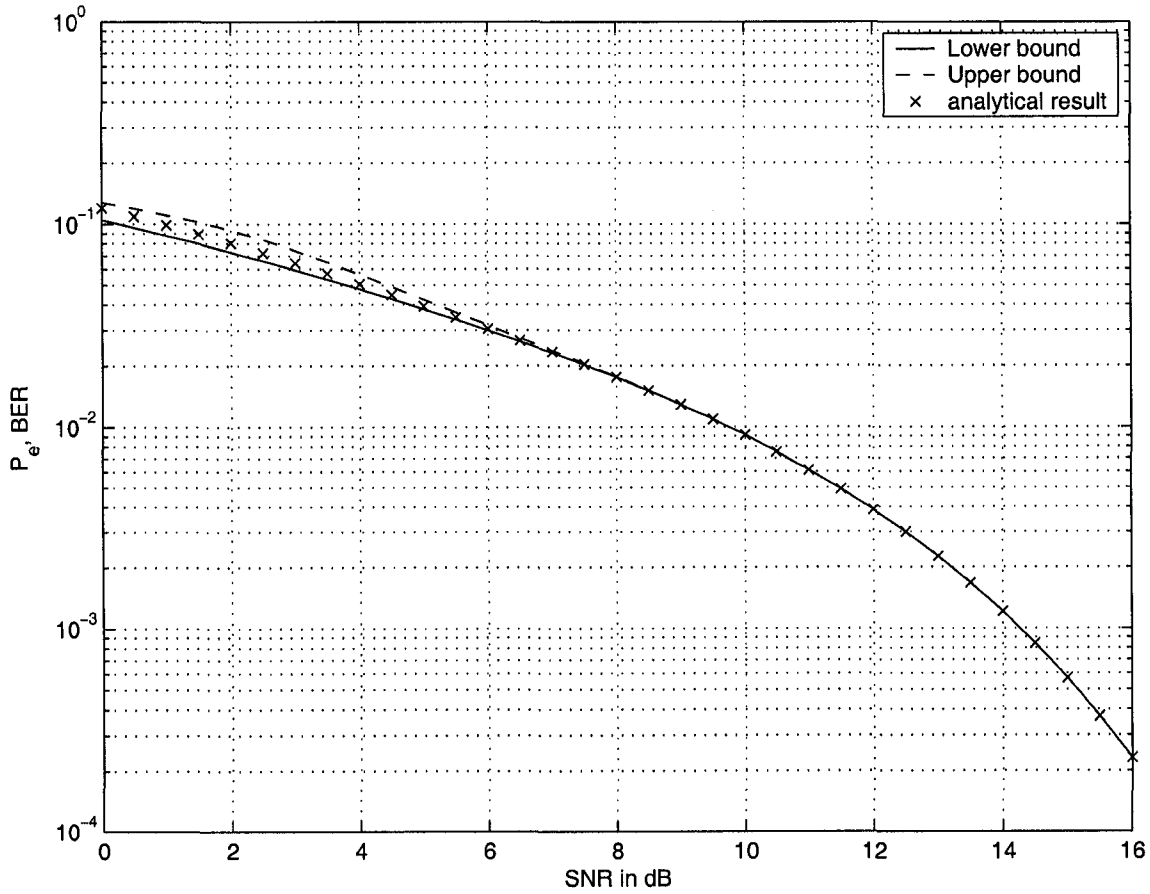

Fig. 3.16. Lower bound and composite upper bound of the BER of the jointly optimal BPSK receiver with one interferer, with θ uniformly distributed over $[0, 2\pi)$, $\Psi = 3$ dB, along with the exact analytical result.

3.5 Summary

Analytical expressions for the error rate performance were derived for a jointly optimal receiver for BPSK signals in the presence of one cochannel interferer. While simulation results were shown in [1], simulation cannot be used for some SIR and SNR values of interest. Nor can simulation be used in some system optimizations.

It is seen that an analytical solution is intricate due to the changing nature of the decision regions. In fact, the expression takes different forms, depending on specific SIR threshold levels. This result (3.9) is a tractable, exact analytical solution for the average error rate performance of a BPSK jointly optimal receiver structure for one cochannel interferer.

These results have been accepted for publication in [32] and [33]. Since these exact results are more precise than previous upper and lower bounds, the derivation in (3.9) is both useful and invaluable to the analysis of the jointly optimal receiver. Eqn. (3.9) is a powerful result that allows one to obtain the precise BER of the jointly optimal receiver, without having to perform extensive simulations.

Chapter 4

Simulating the Jointly Optimal Receiver with Importance Sampling

The case of a BPSK signal in the presence of a single interferer plus AWGN was discussed in Chapter 3. By using the derived analytical result, one can obtain the error rate performance of the the jointly optimal receiver for an arbitrary value of SNR. Thus, one can determine the error rate performance much faster than a standard Monte Carlo simulation, particularly when the BER is at a small value (such as 10^{-10}).

Nonetheless, it is useful to obtain efficient simulation techniques for small values of BER. Moreover, it is desirable to extend the study of this jointly optimal BPSK receiver to situations with multiple interferers, where theoretical results are not available. The following discussion describes how an importance sampling simulation technique can be used to efficiently achieve low BER values.

4.1 A Background to Importance Sampling

Importance sampling has been shown [34], [35] to be a useful method in reducing the computer processing time for a simulation process. In one of the key works on the subject of importance sampling [36], Shanmugan and Balaban describe the usefulness of the IS

technique and how it can be useful for communications systems. This procedure has been used in digital satellite simulations [37], and a rigorous mathematical description of the technique is found in [38].

The conventional IS technique has been modified by others in [5], [39] and [40] to achieve greater sample size savings. In addition, references [41] and [42] remark that the effectiveness of importance sampling decreases as the memory (or dimensionality) increases. This is also an important finding of [18], which is one of the key references in the following discussion.

To understand importance sampling techniques, one must first understand the background to traditional Monte Carlo simulations. Typically, communications systems are simulated using a Monte Carlo approach. Reference [43] gives a good description of Monte Carlo simulation processes. In this type of simulation, the behaviour of a physical system can be described by probability density functions (PDF's). With the known PDF's, a Monte Carlo simulation takes a random sampling from the PDF's. Multiple simulation trials are then performed, and the desired result can be found as an average over the number of observations. In practical communications systems, one can find the statistical error (the variance) in this result. With the variance, one can obtain an estimate of the number of Monte Carlo trials needed to obtain a specific error value.

Monte Carlo simulations are effective because they can be applied to general cases. These simulations can be used to analyze the effects of several disturbances to a communications system. However, one significant drawback of Monte Carlo simulations is the large number of trials needed for low error probabilities. For example, if the BER is at approximately 10^{-6}, one needs approximately 10^{7} trials per simulation run [44].

Since computing resources are finite, one desires to reduce the number of samples or trials needed to generate low error probabilities. Reference [36] describes the IS technique by biasing the trials [45]. In this biasing process, more trials are generated from the tails of the noise process. More tail samples are useful because errors are usually generated by samples in the presence of high noise. If one knows the bias associated with each noise trial, one can then unbias the error count at the output [36] , allowing one to develop an

unbiased estimate of the error probability of the system.

To understand the context of IS in communications system simulation, consider the basic baseband communication system shown in Fig. 4.1. Following the discussion in [44], suppose that the input to the system $S(t)$ has the form

$$S(t) = \sum_j a_j p(t - jT_b) \tag{4.1}$$

where $\{a_j\}$ is the input amplitude sequence, assuming values of $\pm A$ depending on whether the input bit is 0 or 1. The waveform $p(t)$ is a non-return-to-zero pulse, and T_b is the bit duration.

In the model, AWGN $n(t)$ added to the signal to form $X(t)$. The signal $X(t)$ passes through a memoryless system $h(\cdot)$ and is sampled to obtain the sequence $\{Y_k\}$.

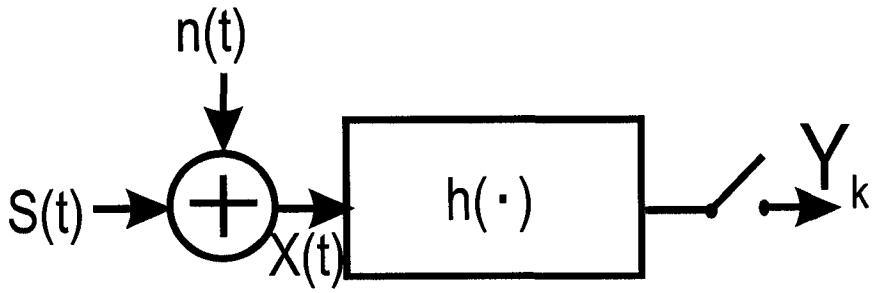

Fig. 4.1. Block diagram of baseband communications system, from [5].

To obtain the probability of the error P_e of the system, one can perform a Monte Carlo simulation. One obtains sampled values of the random processes $S(t)$ and $n(t)$ using random number generators. This forms values of $X(t)$, which generates a corresponding sampled sequence $\{Y_k\}$. The output bit is chosen by comparing $\{Y_k\}$ against some threshold. If this output bit does not match the input bit, an error is generated, and is added to a counter in the simulation program.

If one knows the output PDF $f_Y(y)$ of the system, one can obtain P_e as

$$P_e = \int_{y \in \vartheta} f_Y(y) dy \tag{4.2}$$

where ϑ is the region of y that corresponds to an error. Alternately, one can write P_e in

terms of an error counter function, $I_{\vartheta}(y)$, where

$$I_{\vartheta}(y) = \begin{cases} 1, & y \in \vartheta \\ 0, & y \notin \vartheta. \end{cases} \tag{4.3}$$

Following the discussion in [43], one can then rework (4.2) as

$$\begin{aligned} P_e &= \int_{-\infty}^{\infty} I_{\vartheta}(y) f_Y(y) dy \\ &= E[I_{\vartheta}(Y)] \end{aligned} \tag{4.4}$$

where $E[\cdot]$ is the expectation operation. It can be shown [46] that the sample mean is a natural estimator $\hat{P}_e$ of the expectation. Therefore,

$$\hat{P}_e = \frac{1}{N} \sum_{j=1}^{N} I_{\vartheta}(y_j) \tag{4.5}$$

where N is the number of trials. It can then be shown [43], [44] that the mean and variance of the Monte Carlo estimator are then

$$E(\hat{P}_e) = P_e \tag{4.6}$$

and

$$\sigma_{MC}^2 = \frac{P_e(1-P_e)}{N}. \tag{4.7}$$

Since the mean of the estimator is equal to P_e, the estimator is unbiased.

Another way to use simulation to estimate P_e is to note that if $g_Y(y)$ is another probability density function such that $f_y(y)$ is zero whenever $g_Y(y) = 0$, then one can express P_e as [47]

$$\begin{aligned} P_e &= \int_{-\infty}^{\infty} I_{\vartheta}(y) f_Y(y) dy \\ &= \int_{-\infty}^{\infty} \frac{I_{\vartheta}(y) f_Y(y)}{g_Y(y)} g_Y(y) dy \\ &= \int_{-\infty}^{\infty} I_{\vartheta}(y) W(y) g_Y(y) dy \\ &= E_g[I_{\vartheta}(y) W(y)]. \end{aligned} \tag{4.8}$$

where one defines $W(y)$, the weight of the trial y as

$$W(y) = \frac{f_Y(y)}{g_Y(y)}. \tag{4.9}$$

From (4.8), one can see that P_e can be estimated by generating values of a sequence $\{Y_j\}$ that has a density function $g_Y(y)$, and then by using as an estimator the average of the values of $I_\vartheta(y)W(y)$. When a density function $g_Y(y)$ is chosen such that the random variable $I_\vartheta(y)W(y)$ has a small variance, this "importance sampling" technique can result in an efficient estimator of P_e [47].

Since (4.8) is the same as (4.4), this estimator is also unbiased. From [43], the variance is found by

$$\sigma_{IS}^2 = \frac{\int_{-\infty}^{\infty} I_\vartheta(y) f_Y(y) W(y) dy - P_e^2}{N}. \tag{4.10}$$

In the importance sampling technique, one chooses $g_Y(y)$ such that $f_Y(y) < g_Y(y)$ for all $y \in \vartheta$. This action causes more errors in the simulation. However, each error will be counted with a weight of $W(y)$ for the unbiased result. As shown in [44], this can result in a sample size reduction of

$$\gamma_{samples} = \frac{\sigma_{MC}^2}{\sigma_{IS}^2} = \frac{P_e(1-P_e)}{\int_{-\infty}^{\infty} I_\vartheta(y) f_Y(y) W(y) dy - P_e^2}. \tag{4.11}$$

There are a number of practical difficulties with importance sampling. Firstly, in multi-dimensional cases, it may be difficult to analytically compute $I_\vartheta(y)$, $f_Y(y)$, or $W(y)$. Furthermore, when counting the errors in importance sampling, one needs to compute the weight $W(y)$ for each and every error. This increased computation may lead to increased time to determine the estimation of the error. Finally, in certain communications systems, if P_e is the quantity to be estimated, the boundaries for the error region in signal space may not be actually known. This uncertainty may cause difficulties in choosing a properly biased $g_Y(y)$ to create more error samples.

Thus, it is important to use importance sampling with care. The time savings in simulation using IS techniques can be significant. For efficient simulations, however, one needs to properly bias the noise PDF's and efficiently compute the weight $W(y)$. By using an effective IS technique, one can greatly reduce the sample variance and create quick and effective simulations.

4.2 Importance Sampling in 2-Dimensional Space

When a BPSK signal is in the presence of a cochannel interferer, one can project the resulting signal constellation as four points in a two-dimensional plane. Two-dimensional AWGN is then added to the signal, which can then be detected in the jointly optimal receiver.

Consider two orthogonal axes x and y in signal space. One can then consider the input noise with the joint Gaussian density of

$$f_{x,y}(x,y) = \frac{1}{2\pi}\exp\left(-\frac{x^2+y^2}{2}\right) \tag{4.12}$$

where one is assuming that $\sigma^2 = 1$. A 3-dimensional representation of this joint PDF is shown in Fig. 4.2.

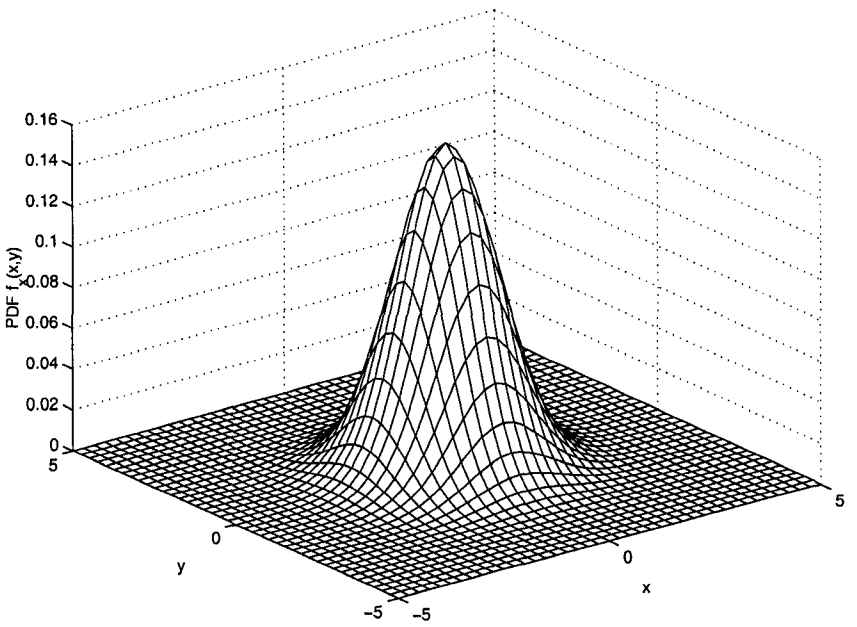

Fig. 4.2. Three-dimensional representation of the jointly Gaussian PDF (versus x and y, from (4.12)), with σ=1.

Following the derivation of the mean and variance in Section 4.1 and in [44], one can derive the estimator for the bit error of the desired 2-dimensional signal. The probability

of bit error is now

$$P_e = \int_{y \in \vartheta} f_{x,y}(x,y)dydx \tag{4.13}$$

where ϑ is the region in signal space that corresponds to an error. Again, one can write P_e in terms of an error counter function, $I_\vartheta(x,y)$, where

$$I_\vartheta(y) = \begin{cases} 1, & (x,y) \in \vartheta \\ 0, & (x,y) \notin \vartheta. \end{cases} \tag{4.14}$$

As in Section 4.1, one can choose another PDF $g_{x,y}(x,y)$ such that the variance of the new estimator is smaller than that of the direct Monte Carlo method. Then, one has

$$\begin{aligned} P_e &= \int_{-\infty}^{\infty} I_\vartheta(x,y) f_{x,y}(x,y)dydx \\ &= \int_{-\infty}^{\infty} \frac{I_\vartheta(x,y) f_{x,y}(x,y)}{g_{x,y}(x,y)} g_{x,y}(x,y)dydx \\ &= \int_{-\infty}^{\infty} I_\vartheta(x,y) W(x,y) g_{x,y}(x,y)dy \\ &= E_g[I_\vartheta(x,y)W(x,y)] \end{aligned} \tag{4.15}$$

where one now defines a two-dimensional weight $W(x,y)$ as

$$W(x,y) = \frac{f_{x,y}(x,y)}{g_{x,y}(x,y)}. \tag{4.16}$$

An appropriate estimator for the bit error rate of the desired BPSK signal is then

$$\hat{P}_e = \frac{1}{N} \sum_{j=1}^{N} I_\vartheta(x_j,y_j) W(x_j,y_j). \tag{4.17}$$

Reference [44] describes the fact that the estimator is unbiased, since

$$\begin{aligned} E[\hat{P}_e] &= \frac{1}{N} \sum_{j=1}^{N} \int\int_{\vartheta} f_{x,y}(x,y)dydx \\ &= P_e. \end{aligned} \tag{4.18}$$

The variance of the estimator is also shown in [44] as

$$\sigma_{IS}^2 = \frac{1}{N} \int\int_{\vartheta} f_{x,y}(x,y)[W(x,y) - P_e]dydx \tag{4.19}$$

and the sample size reduction factor $\gamma_{samples}$ is

$$\gamma_{samples} = \frac{P_e(1-P_e)}{(\int\int_{\vartheta} f_{x,y}(x,y)W(x,y)dydx) - P_e^2}. \tag{4.20}$$

Thus, one wishes to appropriately bias a PDF $g_{x,y}(x,y)$ such that more error samples occur at the tails. As an example, consider the biased PDF of

$$g_{x,y}(x,y) = g(x)g(y) \tag{4.21}$$

where [44]

$$g(x) = \begin{cases} \frac{1}{k\sqrt{2\pi}} \exp\left(-\frac{x^2}{2}\right), & |x| \geq D \\ 2\frac{Q(\sqrt{D^2-x^2})}{k} \frac{1}{\sqrt{2\pi}} \exp\left(-\frac{x^2}{2}\right), & |x| < D \end{cases} \tag{4.22}$$

where

$$k = \exp\left(-\frac{D^2}{2}\right) \tag{4.23}$$

and D is a parameter that controls the degree of biasing of the PDF.

Reference [44] investigates the effectiveness of this biased PDF for importance sampling purposes. However, Beaulieu, Biglieri, and Lai [18] develop a more effective PDF for importance sampling using [48]. Consider the Box-Muller method [49] for generating two independent Gaussian random variables. This transformation yields two independent Gaussian random variables

$$X_1 = \sqrt{-2\ln U_1}\cos(2\pi U_2) \tag{4.24a}$$

$$Y_1 = \sqrt{-2\ln U_1}\sin(2\pi U_2) \tag{4.24b}$$

where U_1 and U_2 are uniformly distributed random variables over the interval (0,1).

By considering the joint PDF created by the two random variables X_1 and Y_1, reference [18] introduces an useful technique to create a hole in the joint PDF. One can now generate two new random variables X and Y, according to

$$X = \sqrt{-2\ln(kU_1)}\cos(2\pi U_2) \tag{4.25a}$$

$$Y = \sqrt{-2\ln(kU_1)}\sin(2\pi U_2) \tag{4.25b}$$

where

$$k = \exp\left(-\frac{R^2}{2}\right), \tag{4.26}$$

where the parameter R can be used to control the degree of the biasing of the generated noise samples.

Through the results of (4.25a) and (4.25b), one would then obtain a 2-dimensional joint PDF with a hole in the middle. Reference [44] describes the joint PDF of the random variables X and Y as

$$f_{x,y}(x,y) = \begin{cases} \frac{1}{k}\frac{1}{2\pi}\exp\left(-\frac{x^2+y^2}{2}\right), & x^2+y^2 \geq R^2 \\ 0, & x^2+y^2 < R^2 \end{cases} \tag{4.27}$$

where R is the same parameter as in (4.26). This parameter can be used to create the radius of the "displaced mass" from the original joint Gaussian PDF.

The results of [18] are worth emphasizing. Consider a basic scatterplot of trials generated from the joint PDF in Fig. 4.2. If we project these trials on a basic orthogonal set of x and y axes, one can have the plot of Fig. 4.3.

Now consider a slice of the joint PDF from Fig. 4.2 along the z-plane at $y = 0$. If one made a similar slice of the joint PDF of (4.27), one would have the result of Fig. 4.4. By examining the slices of these PDF's, one can clearly see that the centre mass has been redistributed to the tails of the joint PDF. This mass redistribution restricts sample points to areas outside the circle of radius R. A scatterplot of this resulting PDF is shown in Fig. 4.5, clearly depicting the exclusion of trials inside the hole of radius R.

Reference [18] further describes that the weighting function is undefined whenever one is within the radius R:

$$W(x,y) = \begin{cases} k, & x^2+y^2 \geq R^2 \\ \text{undefined}, & x^2+y^2 < R^2. \end{cases} \tag{4.28}$$

Eqn. (4.28) is undefined within R because sample points never occur in that region. This is an important fact; it is thus important that the region of integration ϑ lies outside the disk if the estimator is to be unbiased.

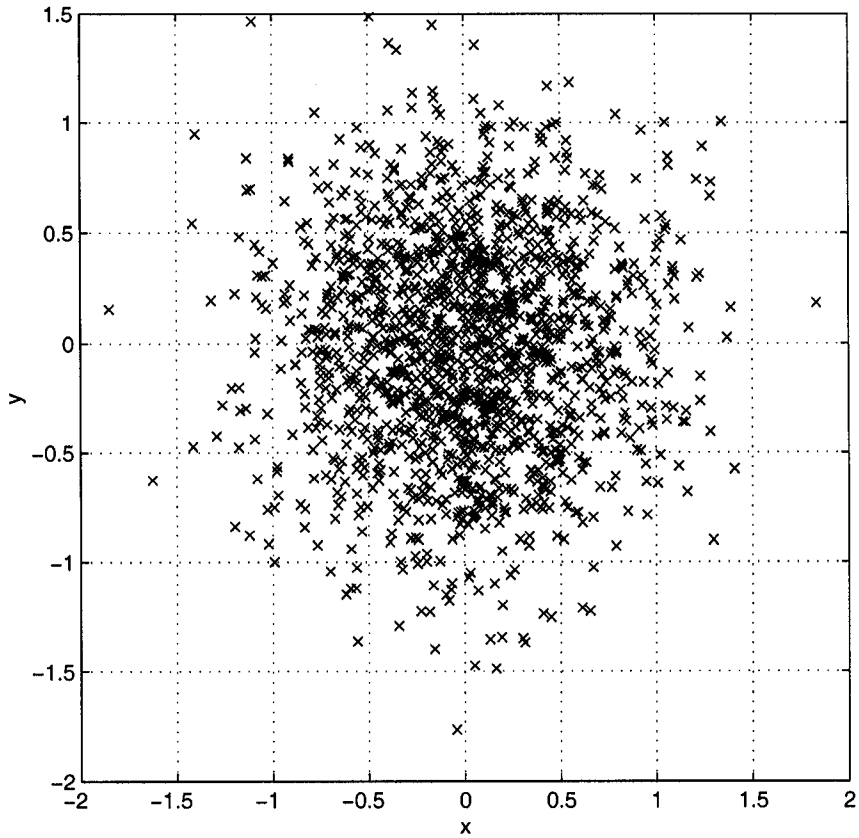

Fig. 4.3. Scatterplot of 2-dimensional Gaussian noise simulation (with N=1500, and σ = 1), centered at the origin.

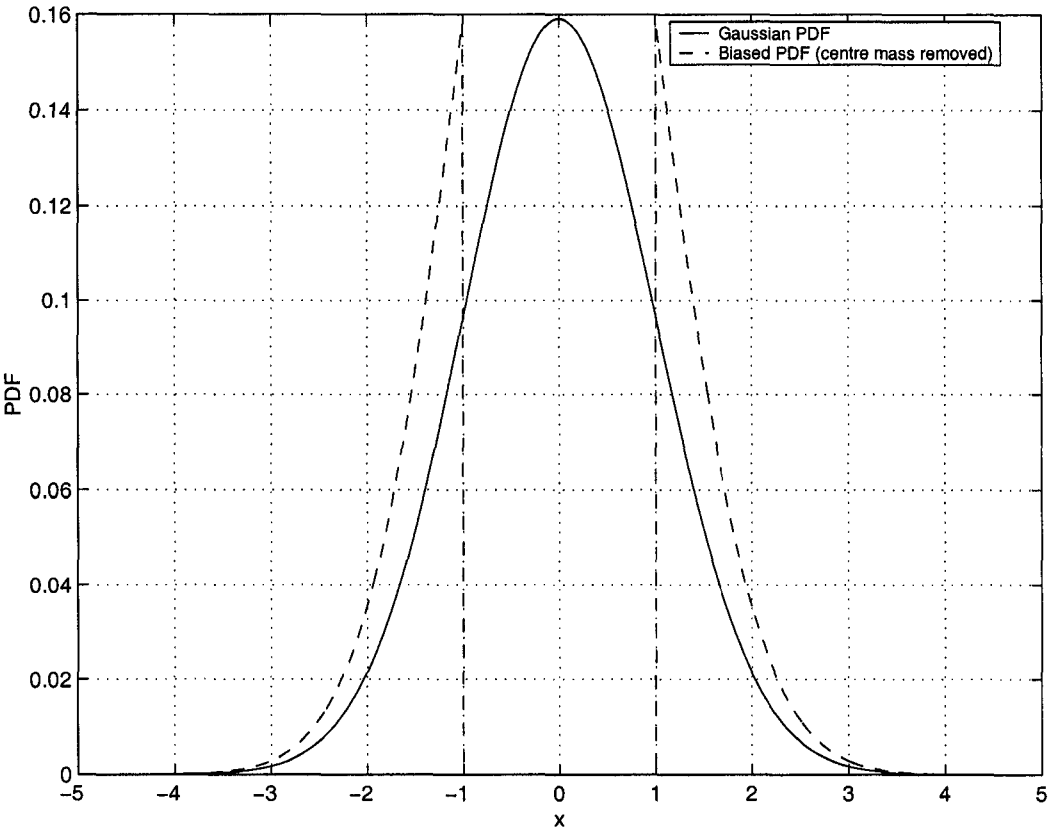

Fig. 4.4. Slice of 2-dimensional joint Gaussian PDF, from (4.12), and the biased PDF from (4.27), with y=0, σ=1, and R=1.

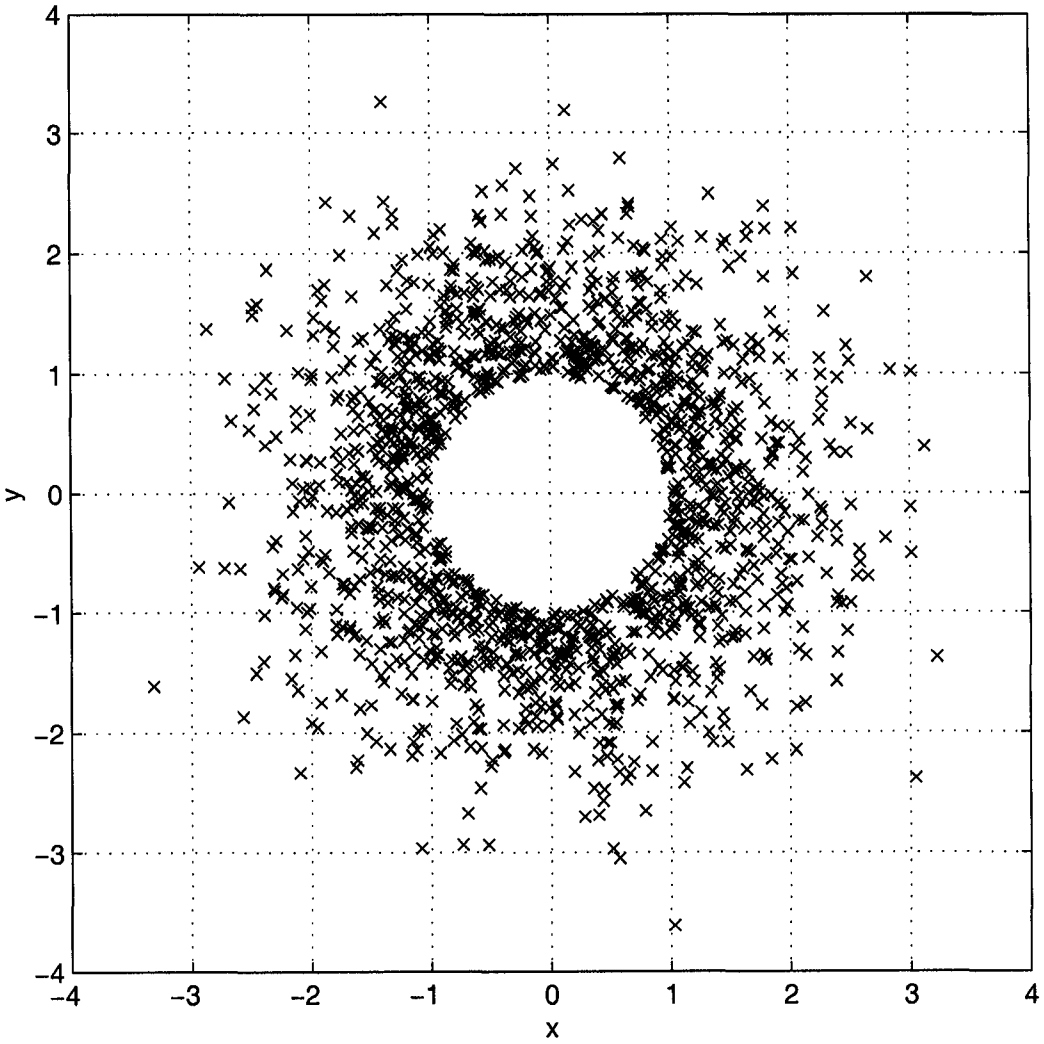

Fig. 4.5. Scatterplot of biased noise simulation, using the PDF in (4.27), centered at the origin, with N=1500, and R=1.

Let d be the minimum distance from the signal point to the decision boundary. Reference [18] shows that the variance of the estimator is minimized when k is minimized. Because of this fact, [44] describes that *the smallest variance occurs when R is set equal to the threshold distance d.*

Therefore, it is desirable to set the noise sample points greater than a radius d away from the signal points (since no errors occur when the radius is less than d). Using this distance, one minimizes the variance and appropriately biases the PDF's so that one can achieve low-BER simulations. An example of this effect with a two-point orthogonal signal constellation is shown in Fig. 4.6. In this Figure, the noise points are distributed so that they lie beyond a distance d. This creates more sample points in the error region, and by counting each error sample with weight k, one can obtain very low BER's.

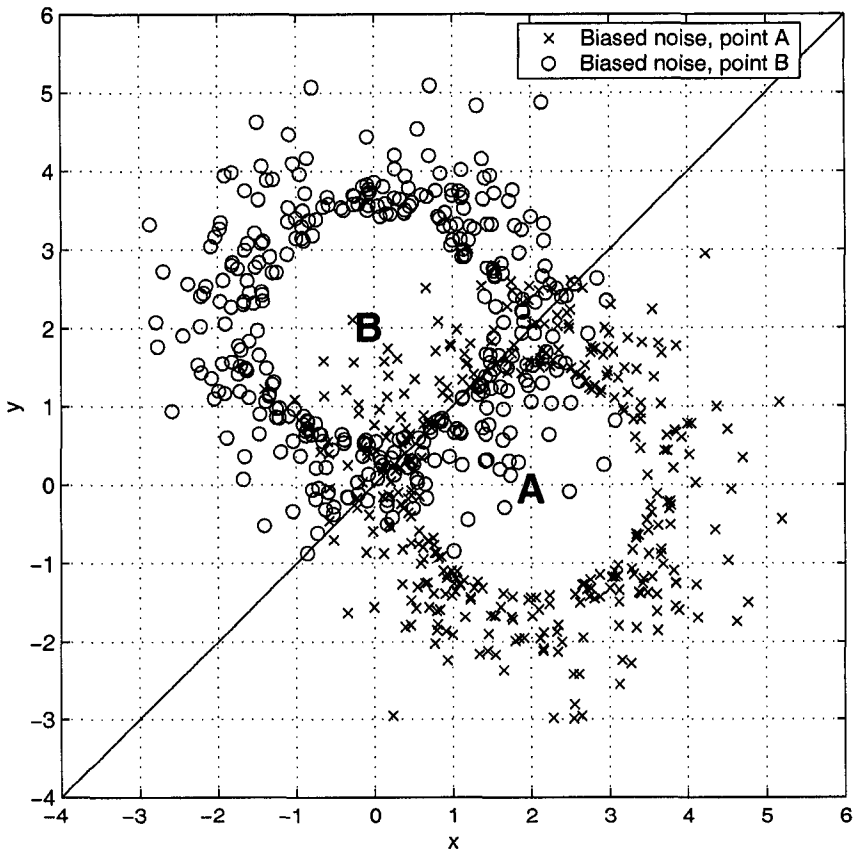

Fig. 4.6. Scatterplot simulation points of 2-dimensional biased Gaussian noise for 2 points centered at A and B, with a straight line decision boundary, with N=350, and $R = d$.

By using an importance sampling technique in 2-dimensional signal space, one now has a method to efficiently simulate the jointly optimal BPSK receiver. This powerful technique will reduce simulation time and allow one to extend the simulation to small levels of BER.

4.3 Importance Sampling and the Jointly Optimal 2-User Receiver

The technique developed in Section 4.2 will allow one to obtain accurate simulations for the jointly optimal 2-user receiver. The basic method for the simulation follows:

- For N number of points, a uniformly distributed random variable between 0 and 1 is created by a random number generator. If the random variable is less than 0.5, one assigns the input bit b_0 to the BPSK signal as "0". Otherwise, b_0 is "1".
- The process above is repeated for b_1, the interferer's bit.
- If the phase difference θ is random, N uniformly random θ values in the interval [0, 2π) are created.
- Based on the values of SNR, SIR, and theta, the signal constellation points from Chapter 2 are calculated for the orthogonal axes for $\phi_0(t)$ and $\phi_1(t)$, i.e.

$$y_1(t) = \left(A_0 + A_1 \cos\theta\right)\phi_0(t) + \left(A_1 \sin\theta\right)\phi_1(t) \tag{4.29a}$$

$$y_2(t) = \left(A_0 - A_1 \cos\theta\right)\phi_0(t) - \left(A_1 \sin\theta\right)\phi_1(t) \tag{4.29b}$$

$$y_3(t) = -\left(A_0 - A_1 \cos\theta\right)\phi_0(t) + \left(A_1 \sin\theta\right)\phi_1(t) \tag{4.29c}$$

$$y_4(t) = -\left(A_0 + A_1 \cos\theta\right)\phi_0(t) - \left(A_1 \sin\theta\right)\phi_1(t). \tag{4.29d}$$

- Consider the constellation point $(b_0, b_1) = (1,0)$ (i.e. the "desired" bit is equal to "1"). One will then calculate the distance between these points and each of $(b_0, b_1) = (0,0)$ and (0,1). The smallest distance determines the decision boundary. The threshold

length $d_{(1,0)}$ is equal to half this distance, as shown in Fig. 4.7. This process is repeated for $(b_0, b_1) = (1,1)$ to find $d_{(1,1)}$. One does not have to repeat the process for either of $(b_0, b_1) = (0,0)$ or $(0,1)$, since the problem has symmetry. That is, the decision regions for points $(b_0, b_1) = (0,0)$ and $(0,1)$ are mirror images of those for points $(b_0, b_1) = (1,0)$ and $(1,1)$. With this knowledge, one reduces the number of simulation samples required.

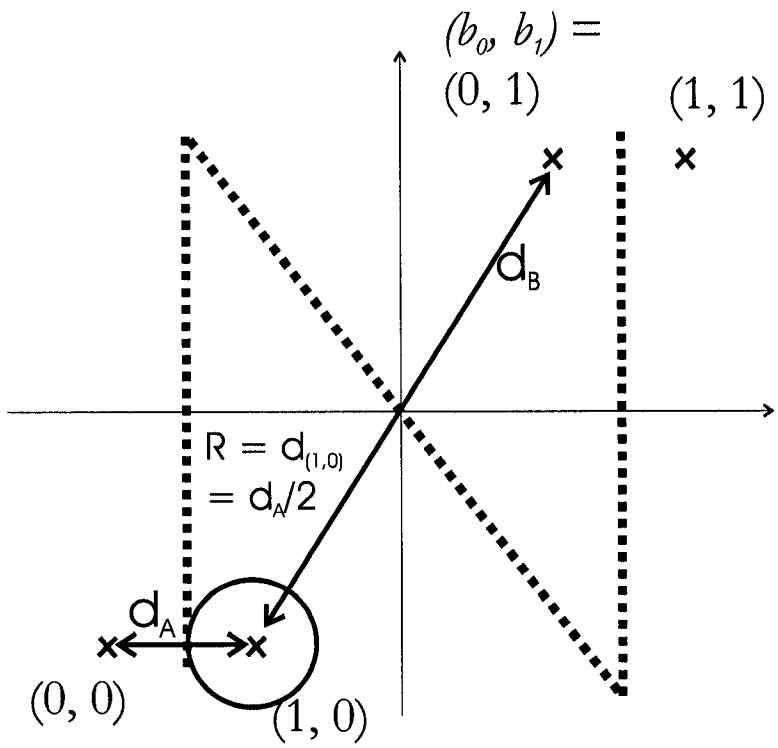

Fig. 4.7. Constellation points and decision boundary calculation (dotted line) for a jointly optimal BPSK receiver for 2 users. The value of R (in this case, $d_{(1,0)}$) is also shown.

- Using $d_{(1,0)}$ and $d_{(1,1)}$, one can calculate a corresponding $k_{(1,0)}$ and $k_{(1,1)}$ from (4.26).
- The values of $k_{(1,0)}$ and $k_{(1,1)}$ are then used with (4.25a) and (4.25b) to create biased noise trials. The resulting signal plus noise constellation points are (v_0, v_1).
- The jointly optimal receiver decodes the point by determining the closest (b_0, b_1) point to (v_0, v_1). The bit $\hat{b}_0$ is chosen based on this operation. If $\hat{b}_0 \neq b_0$, an error

occurs.

- Because the original PDF was biased, every error is counted with a weight $W(x,y)$ (4.28). The weight $W(x,y)$ is either $k_{(1,0)}$ or $k_{(1,1)}$, depending on the original PDF.
- The weighted errors are counted, and are then divided by N to yield the estimate of the BER of the jointly optimal receiver.

Importance sampling results in tremendous time savings when simulating the results for the jointly optimal receiver. In a tradtional Monte Carlo process, one needs to sample 10^{15} to 10^{16} points to simulate BER's of the order of 10^{-14}. With importance sampling, one can have many orders of magnitude fewer samples to achieve the same BER's with similar variance.

It is important to verify this simulation technique with known results. Since Chapter 3 determined an exact analytical result, one can compare the results of IS simulations with the analytical formulae in Chapter 3. The results are shown in Fig. 4.8. Relatively large values of SNR are used in the simulation (10 dB, 12 dB, and 14 dB), and yet one is still able to simulate BER's of 10^{-12}. As in Chapter 3, the curves asymptotically reach the BER value of a single BPSK signal in AWGN. Fig. 4.8 shows that the IS simulation works well, matching the curves obtained by analytical expressions.

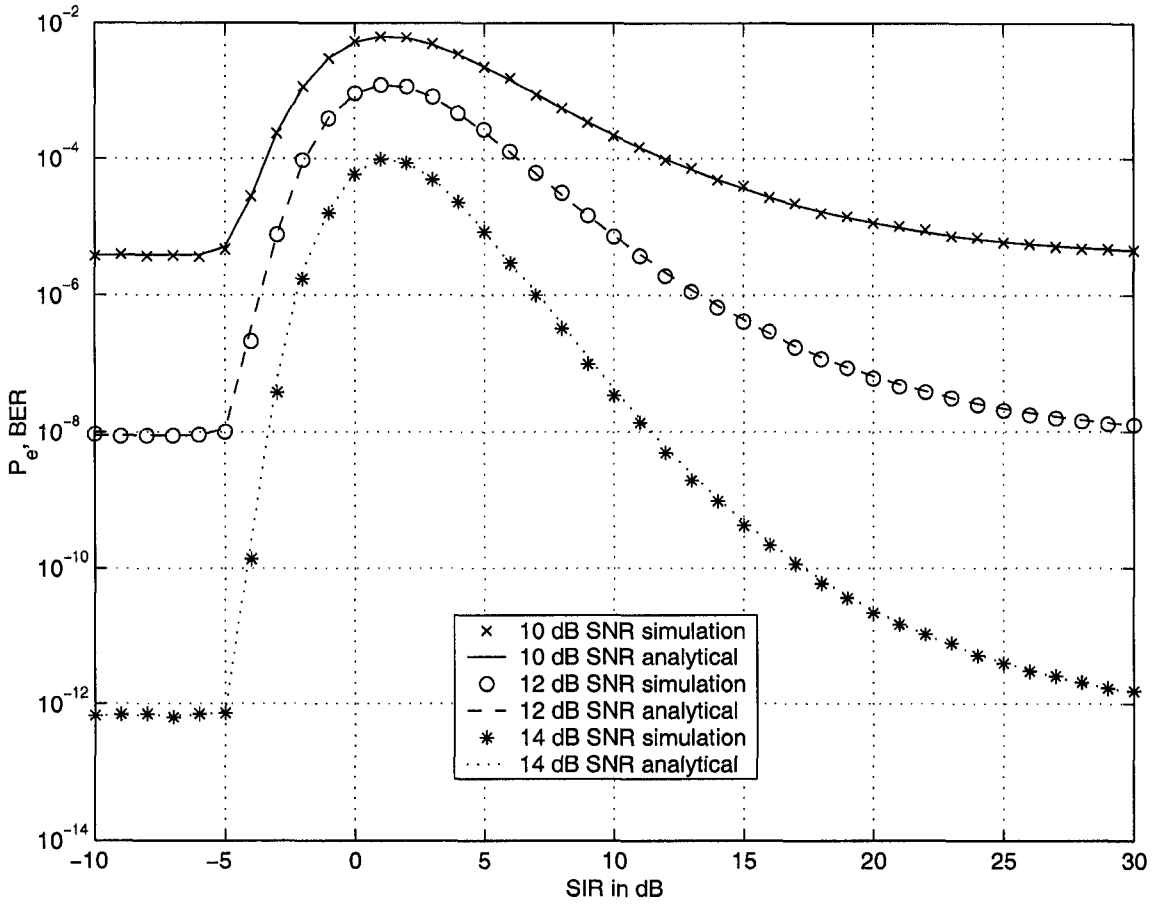

Fig. 4.8. The BER performance versus SIR of a jointly optimal receiver for a BPSK signal plus one interferer, determined by analysis and IS simulations, with $\theta=\pi/6$.

This importance sampling technique also allows one to see how the BER changes in relation to a non-random θ. While these changes could have been observed using the analytical method from Chapter 3, a quick simulation technique is also useful. Figs. 4.9 and 4.10 demonstrate how the error rate curve changes according to θ. In Fig. 4.9, one sees that as θ approaches zero, the SIR bump in the error rate curve increases significantly. Conversely, as θ approaches $\frac{\pi}{2}$, the curve flattens out. This is intuitively correct, as when the BPSK signals differ by a value of $\frac{\pi}{2}$, the signals' orthogonality makes it easier to detect the desired signal.

The effect of a changing θ is also seen in Fig 4.10. This Figure shows that as θ approaches $\frac{\pi}{2}$, the SNR curve approaches that of a single BPSK signal in AWGN. However, as θ approaches zero, the error rate performance does not decrease as sharply.

Importance sampling has a significant effect on the simulation of the jointly optimal BPSK receiver. Moreover, this simulation technique reinforces the analytical results of Chapter 3. In the case of a desired signal plus one interferer, the simulation time savings are large. One can achieve low BER's with small variances. This allows the technique to apply to many values of SNR, SIR, and θ, which reinforces the power of the IS procedure.

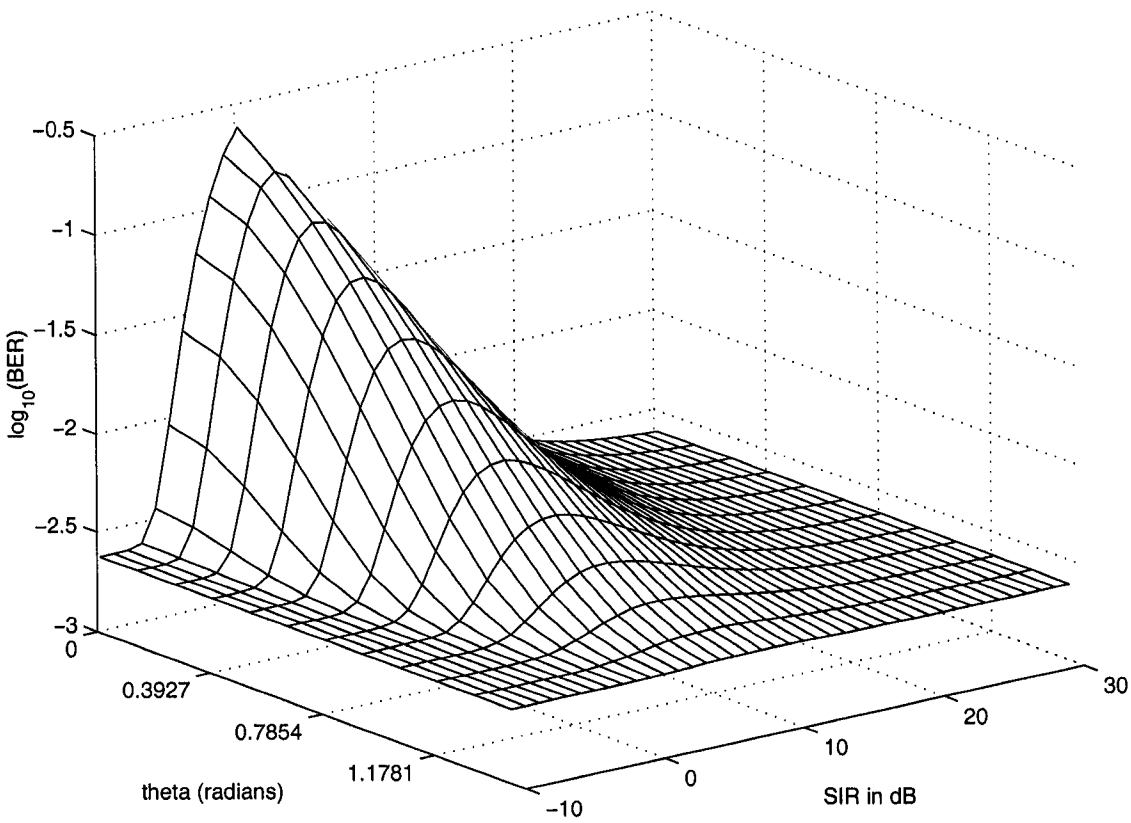

Fig. 4.9. Error rate performance versus θ and SIR, of the jointly optimal receiver for a BPSK signal plus one interferer, with $\gamma = 6$ dB.

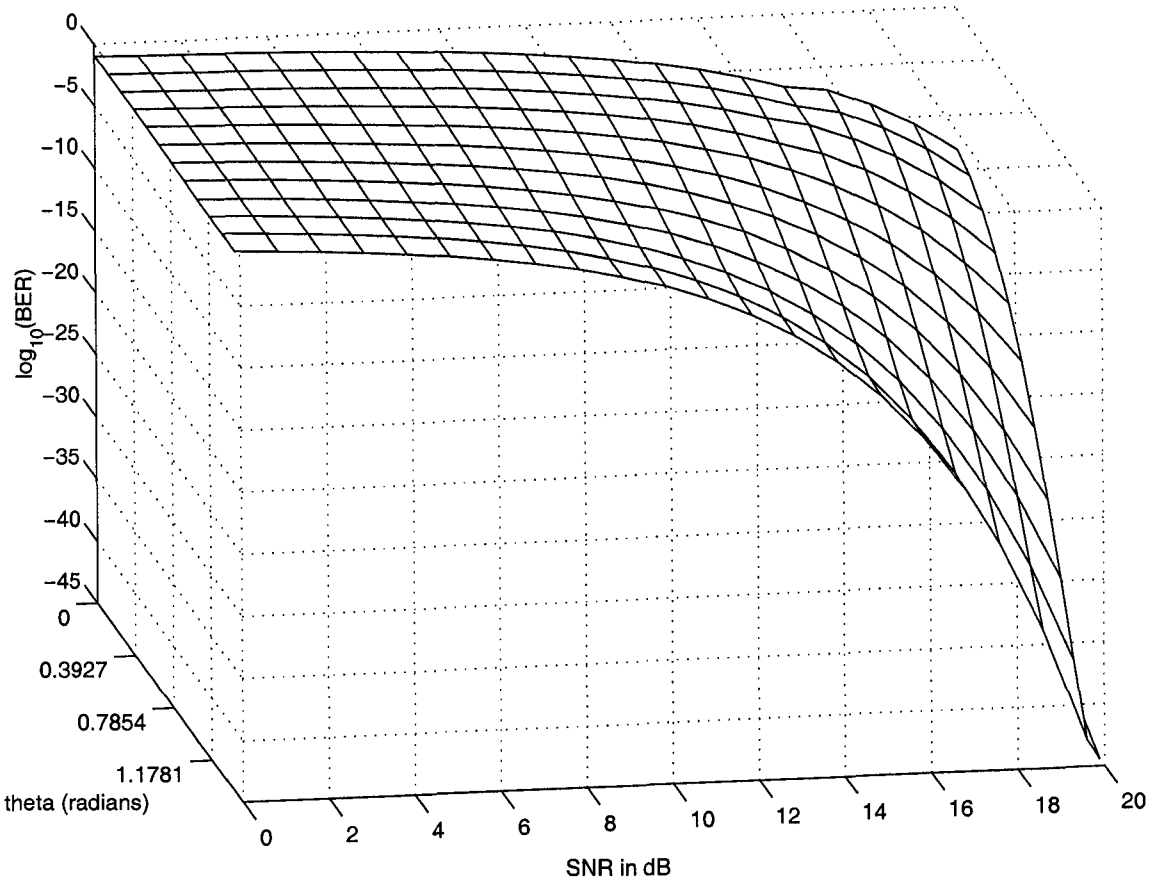

Fig. 4.10. Error rate performance versus θ and SNR, of the jointly optimal receiver for a BPSK signal plus one interferer, with SIR of $\Psi = 6$ dB.

4.4 Importance Sampling Simulation Gains

4.4.1 Comparing Monte Carlo Simulations to Importance Sampling Simulations

To assess the value of the importance sampling technique, it is useful to examine the savings in simulation time. One can determine these savings by finding the appropriate number of necessary simulation samples.

References [18] and [44] describe certain run-time considerations for efficient simulations. Consider N iterations by a typical Monte Carlo simulation. Suppose that the time to generate a random noise variate is t_G, and the time to compute the rest of the decoding is t_D. Then, the total time for simulation is

$$T_{MC} = N(t_G + t_D). \tag{4.30}$$

For a similar variance in the estimate, N_{IS} trials will be used, with $\frac{N}{N_{IS}} = \gamma_{samples}$. Let the generation of each IS random noise sample be of duration time t_{G2}. This yields the total time of importance sampling simulation as

$$T_{IS} = N_{IS}(t_{G2} + t_D), \tag{4.31}$$

assuming that the calculation of weight $W(x,y)$ is not large, relative to the decoding time t_D.

The simulation time savings is

$$\frac{T_{MC}}{T_{IS}} = \frac{N(t_G + t_D)}{N_{IS}(t_{G2} + t_D)}. \tag{4.32}$$

If $t_D \gg t_G$ or if $t_D \gg t_{G2}$, an approximation is

$$\frac{T_{MC}}{T_{IS}} \cong \frac{N}{N_{IS}} = \gamma_{samples}. \tag{4.33}$$

Thus, if one can find the value of $\gamma_{samples}$, one can find the approximate simulation time savings. This is a useful result, since the value of $\gamma_{samples}$ was defined in (4.20).

Furthermore, it is shown in [44] that when the threshold distance d is used as the radius R, the sample size saving can be approximated by

$$\frac{T_{MC}}{T_{IS}} \cong \frac{1-P_e}{\exp\left(-\frac{d^2}{2}\right)-P_e}. \tag{4.34}$$

The result of (4.34) indicates that with specific values of d and P_e, one can determine the simulation savings time.

To find the savings time, it is useful to determine the number of trials required for a typical Monte Carlo simulation. A typical rule of thumb is to choose N to be on the order of $10/P_e$ to $100/P_e$ [34], [43], [50]. Choosing an N value of $100/P_e$ should yield a relatively small sample variance. Reference [43] describes the 95% confidence interval of this simulation to be about $(0.8\hat{P}_e, 1.25\hat{P}_e)$. If one wishes to have small graphical variance in simulation plots, one could choose an N value of $1000/P_e$, which has a 95% confidence interval of about $(0.94\hat{P}_e, 1.06\hat{P}_e)$ [43].

Using the rule of thumb of $N = 100/P_e$, it can be seen that a large number of trials is needed for good simulations. From the number of Monte Carlo trials in Figs. 4.11 and 4.12, one observes the inverse relationship between the number of trials and $\hat{P}_e$, the sampled BER.

One can also use (4.34) to examine the sample size savings $\gamma_{samples}$ of the simulation. Plots of $\gamma_{samples}$ versus SIR and SNR are shown in Figs. 4.13 and 4.14. An arbitrary value of θ is chosen for illustrative purposes, and the minimum value of d is chosen in the calculations.

As discussed, the value of $\gamma_{samples}$ is a rough indication of the ratio of time elapsed between a Monte Carlo simulation and an importance sampling one. However, the plots of Figs. 4.13 and 4.14 are very similar to those of Figs. 4.11 and 4.12. This seems to indicate that for the specific rule of thumb ($N = 100/P_e$), there is not a significant increase in the number of IS sample points.

Fig. 4.13 shows that importance sampling benefits when the SNR increases. In general, this is because high-SNR regions have larger values of d and lower values of P_e, which would decrease the value of the denominator in (4.34). For a similar reason, importance

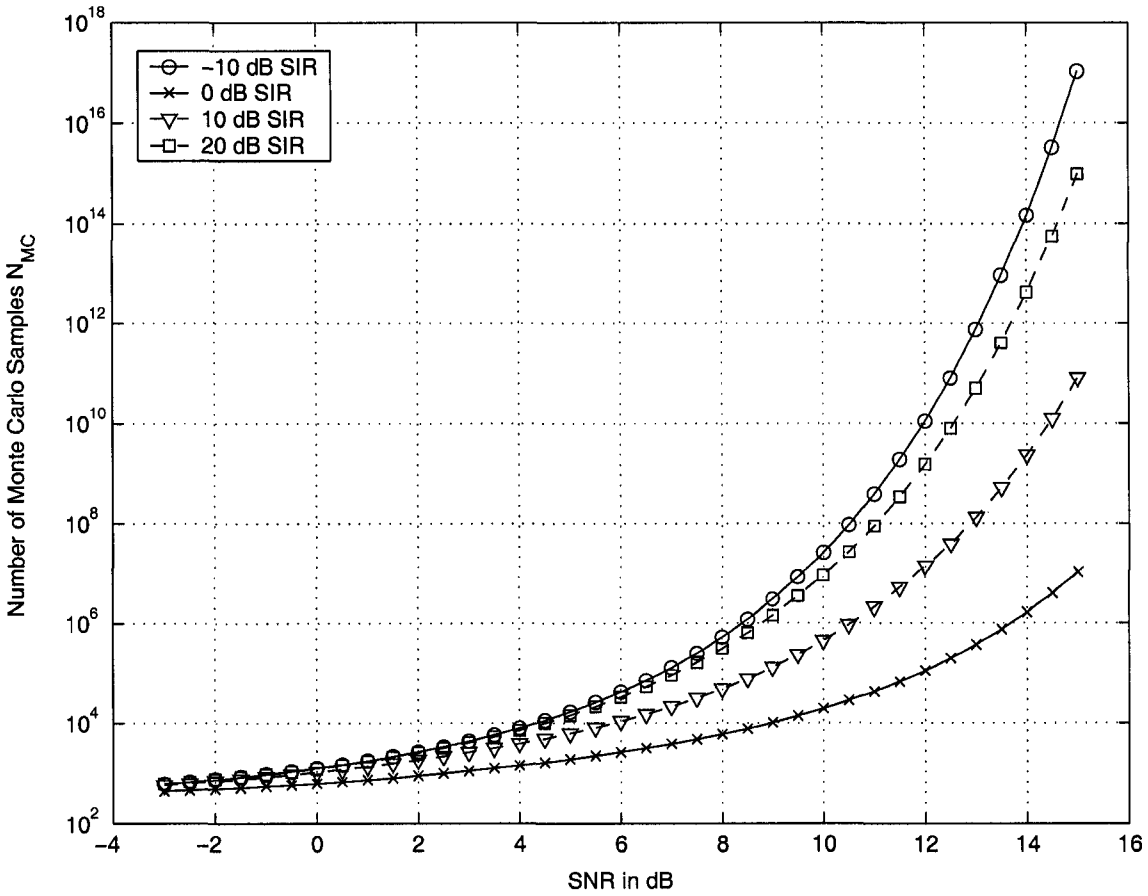

Fig. 4.11. Number of Monte Carlo samples versus SNR for $N = \frac{100}{P_e}$, with $\theta = \frac{\pi}{6}$.

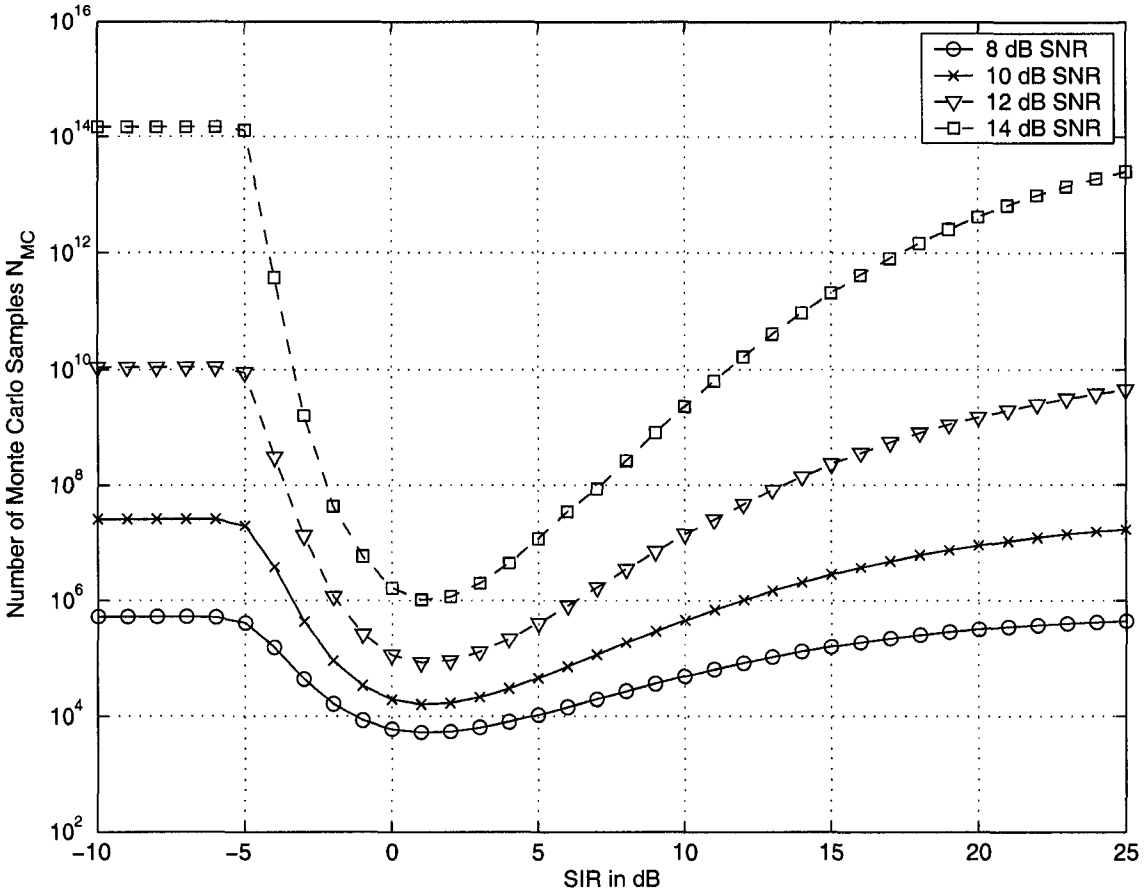

Fig. 4.12. Number of Monte Carlo samples versus SIR for $N = \frac{100}{P_e}$, with $\theta = \frac{\pi}{6}$.

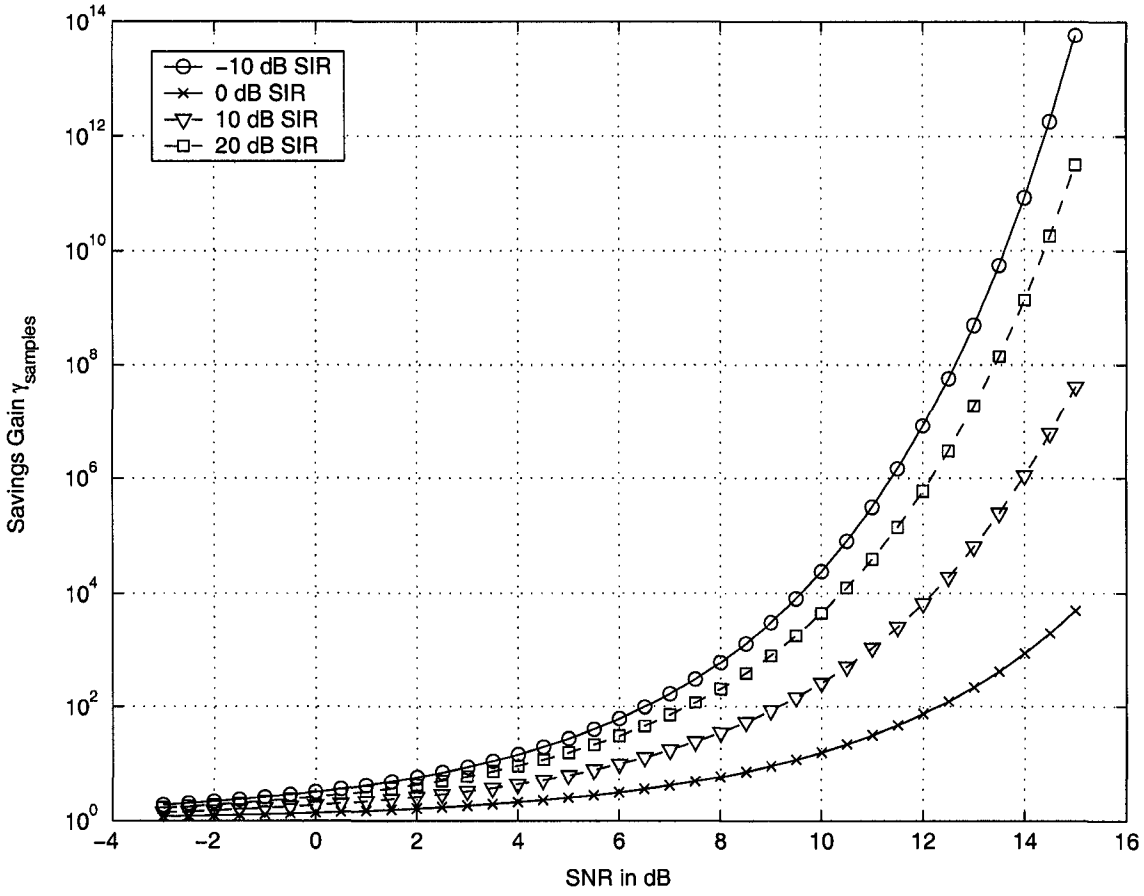

Fig. 4.13. Sample savings gain versus SNR for a similar variance σ as that in Fig. 4.11, with $\theta = \frac{\pi}{6}$.

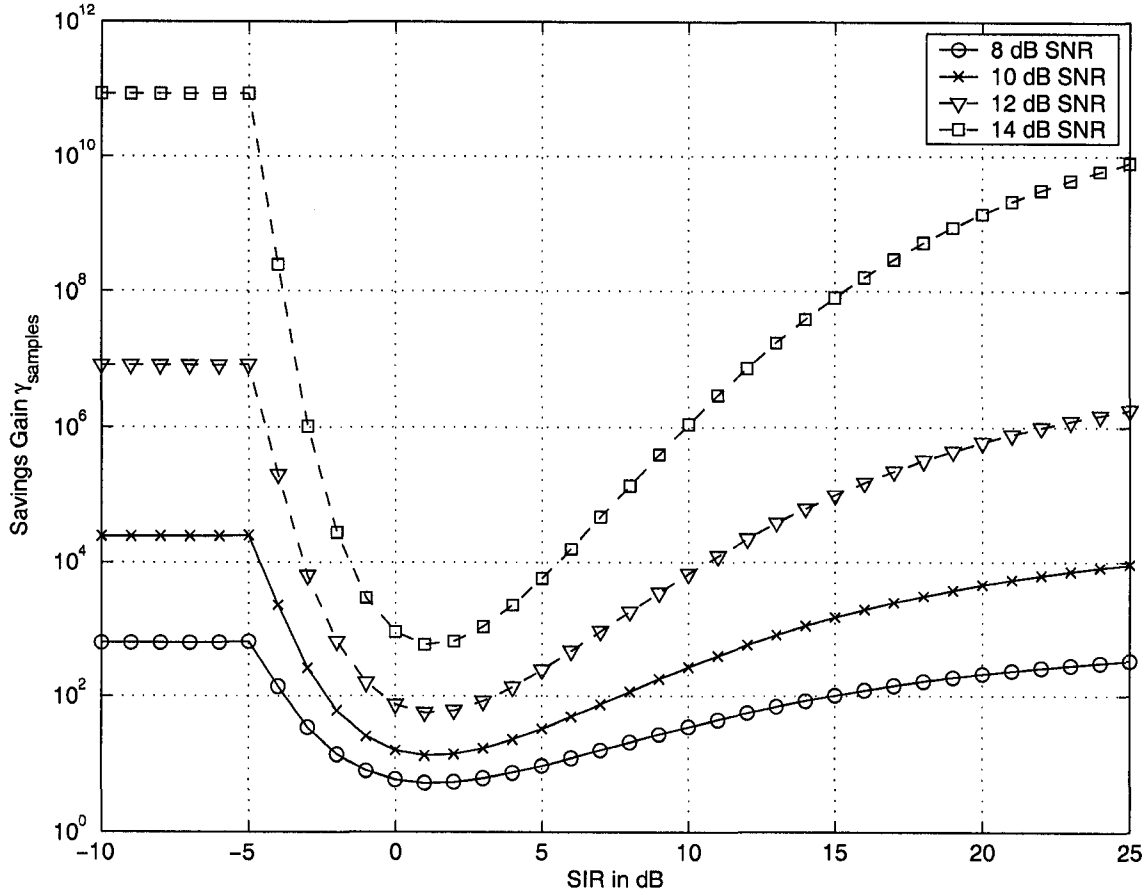

Fig. 4.14. Sample savings gain versus SIR for a similar variance σ as that in Fig. 4.12, with $\theta = \frac{\pi}{6}$.

sampling has greater benefits when the SIR is either really large or really small.

4.4.2 Number of Trials for Importance Sampling and Monte Carlo Simulations

Subsection 4.4.1 introduces the rule of thumb for Monte Carlo simulations of $N_{MC} = c_{MC}/P_e$, where c_{MC} is some constant. Thus, the number of Monte Carlo simulation points is inversely proportional to the error rate P_e. This relationship is why so many trials are required to simulate low error rates.

However, the results of Subsection 4.4.1 indicate that N_{IS} is not as dependent on P_e. To verify this, one can examine the variance σ^2. In the case of Monte Carlo simulation, [44] states that the variance of the Monte Carlo estimator is

$$\sigma_{MC}^2 = \frac{P_e(1-P_e)}{N_{MC}}. \tag{4.35}$$

Set the normalized variance σ^2/P_e^2 as a constant c_{var}, i.e.

$$\frac{\sigma_{MC}^2}{P_e^2} = \frac{(1-P_e)}{P_e N_{MC}} = c_{var}. \tag{4.36}$$

An approximation for N_{MC} can be made by noting that as P_e approaches small values (such as 10^{-6}), the numerator in (4.36) approaches 1. Then,

$$\frac{\sigma_{MC}^2}{P_e^2} \approx \frac{1}{P_e N_{MC}} \approx c_{var}, \tag{4.37}$$

or, by rearranging terms with $c_{MC} = 1/c_{var}$,

$$N_{MC} \approx \frac{c_{MC}}{P_e}, \tag{4.38}$$

where c_{MC} is an arbitrary constant. Thus, for an arbitrarily-sized variance, choose a c_{MC} for the variance (for example, 10, 100, or 1000), which leads to the rule of thumb in Subsection 4.4.1.

A similar calculation can be performed for the normalized importance sampling variance σ_{IS}^2/P_e^2. The variance is [44]

$$\sigma_{IS}^2 = \frac{1}{N_{IS}} \int \int_{\vartheta} f_{x,y}(x,y)[W(x,y) - P_e]dydx, \tag{4.39}$$

where k is from (4.26). Since, from (4.28), $W(x,y) = k$ beyond the radius d, (4.39) can be rearranged to

$$\sigma_{IS}^2 = \frac{P_e W(x,y) - P_e^2}{N_{IS}} = \frac{P_e k - P_e^2}{N_{IS}}. \tag{4.40}$$

Set the normalized variance equal to some constant c_{var2}, i.e.

$$\frac{\sigma_{IS}^2}{P_e^2} = \frac{k - P_e}{P_e N_{IS}} = \frac{\frac{k}{P_e} - 1}{N_{IS}} = c_{var2}. \tag{4.41}$$

Again, one can make a rearrangement where $c_{IS} = 1/c_{var2}$, yielding

$$N_{IS} = c_{IS}\left(\frac{k}{P_e} - 1\right) \tag{4.42}$$

One can now find an approximate value of P_e. Consider a constellation point in two-dimensional signal space. If d were the perpendicular distance from the point to a straight-line decision boundary, then an approximate value of P_e is

$$P_e \approx Q(d), \tag{4.43}$$

assuming a normalized noise variance equal to 1. The function $Q(\cdot)$ is the Q function. Note that in the jointly optimal receiver case, the decision boundary is not simply a straight line. However, as d increases, the value of P_e in (4.43) approaches $Q(d)$.

An asymptotic approximation to the function $Q(d)$ can now be made as [51]

$$\text{erfc}(z) \approx \frac{\exp(-z^2)}{z\sqrt{\pi}}, \tag{4.44}$$

where erfc$(\cdot)$ is the complimentary error function, related to $Q(\cdot)$ by

$$Q(x) = \frac{1}{2}\text{erfc}\left(\frac{x}{\sqrt{2}}\right). \tag{4.45}$$

A rough approximation of (4.43) is then

$$P_e \approx Q(d) \approx \frac{\exp\left(-\frac{d^2}{2}\right)}{d\sqrt{2\pi}}. \tag{4.46}$$

Combine (4.26) with (4.42) and (4.46) to yield

$$N_{IS} = c_{IS}\left(\frac{k}{P_e} - 1\right) \approx c_{IS}\left(\frac{\exp\left(-\frac{d^2}{2}\right)}{\frac{\exp\left(-\frac{d^2}{2}\right)}{d\sqrt{2\pi}}} - 1\right) \approx \sqrt{2\pi}c_{IS}d - c_{IS}. \tag{4.47}$$

That is, N_{IS} is approximately linearly dependent on d, the minimum distance to the decision boundary. This is a useful result. Empirically, we have observed that N_{IS} is approximately independent of P_e. This is a very important result because it implies that one can simulate arbitrarily small values of P_e using this importance sampling technique. While there is still dependency on d, this value does not fluctuate as significantly as P_e, allowing one to efficiently simulate small P_e values. In fact, *a slight change in d results in a significant change in* P_e. For example, using the approximation in (4.43), P_e is approximately 3×10^{-5} for a value of $d = 4$, while it is approximately 1×10^{-7} for a value of $d = 7$. For this reason, one can simulate extremely small BER's using a slowly-increasing N_{IS}.

Note that this is only an approximation; there is a fluctuation in the required number of trials. Even so, the variation in N_{IS} is much smaller than the resulting increase in N_{MC}. Thus, importance sampling in this particular two-dimensional problem results in significant savings in the number of required trials. Consequently, the time for simulation is decreased by several orders of magnitude, particularly for low values of BER. This benefit of importance sampling allows one to efficiently simulate the jointly optimal BPSK receiver.

4.5 Summary

The importance sampling simulation technique in [18] is a very useful procedure in the simulation of a jointly optimal BPSK receiver. Since the two BPSK signals create a 4-point signalling constellation in 2-dimensional space, appropriate decision boundaries can be found. One can then bias the PDF to that of (4.27) and count the sample errors accordingly.

For this 2-dimensional jointly optimal receiver problem, importance sampling is a powerful technique. It has 2 main benefits:

- For a given constellation point, the weight $W(x,y)$ is constant; $W(x,y) = k$. This can lead to substantial gains in computational time. Whereas traditional importance sampling causes continuous recalculation of $W(x,y)$ and $f_{x,y}(x,y)$, the IS technique developed in [18] has $W(x,y) = k$.

- As shown in [18], this version of IS is most effective only when we can accurately estimate the minimum distance d. However, with the assumptions made in this investigation, d is known in this receiver. In fact, d is half the minimum distance between two points in the 4-point signalling constellation.

Importance sampling has been shown to be an efficient simulation technique. It results in a significant decrease in sample points for a small variance. Moreover, by calculating the minimum threshold distance d between points, one has an effective method of extending this case to scenarios where there are more than 4 constellation points. These multiple-interferer situations will be analyzed in the following chapter.

Chapter 5

Performance of Multiple-Interferer Jointly Optimal Receivers

The procedure of Chapter 4 provides a useful technique in simulating the jointly optimal receiver for BPSK signals in the presence of multiple interferers. Using importance sampling, one can obtain efficient simulations for multiple interferers.

One can better understand the nature of the jointly optimal receiver when considering these multiple-interferer cases. Indeed, the results of this Chapter verify that additional interferers worsen the error rate performance of the jointly optimal receiver.

5.1 Simulating the Multiple-Interferer Jointly Optimal Receivers

In [52], Kwan and Leung consider an individually optimal receiver in the case of a BPSK signal in the presence of 2 interferers [53].

The description of the problem follows that of the 2-user case in Chapter 2. Consider again the desired BPSK signal $A_0 b_0 s_0(t)$ transmitted over an AWGN channel. This transmission is now in the presence of additional interfering BPSK signals, $A_i b_i s_i(t)$, where $i = 1, 2, ...K$ (K is the total number of interferers). Again, A_i is the amplitude of the signal

from user i, while b_i is the bit transmitted (either -1 or $+1$) by user i. The deterministic signal assigned to the ith user is $s_i(t)$. Synchronous signals are assumed. One can then write the received signal as

$$\begin{aligned} v(t) &= \sum_{i=0}^{K} A_i b_i s_i(t) + n(t), \ 0 \le t \le T \\ &= \sum_{i=0}^{K} \left(A_i b_i \sqrt{\frac{2}{T}} \cos(\omega_i t + \theta_i) \right) + n(t), \ 0 \le t \le T \end{aligned} \tag{5.1}$$

where $n(t)$ is white Gaussian noise with two-sided power spectral density $N_0/2$, T is the bit duration, and ω_i is the angular frequency of signal i. Since one is considering cochannel interference scenarios, let $\omega_i = \omega_0 = \omega$ for all i. The phase difference between signals 0 and i is θ_i ($\theta_0 = 0$).

An individually optimal receiver using a maximum likelihood ratio was developed in [52]. Previously, in [2] and [54], jointly and individually optimal receivers are described. In essence, an individually optimal receiver selects the appropriate bit $b_0 \in \{-1, +1\}$ that maximizes the a posteriori probability

$$P[(b_0)|v(t), \ 0 \le t \le T], \tag{5.2}$$

while the jointly optimal receiver selects the bit *vector* $\mathbf{b} = [b_0 \, b_1 \, ... \, b_k]$ that maximizes the joint a posteriori probability

$$P[(\mathbf{b})|v(t), \ 0 \le t \le T]. \tag{5.3}$$

It is shown in [2] that as the SNR increases in the multi-user channel, the jointly optimal receiver performs nearly as well as the individually optimal receiver. This result is similar to the two-user case discussed in Chapter 2.

Following [1], [52], and Chapter 2, project $v(t)$ on a pair of orthonormal basis functions determined by the Gram-Schmidt procedure as

$$\phi_0(t) = \phi_0'(t) = \sqrt{\frac{2}{T}} \cos(\omega_0 t) \tag{5.4a}$$

$$\phi_1(t) = -\frac{\cos\theta_1}{\sin\theta_1}\phi_0'(t) + \frac{1}{\sin\theta_1}\phi_1'(t) = -\sqrt{\frac{2}{T}} \sin(\omega_0 t) \tag{5.4b}$$

where $\phi_0'(t) = \sqrt{\frac{2}{T}}\cos(\omega_0 t)$ and $\phi_1'(t) = \sqrt{\frac{2}{T}}\cos(\omega_0 t + \theta_1)$.
where $\phi_0'(t) = \sqrt{\frac{2}{T}}\cos(\omega_0 t)$ and $\phi_1'(t) = \sqrt{\frac{2}{T}}\cos(\omega_0 t + \theta_1)$.

One important aspect of this orthogonalization is that all signals $A_i b_i s_i(t)$ can be expressed as the sum of the two orthonormal signals in (5.4a) and (5.4b). That is, one can express $s_i(t)$ as the sum of two orthonormal functions:

$$s_0(t) = \phi_0(t) \tag{5.5a}$$

$$s_i(t) = (\cos\theta_i)\phi_0(t) + (\sin\theta_i)\phi_1(t), \quad i = 1,2,...K \tag{5.5b}$$

Thus, the dimensionality of this problem is 2, *independent of the value of K.*[1] The consistently two-dimensional nature of this problem is beneficial. Importance sampling techniques from Chapter 4 can be used for any number, K, of cochannel interferers.

One can now consider the received signal without noise, $y(t) = v(t) - n(t)$. There are 2^{K+1} possible received signal combinations, $\pm A_0 s_0(t) \pm A_1 s_1(t) ... \pm A_K s_K(t)$.

For example, if there are 2 interferers, there are 8 possible received signal combinations, as shown on the scatter plot of Fig. 5.1:

$$y_{000}(t) = \left(-A_0 - A_1\cos\theta_1 - A_2\cos\theta_2\right)\phi_0(t) + \left(-A_1\sin\theta_1 - A_2\sin\theta_2\right)\phi_1(t) \tag{5.6a}$$

$$y_{001}(t) = \left(-A_0 - A_1\cos\theta_1 + A_2\cos\theta_2\right)\phi_0(t) + \left(-A_1\sin\theta_1 + A_2\sin\theta_2\right)\phi_1(t) \tag{5.6b}$$

$$y_{010}(t) = \left(-A_0 + A_1\cos\theta_1 - A_2\cos\theta_2\right)\phi_0(t) + \left(+A_1\sin\theta_1 - A_2\sin\theta_2\right)\phi_1(t) \tag{5.6c}$$

$$y_{011}(t) = \left(-A_0 + A_1\cos\theta_1 + A_2\cos\theta_2\right)\phi_0(t) + \left(+A_1\sin\theta_1 + A_2\sin\theta_2\right)\phi_1(t) \tag{5.6d}$$

$$y_{100}(t) = \left(+A_0 - A_1\cos\theta_1 - A_2\cos\theta_2\right)\phi_0(t) + \left(-A_1\sin\theta_1 - A_2\sin\theta_2\right)\phi_1(t) \tag{5.6e}$$

$$y_{101}(t) = \left(+A_0 - A_1\cos\theta_1 + A_2\cos\theta_2\right)\phi_0(t) + \left(-A_1\sin\theta_1 + A_2\sin\theta_2\right)\phi_1(t) \tag{5.6f}$$

$$y_{110}(t) = \left(+A_0 + A_1\cos\theta_1 - A_2\cos\theta_2\right)\phi_0(t) + \left(+A_1\sin\theta_1 - A_2\sin\theta_2\right)\phi_1(t) \tag{5.6g}$$

$$y_{111}(t) = \left(+A_0 + A_1\cos\theta_1 + A_2\cos\theta_2\right)\phi_0(t) + \left(+A_1\sin\theta_1 + A_2\sin\theta_2\right)\phi_1(t) \tag{5.6h}$$

[1]This is a result of the cochannel nature of the signals, i.e. $\omega_i = \omega_0 = \omega$. It is shown in [1] and [52] that if the K interferers do not have common ω_i, there could be up to K required orthonormal vectors.

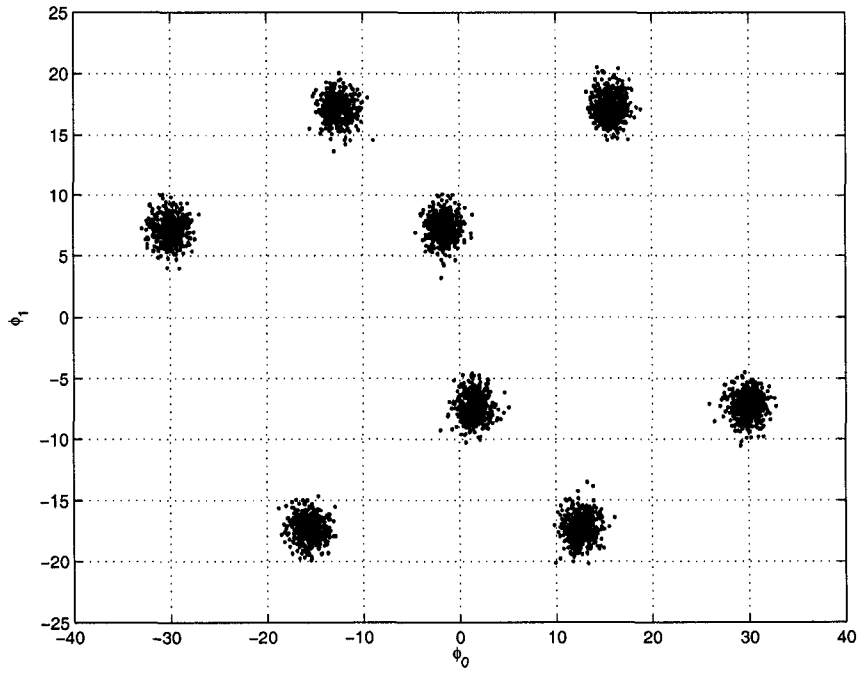

Fig. 5.1. Scatterplot of BPSK signal plus 2 interferers and AWGN, with SNR=20 dB, Ψ_1=3 dB, Ψ_2=0 dB, $\theta_1 = \pi/6$, and $\theta_2 = 2\pi/3$.

The process can also be repeated for 3 interferers. A scatter plot of this scenario is shown on Fig. 5.2. On Fig. 5.2, the noise of two pairs of constellation points causes the scatter plot to overlap (where $\phi_0 = -20$ to -10), giving the appearance of 14 points. This overlap is for illustrative purposes; this plot shows the difficulty in having a 4-user (16-point) constellation with easily separated points.

One can continue this process continues for K interferers, although the number of constellation points exponentially increases relative to K. For any K number of interferers, with the bit vector $\mathbf{b} = [b_0\, b_1\, \ldots\, b_k]$, one could represent $y(t)$ as

$$y(t) = \sum_{i=1}^{K} \left(A_i b_i \cos\theta_i \phi_0(t) + A_i b_i \sin\theta_i \phi_1(t) \right). \tag{5.7}$$

Note that this remains a two-dimensional problem, and the decision boundaries can be shown in two-dimensional signal space.

The simulation of the jointly optimal BPSK receiver for K interferers is similar to the simulation of the jointly optimal receiver for 1 interferer. The process in Section 4.3 applies,

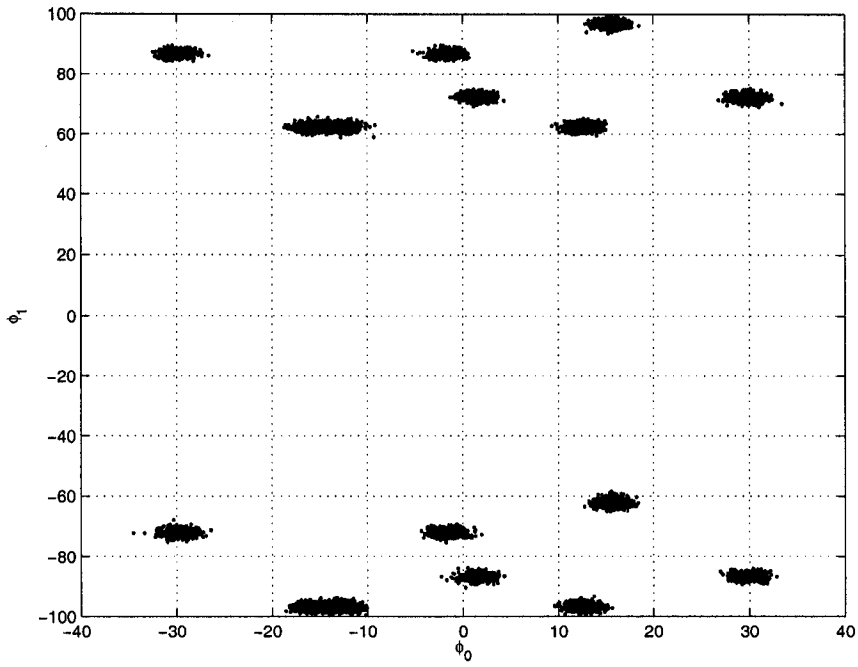

Fig. 5.2. Scatterplot of BPSK signal plus 3 interferers and AWGN, with SNR=20 dB, Ψ_1=3 dB, Ψ_2=0 dB, Ψ_3=−15 dB, $\theta_1 = \pi/6$, $\theta_2 = 2\pi/3$, and $\theta = 3\pi/2$.

since this is still a two-dimensional signal space. However, there are two major differences:

- Finding the threshold distances d requires more calculation. For example, in the single-interferer case of Section 4.3, one needed to calculate the minimum distance between 2 pairs of points. However, in the case of 2 interferers, each threshold distance d is found by minimizing the distance for *4* pairs of points. For a 3-interferer case, the distance between *8* pairs of points must be calculated. For K interferers, one must calculate 2^K distances to find the value of d.

- Not only do the values of d require more calculation, but there are also more values of d to be found. Consider Section 4.3, where one requires the threshold lengths $d_{(1,0)}$ and $d_{(1,1)}$. This is because there are $2^2 = 4$ constellation points, and $2^1 = 2$ possible combinations where the desired bit is equal to one.

  However, in the case of K interferers, there are 2^{K+1} constellation points, and 2^K possible combinations where the desired bit is equal to one. This results in more d

values to be calculated, which causes more k values to be calculated, which causes more biased PDF's in Equation (4.27).

Given this additional complexity, the importance sampling technique developed in Chapter 4 is all the more needed. This simulation procedure is still effective for the following reasons:

- For a given constellation point, the weight $W(x,y)$ is still constant; $W(x,y) = k$. On an overall basis, this allows the IS simulation to require fewer calculations. Granted, there are more constellation points, which requires more $W(x,y)$ calculations. However, this is still preferable over a continuous calculation of $W(x,y)$ for each and every sample point, which often occurs in IS simulation.

- The assumption in [18] is still valid – this IS simulation is most effective if one can accurately calculate the minimum threshold distance d. Regardless of the number of interferers in the system, this value can be calculated within reasonable time.

- In addition, this simulation technique emphasizes the importance of two-dimensional decision boundaries. This is not the only way to make a jointly optimal decision; joint-likelihood decision statistics are discussed in [2], and achieve the same result. However, in order to implement joint-likelihood decision statistics for K interferers, one may require more complex calculations. The "minimum-distance" jointly optimal receiver is fairly straightforward to simulate, and achieves good results.

In summary, the importance sampling technique developed in Chapter 4 is equally effective for multiple-interferer BPSK cases. This is a result of the continued 2-dimensional nature of the problem. However, one requires more time to calculate the biased points in IS. As the number of constellation points exponentially increase as K increases, more preliminary calculations are required for K interferers. Nonetheless, importance sampling is still a useful procedure to examine the multiple-interferer problem.

5.2 Results and Discussion

The jointly optimal receiver for multiple interferers is simulated. Simulation results were obtained for $K = 2$ and $K = 3$ interferers. Results for $K = 6$ were also obtained, as this is a practical example for a cellular network environment.

One first compares the multiple-interferer results with similar simulations in certain peer-reviewed publications. Reference [52] simulates an individually optimal receiver for a BPSK signal in the presence of two interferers. One of the simulation curves from [52] is shown in Fig. 5.3. Also recall that according to [2], as the SNR increases in the multi-user channel, the jointly optimal receiver performs nearly identically to the individually optimal receiver. As a result, some jointly optimal simulations are also present in Fig. 5.3. Fig. 5.3 shows the BER versus the SIR for the two-interferer case. Curves for three different SNR values are plotted on the graph.

The results of Fig. 5.3 indicate that the importance sampling simulations from Section 5.1 are valid. The simulation from [52] matches that of the IS simulation that uses the same input parameters (the curve for 7 dB SNR in Fig. 5.3). This result thus implies that the IS simulation technique works for the multiple-interferer scenario.

One can obtain other useful observations from Fig. 5.3. Firstly, as the SIR increases, the curves progress towards the "error floor" of a single BPSK signal in AWGN, i.e.

$$P_{e(BPSK)}(\gamma_s) = Q\left(\sqrt{2\gamma_s}\right), \tag{5.8}$$

where γ_s is the signal-to-noise ratio. However, compared to the single-interferer case, this does not rapidly occur as the SIR decreases (i.e. when the SIR achieves a large negative dB value). The SNR curves for 7 dB and 10 dB indicate that once a value of approximately -5 dB SIR is reached, the "tail" of the curve slows down significantly. These curve shapes can be compared to the curve shapes of single BPSK interferer scenarios (for an example, see Fig. 4.8).

Other observations can be made in this Figure. The maxima of the curves still occurs at 0 dB when θ is a random variable between $[0, 2\pi)$, which is also the case in a single-interferer scenario. In addition, the 10 dB SNR curve offers an interesting result. There

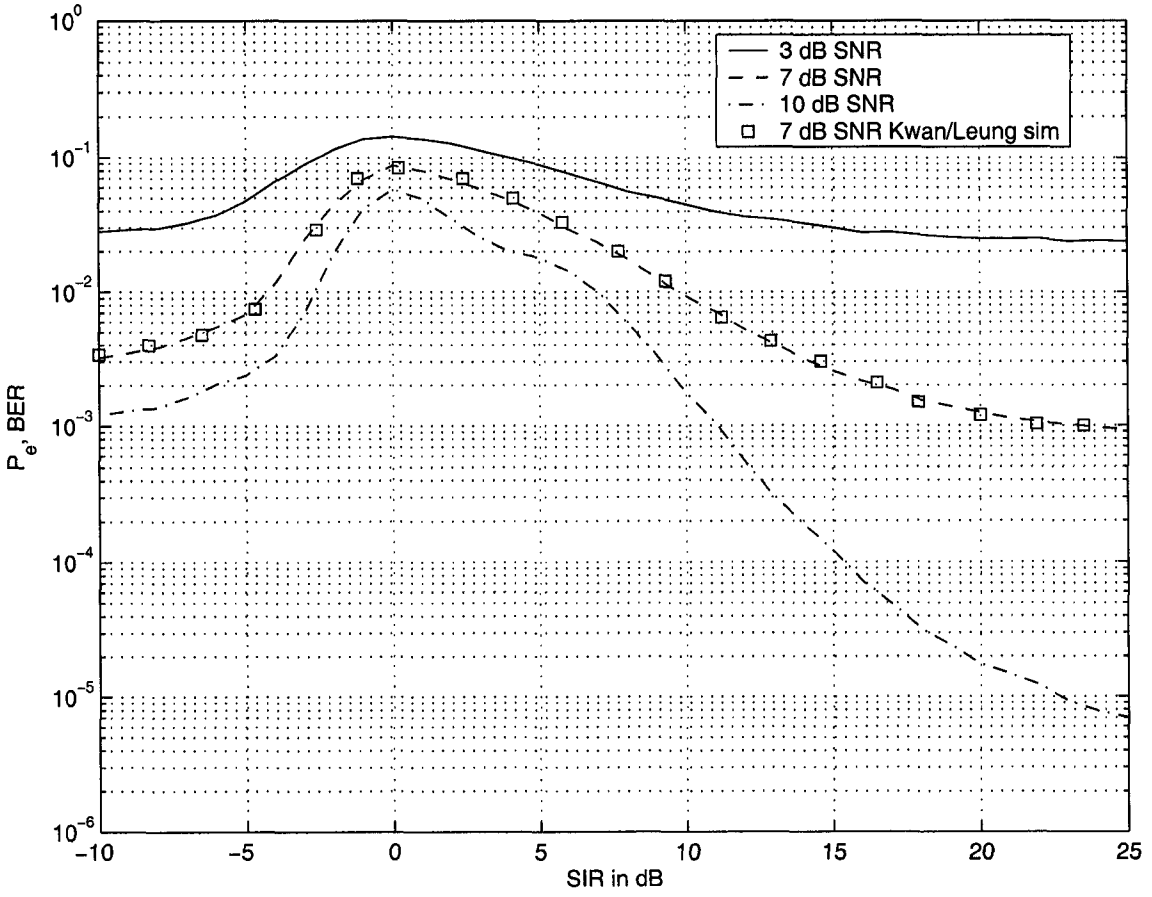

Fig. 5.3. The BER performance of a jointly optimal receiver versus SIR_1, for a BPSK signal plus two interferers, with SIR_1=SIR_2, and θ uniformly distributed over $[0,2\pi)$.

is a "bulge" in the curve where the SIR is approximately +5 dB. The slope of the BER-versus-SIR curve is still negative at this inflection point, but the result is still interesting, particularly when compared with Fig. 5.4.

Fig. 5.4 shows the same scenario as that in Fig. 5.3, but 3 interferers are in the system instead of two. This graph emphasizes the nature of the multi-interferer "bulge" in the BER/SIR curve. To the best of the author's knowledge, this bulge has not been reported in previous works. The bulge is again present at the region around +5 dB SIR, and is emphasized for the curves where the SNR is 7 dB and 10 dB. Again, as in Fig. 5.3, the curves tend towards an asymptotic limit as the SIR increases. However, as the SIR *decreases* (i.e. as the SIR in units of dB's becomes much more negative), the curves do not have a sharp decrease in BER. Thus, for most reasonable negative dB values of SIR, the performance benefits are not significant in the jointly optimal receiver.

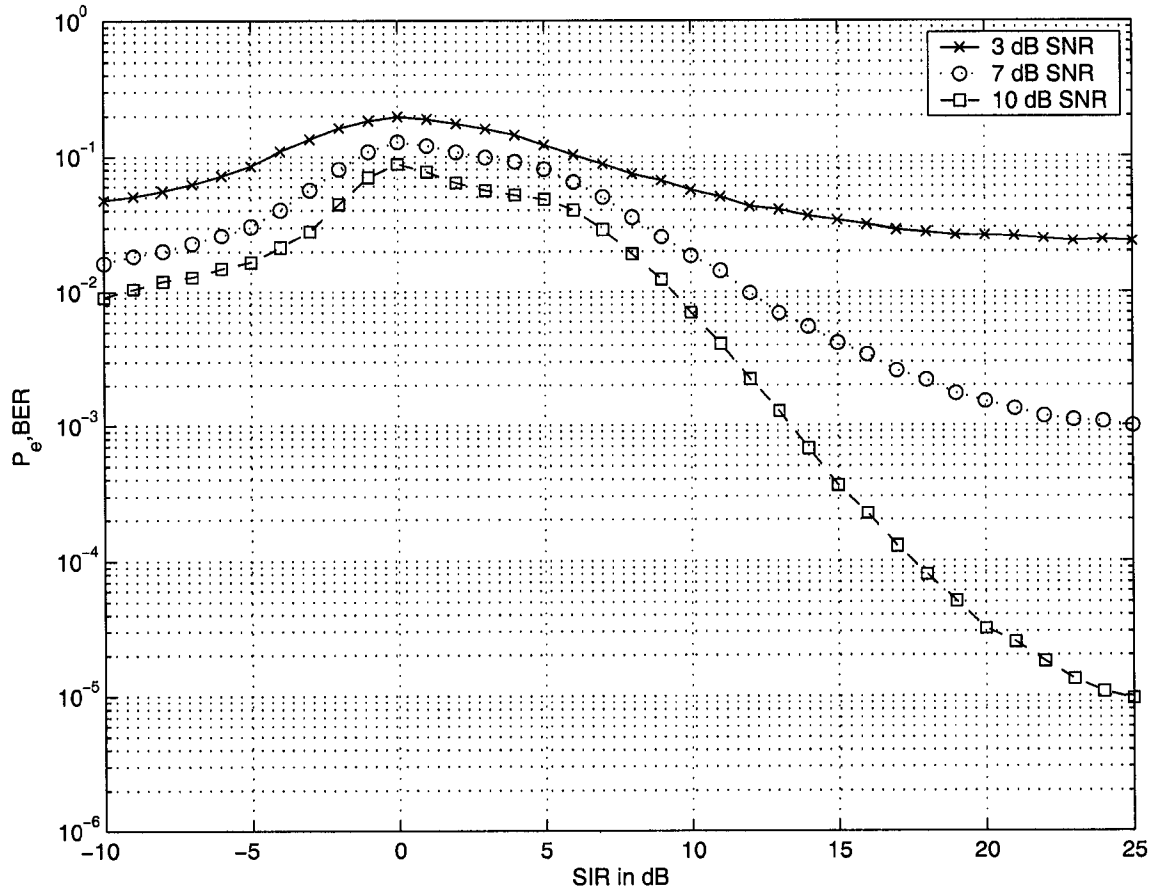

Fig. 5.4. The BER performance of a jointly optimal receiver versus SIR_1, for a BPSK receiver with three interferers, with $SIR_1 = SIR_2 = SIR_3$, and θ a uniformly distributed random variable on $[0,2\pi)$.

Why is the small SIR case so different with multiple interferers compared with one interferer? This is partly a result of the nature of the simulation models used in Figs. 5.3 and 5.4. In these two figures, the SIR for each interferer was identical; i.e.

$$\Psi_1 = \Psi_2 = \Psi_3 = \frac{A_0^2}{A_1^2} = \frac{A_0^2}{A_2^2} = \frac{A_0^2}{A_3^2}. \tag{5.9}$$

Thus, in Figs. 5.3 and 5.4, a large amount of signal energy resides with the interferers at very negative dB SIR. On a relative scale, compare this with the single-interferer case (for an example, see Fig. 4.8). At an SIR_1 of -3 dB, for example, the interferers have twice the energy of the desired signal in the case of one single interferer. However, with three interferers, where $SIR_1 = SIR_2 = SIR_3$, the combined interferers now have *six times* the energy of the desired signal. This increased interferer energy makes it more difficult to detect the desired signal, resulting in decreased performance in the negative dB regions of the curve. This is seen in Figs. 5.3 and 5.4, which reaches a BER of 10^{-3} in the case of 2 interferers at 10 dB SNR and -10 dB SIR, but only 10^{-2} in the case of three interferers in the same conditions.

The comparison among one, two, and three BPSK interferers is shown in Fig. 5.5. Two levels of SNR are shown on this plot (4 dB and 12 dB). Note that this plot also shows the features of the importance sampling technique. Most of the 12 dB SNR curves reach a BER of the order of 10^{-7} to 10^{-8}. This is achieved with N_{IS} only on the order of 40,000 to 100,000 trials. As discussed in Chapter 4, importance sampling is a powerful technique in this problem. The technique allows one to simulate very low BER's in reasonable time.

Upon examination of Fig. 5.5, the following observations can be made:

- While the single-interferer receiver performs fairly well at reasonably low values of SIR (from an SIR of -10 to -5 dB), this is not the case for multiple interferers. As previously discussed, this occurs because there is more interferer energy in the multiple-interferer scenario. This increased energy makes the desired signal harder to detect.

- At large values of SIR, the curves progress towards the "error floor" of a single BPSK

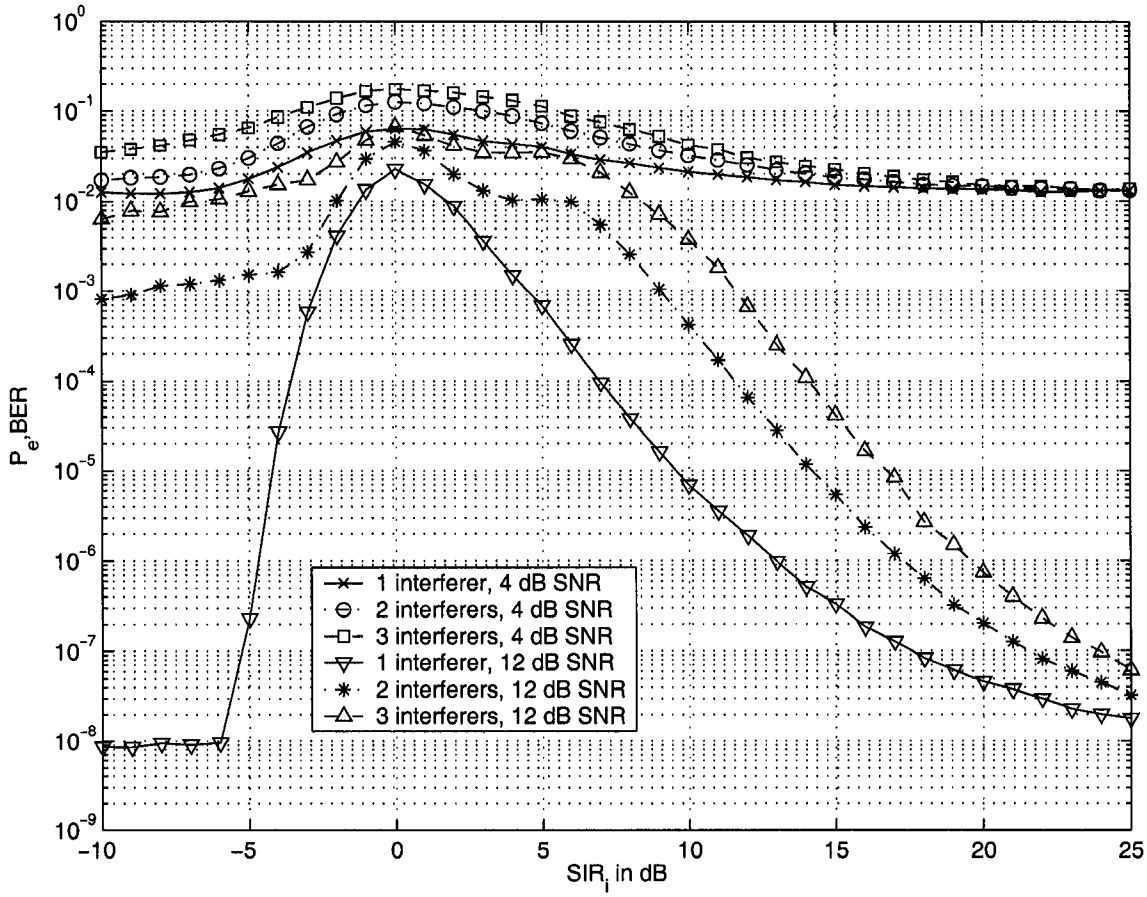

Fig. 5.5. The BER performance of a jointly optimal BPSK receiver versus SIR_i ($i = 1,2,3$), in the presence of one, two, or three interferers, with $SIR_1 = SIR_2 = SIR_3$, and θ_i uniformly distributed over $[0,2\pi)$.

signal in AWGN. With more interferers, one needs larger values of SIR to achieve the error floor.

- The "bulge" in the SIR curve still occurs at a value of around +5 dB SIR for two or three interferers.

- Except for very high values of SIR, there is significant performance degradation in the jointly optimal receiver as one increases the number of interferers. Even for a relatively poor BER value (at 0 dB SIR), the BER for three interferers is nearly four times worse than the BER for one interferer.

Simulations for $K = 6$ interferers are introduced in Fig. 5.6. The simulation of 6 interferers is of particular use in a practical wireless cellular environment. Since there is a finite number of channels in a mobile telephone environment, cellular frequencies must be reused. Typical network design thus divides a geographical area into hexagons, where each hexagon represents the coverage area of an omnidirectional base station. As a result of this hexagonal design, one can have 6 equidistant cochannel interferers to a desired signal. Thus, it is useful to simulate a 6-interferer case.

The following observations can be made upon examination of Fig. 5.6:

- At any arbitrary value of SIR in Fig. 5.6, the net interferer energy is equal for all cases of interferers. Even so, an increased number of interferers causes a degradation of performance. For example, at a total SIR of 5 dB, the 2-interferer case performs approximately 1.5 dB worse than the single-interferer scenario with the same total interferer energy. The six-interferer case performs about 3 dB worse than the single-interferer case with the same total interferer energy.

- The error rate curves in Fig. 5.6 cross at certain values of SIR. One could surmise that this occurs because the energy is distributed among different numbers of interferers. For example, at 0 dB total SIR, the single-interferer case has one BPSK signal with the same energy as the (only) interferer. However, the two-interferer case has the one

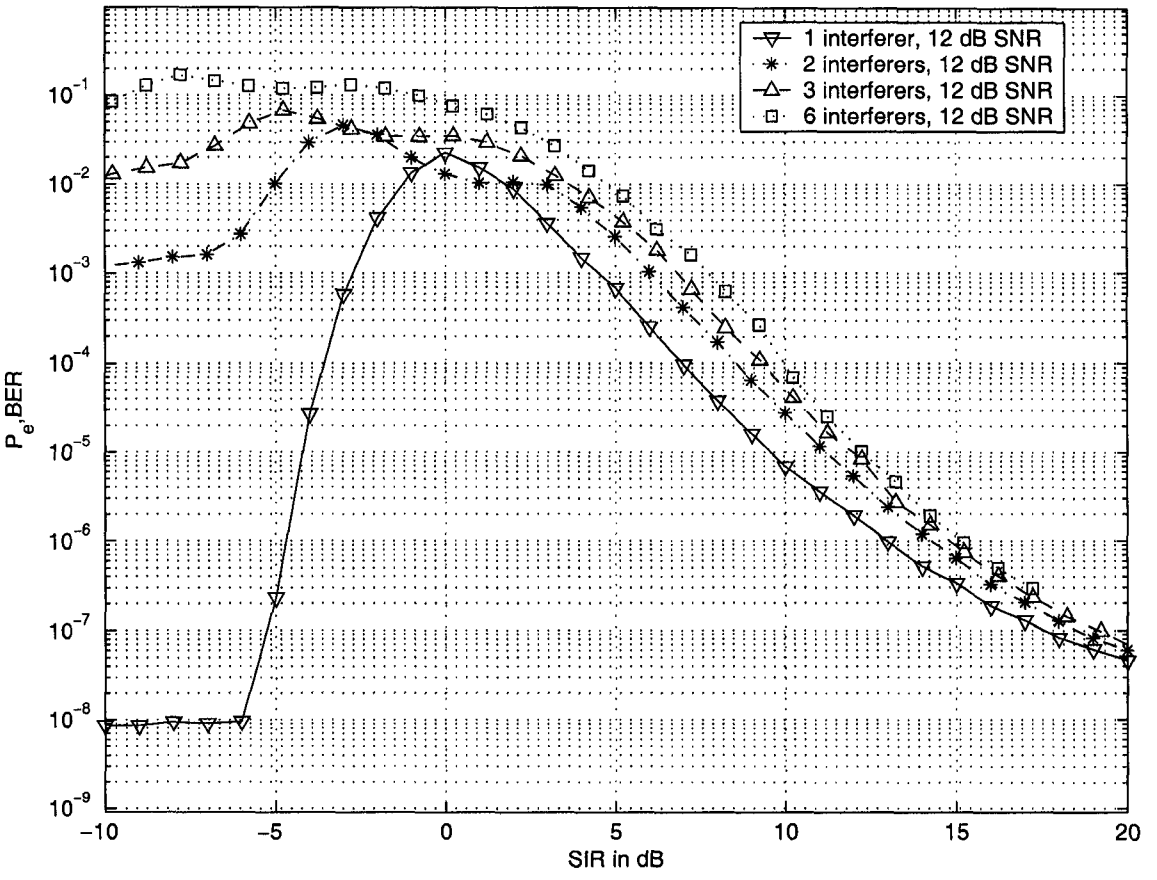

Fig. 5.6. The BER performance of a jointly optimal BPSK receiver versus total SIR, in the presence of one, two, three, or six interferers, with all interferer SIR_i equal, an SNR of 12 dB, and θ_i uniformly distributed over $[0,2\pi)$.

BPSK signal with twice the energy as each cochannel interferer. The variety in the distribution of energy causes different performance results.

- Note that the absolute maximum of the error rate curves still occurs at a level where the desired signal has the same energy as each of the single interferers (0 dB SIR for 1 interferer, -3 dB SIR for 2 interferers, etc.) This is verified when observing Fig. 5.5.

Further observations can be made if one places the SNR along the x-axis and plots the results. Fig. 5.7 displays this scenario, and again shows the power of the importance sampling technique, obtaining simulation points for BER's of nearly 10^{-25}. At a relatively high SIR_i value (12 dB), it is shown that the jointly optimal receiver has sharply different performance characteristics as one increases the SNR.[2] For example, at a (relatively high) SNR value of 10 dB, the single-interferer jointly optimal receiver performs with a gain of almost 2 dB, compared to the 2-interferer receiver. This gain increases as one increases the SNR. In addition, the performance gain between receivers with one and three interferers is very large. Upon examination of this plot, one can conclude that increasing the number of interferers K significantly degrades the performance in detecting a single desired BPSK signal.

One reason that an increased number of interferers K causes such a performance degradation lies in the energy of the interferers. When the interferers have more energy than the desired signal, the decision boundaries in two-dimensional signal space may be very near the desired signal constellation points. As an example, if a dominant A_1 or A_2 is present in (5.6a) – (5.6h), the orientation of the constellation points changes. If the constellation is such that a $-A_0$ is fairly indistinguishable from a $+A_0$, it would make the desired bit b_0 more difficult to detect.

Another reason why Fig. 5.7 has such a performance degradation lies in the nature of the curves. In Fig. 5.7, all curves had a SIR_i value equal. However, this means that the

[2]Also recall that as the SNR increases, the jointly optimal detector converges to the individually optimal (minimum-BER) detector [2]; thus, these results are equally valid for individually optimal detectors.

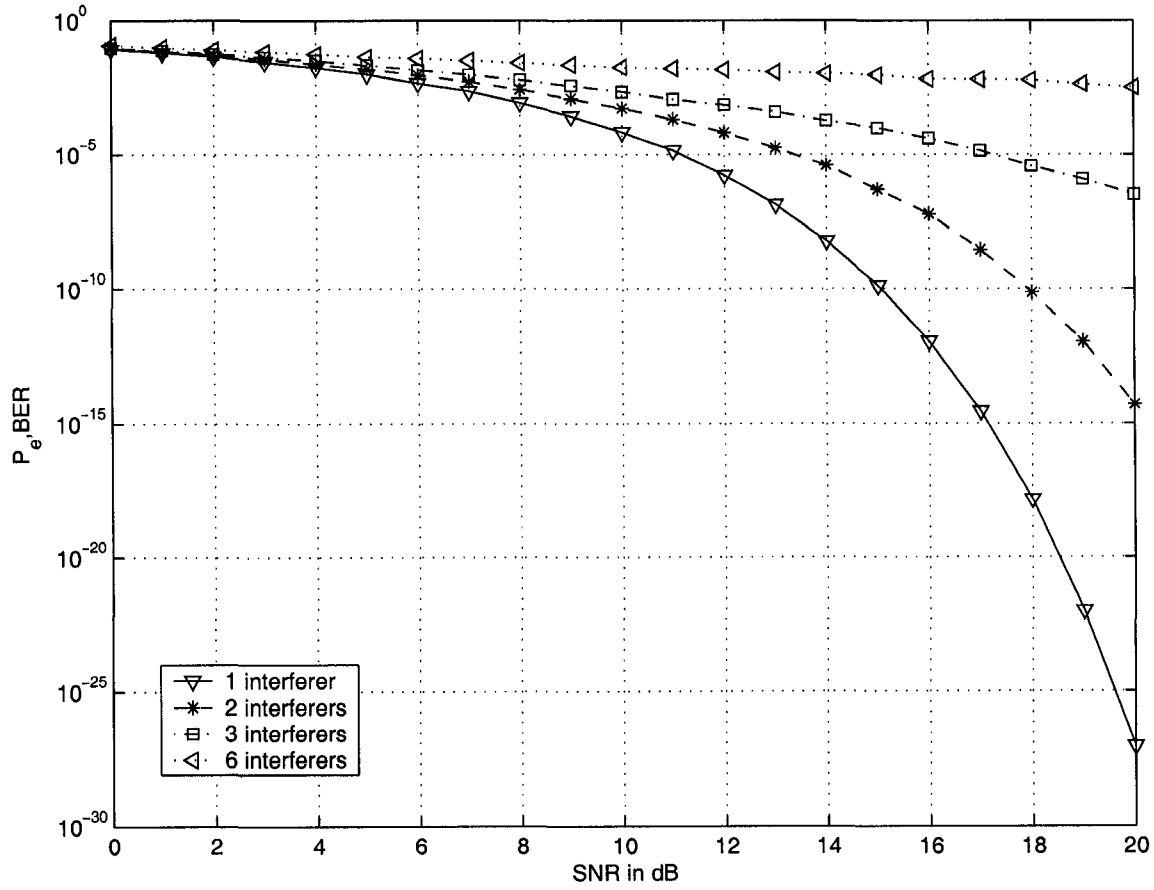

Fig. 5.7. The BER performance of a jointly optimal BPSK receiver versus SNR, in the presence of one, two, three, and six interferers, with all interferer SIR_i = 12 dB, and θ_i uniformly distributed over $[0,2\pi)$.

3-interferer case has more interferer energy than the single-interferer case. In this plot, the multiple-interferer case has more energy, which makes the desired signal more difficult to detect.

To specifically examine the performance of the jointly optimal receiver, it is useful to examine the case of multiple interferers *with the same net interferer energy*. That is, one wants the interferer energy for 1 interferer to be equal to that for 3 interferers. Thus, the individual SIR_i for the 3-interferer case is larger than that for the single-interferer case. Thus, for these curves, the total SIR will be equal. This is shown in Fig. 5.8. Note that there is still a performance degradation between the single-interferer case and the 3-interferer case, but it is not as large as that in Fig. 5.7.

An expanded version of a region of Fig. 5.8 is shown in Fig. 5.9. This plot shows that for a range of SNR between 0 and 6 dB, the error rate performance for one, two, three, and six interferers is similar. The error rate curves diverge significantly once an SNR of 10 dB is reached. Thus, one sees that when the interferer energy is constant, performance degradation in the multiple-interferer case occurs mainly at SNR values above 10 dB. The error function becomes more non-linear at values greater than 10 dB, causing the curves to diverge at this value. In fact, it is shown in [55] and [56] that the degradation in error rate performance is a result of the upward-concavity of the Q-function.

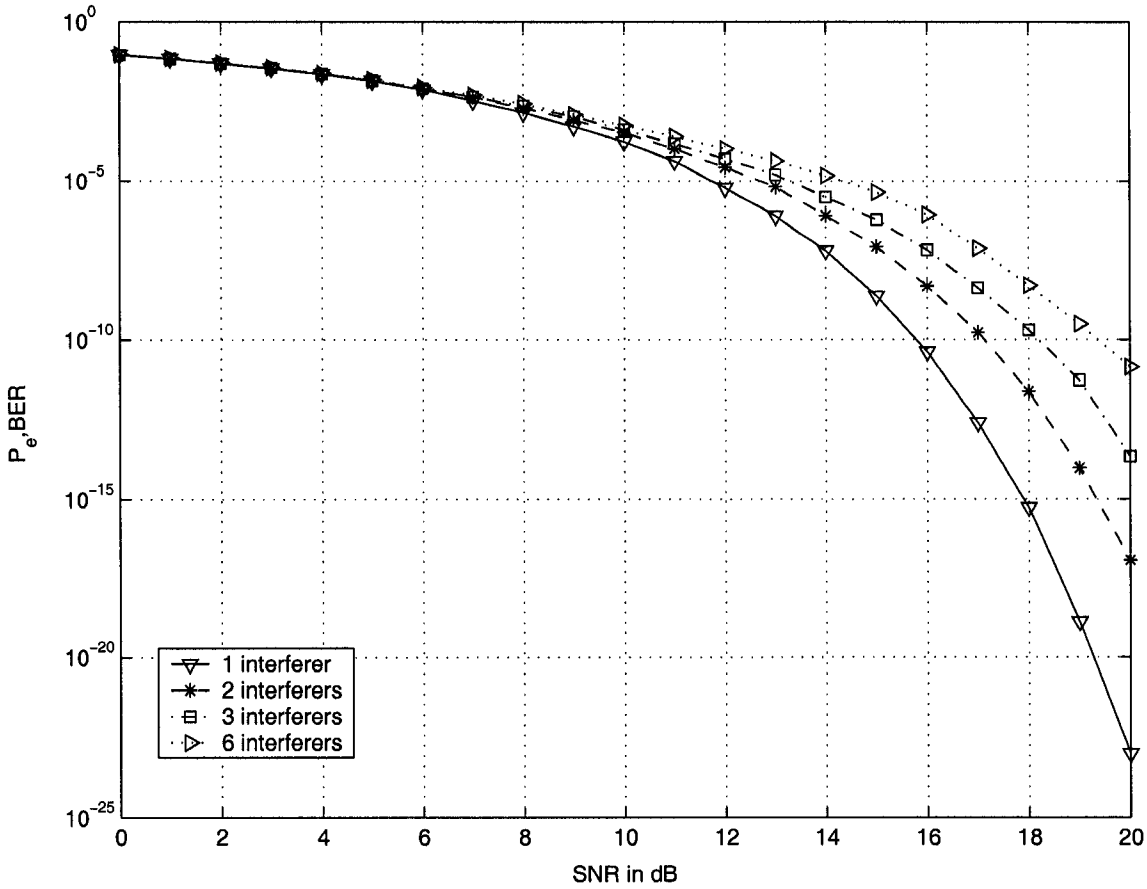

Fig. 5.8. The BER performance of a jointly optimal BPSK receiver versus SNR, in the presence of one, two, three, and six interferers, with the net interferer energy constant (i.e. the total SIR is 10 dB), and θ_i uniformly distributed over $[0,2\pi)$.

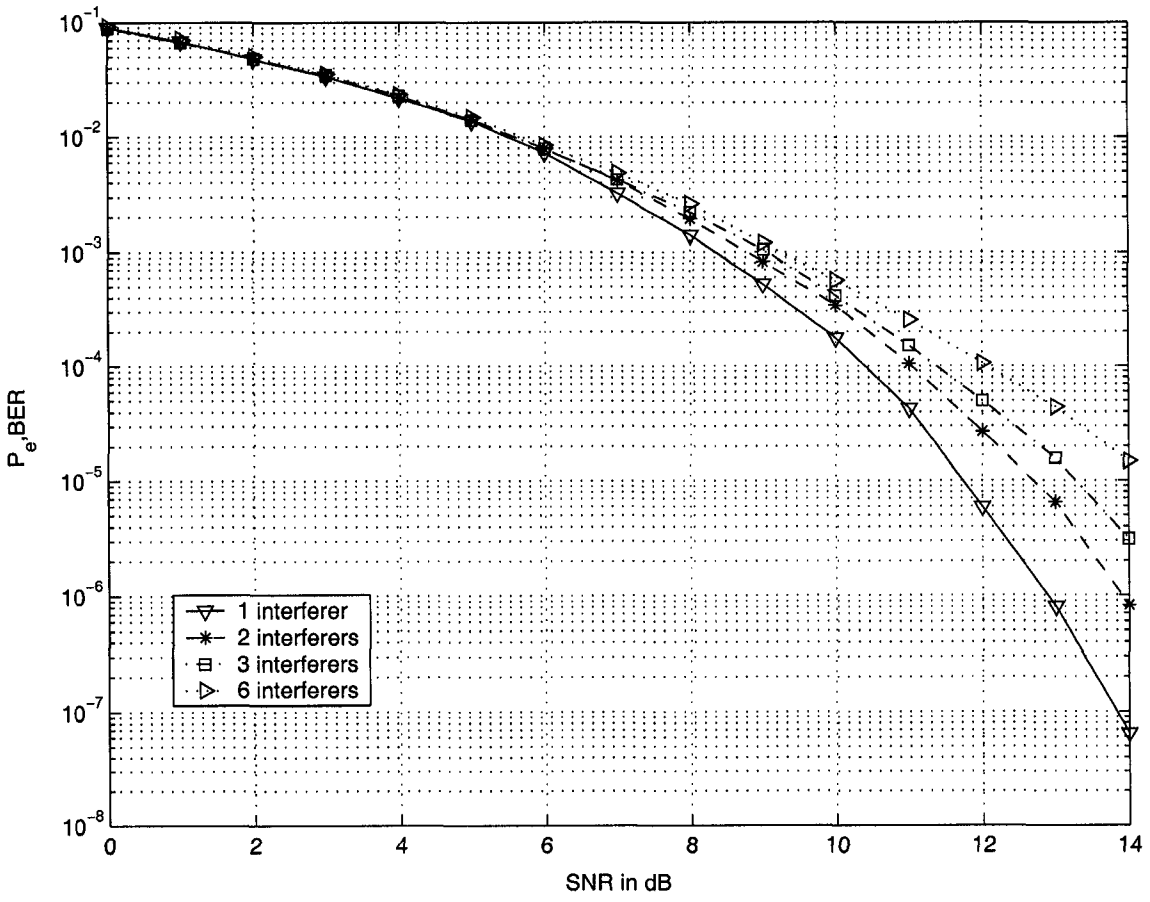

Fig. 5.9. The BER performance of a jointly optimal BPSK receiver versus SNR, in the presence of one, two, three, and six interferers, with the SNR between 0 and 14 dB, the net interferer energy constant (i.e. the total SIR is 10 dB), and θ_i uniformly distributed over $[0,2\pi)$.

As a further example, consider Fig. 5.10, where the SIR among interferers is *not* equal, but with a constant dB difference. An IS simulation was done to achieve the curves in Fig. 5.10, which allowed one to achieve BER values down to 10^{-15}. These curves yield some interesting results. Firstly, local maxima of the BER curve occur *whenever* SIR_i *is equal to 0 dB, for any* $i=1,..K$. That is, the two-interferer curve has 2 local maxima, while the 3-interferer curve has 3 local maxima, where the BER is poorest. One can thus conclude that whenever an interferer's energy is the same as that of the desired signal, the BER would be poor (many bit errors will occur).

Other interesting observations arise from Fig. 5.10. If there is enough difference in the energies of the individual interfering signals, the curve obtains a "multiple-bump" shape, achieving its local maxima, then sharply decreasing towards the error floor of a single BPSK signal in AWGN. This is seen in the 3-interferer curve in Fig. 5.10. However, if the difference among interferer SIR is not that large, the "bumps" converge, as seen in the two-interferer case. As well, note that at very low values of SIR_1, the 3-interferer case still performs relatively poorly.

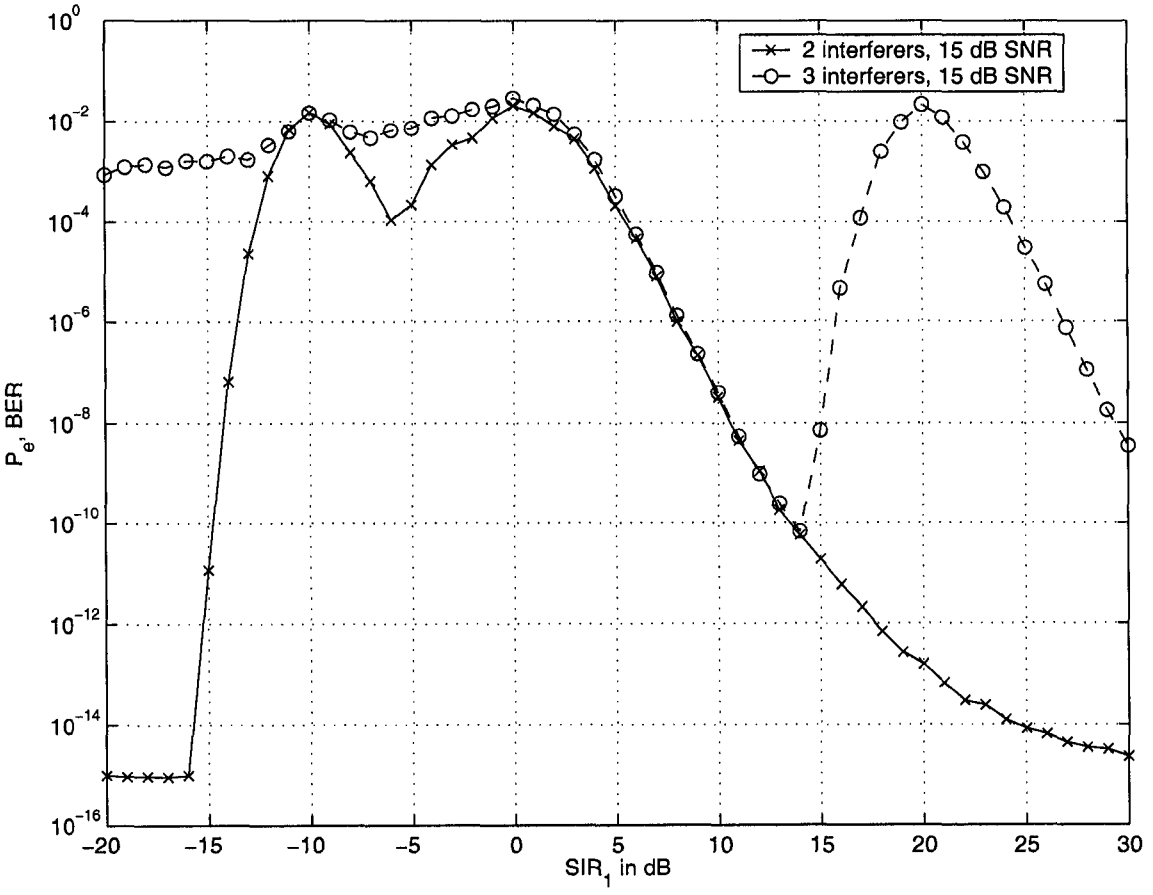

Fig. 5.10. The BER performance of a jointly optimal BPSK receiver versus SIR_1, with two and three interferers, where $SIR_2 = 10$ dB + SIR_1. In the case of three interferers, $SIR_3 = SIR_1 - 20$ dB.

With a variety of input parameters (from the SIR of each interferer, to the SNR, to the θ, to the importance sampling technique), there are a large number of parameters affecting the performance of the jointly optimal BPSK receiver in the presence of K interferers. In this section, one has highlighted the main points. Adding interferers causes a performance degradation in the system. While this is not a surprising result, what is surprising is the relative *magnitude* of the degradation. As well, because there is more interferer energy, the jointly optimal multiple-interferer receiver does not perform as well at largely negative dB values of SIR. These observations, along with others made in this section, point to the difficulties in detecting a BPSK signal in the presence of multiple interferers.

5.3 Summary

One needs a technique to efficiently simulate the jointly optimal BPSK receiver in the presence of multiple cochannel interferers. The importance sampling technique from Chapter 4 provides a very useful tool in examining this scenario. This is a result of the consistently two-dimensional nature of the problem, regardless of the number of interferers K.

It is seen that the IS simulation technique allows one to achieve very low BER's for the receiver in the presence of multiple interferers. However, when extending the IS technique to multiple interferers, more preliminary calculations are required. This is because there is an exponential increase in the number of constellation points 2^{K+1}, causing more weighting functions $W(x,y)$ to be needed. Still, this is preferred over continued recalculation of $W(x,y)$ for each and every sample point.

One observes that for a given value of SNR and SIR, the performance of a multiple-interferer jointly optimal receiver is worse than one with only one single interferer. This can be explained as a result of increased interferer signal energy, which makes the desired signal more difficult to detect.

The results of this Chapter show that adding BPSK interferers to the system causes performance degradation. While this is generally known, what this Chapter offers is a quantifiable measure of how much better a single-interferer receiver performs. Further-

more, throughout this chapter, one applies a useful IS technique to a problem well-suited for the procedure. The techniques and observations are useful for practical cellular system design, particularly in areas such as power control. These new results allow one to examine the behaviours of multiple-interferer scenarios.

Chapter 6

Conclusions

It is important to analyze the effects of communications systems in the presence of cochannel interference plus noise. The addition of cochannel interferers makes the desired signal more difficult to detect, and degrades the BER performance of the communications system. In addition, when analyzing optimal receiver structures, it is often difficult to make effective observations of BER performance. Exact, analytical mathematical expressions are not always obvious, and bounds to the error rate performance are often needed. One could also simulate the communications system, but it is usually time-consuming to simulate a very large number of trials.

This thesis examines the case of a jointly optimal receiver for a desired BPSK signal in the presence of cochannel interference plus noise. An efficient importance sampling technique is used to simulate the system using a relatively small number of samples. This technique is valuable because it allows one to examine the case of multiple interferers. This work also derives a new, exact, analytical expression for the BER performance of a BPSK signal in the presence of one cochannel interferer plus noise. In summary:

1. The optimality of the BPSK receiver in [1] is clarified. While the signal constellation diagrams in [1] imply the use of a jointly optimal receiver, one determines that a minimum-BER individually optimal receiver is used. The BER performance of this receiver is seen to be good in regions of small and large SIR.

2. This thesis clarified the definition of individually optimal and jointly optimal receivers. Individually optimal receivers have a decision boundary that is a curved line in two-dimensional signal space. Jointly optimal receivers, on the other hand, have a decision boundary composed of straight line segments. While individually optimal receivers perform better than jointly optimal ones, the performance of these two receivers is significantly different only at very small values of SNR. Thus, it is useful to analyze the BER performance of jointly optimal receivers.

3. A new, exact analytical expression for the BER performance of the jointly optimal BPSK receiver is derived. This expression is derived using Craig's method [3]. This analytical expression takes different forms, depending on specific SIR threshold levels. The result is a tractable, exact analytical solution. Upper and lower analytical bounds are also analyzed, and are tight to the derived expression.

4. An efficient simulation technique is applied to the jointly optimal BPSK receiver. This is a new application of the importance sampling method of [18], and is a powerful technique in the simulation of this receiver. Since the decision boundary of this receiver is composed of straight line segments, this IS technique introduces significant savings in simulation time. The technique allows one to use significantly fewer trials for a small variance in BER.

5. The new IS simulation application is used for the case of a BPSK signal in the presence of multiple cochannel interferers. This simulation is useful and powerful because it allows for significant time savings over traditional Monte Carlo simulation. The IS technique allows one to make useful performance observations that would otherwise be unaddressed. One sees that adding BPSK interferers to the system causes performance degradation, and one makes quantifiable observations of how much better a single-interferer receiver performs. By exploiting the significant time savings in importance sampling, one is able to thoroughly analyze the performance of the jointly optimal receiver.

References

[1] R. Kwan and C. Leung, "Optimal detection of a BPSK signal contaminated by interference and noise," *IEEE Communications Letters*, vol. 6, no. 6, pp. 225–227, June 2002.

[2] S. Verdú, *Multiuser Detection*. New York: Cambridge University Press, 1998.

[3] J. W. Craig, "A new simple and exact result for calculating the probability of error for two-dimensional signal constellations," in *Proc. IEEE Military Communications Conference MILCOM '91*, Boston, MA, Nov. 1991, vol. 2, pp. 0571–0575.

[4] X. Dong, N. C. Beaulieu, and P. H. Wittke, "Signaling constellations for fading channels," *IEEE Transactions on Communications*, vol. 47, no. 5, pp. 703–714, May 1999.

[5] N. C. Beaulieu, "A investigation of Gaussian tail and Rayleigh tail density functions for importance sampling digital communication system simulation," *IEEE Transactions on Communications*, vol. 38, no. 9, pp. 1288–1292, Sept. 1990.

[6] A. S. Rosenbaum, "Binary PSK error probabilities with multiple cochannel interferences," *IEEE Transactions on Communications*, vol. COM-18, no. 3, pp. 241–253, June 1970.

[7] C. W. Helstrom, "Calculating error probabilities for intersymbol and cochannel interference," *IEEE Transactions on Communications*, vol. COM-34, no. 5, pp. 430–435, May 1986.

[8] N. C. Beaulieu, "The evaluation of error probabilities for intersymbol and cochannel interference," *IEEE Transactions on Communications*, vol. 39, no. 12, pp. 1740–1749, Dec. 1991.

[9] N. C. Beaulieu and A. A. Abu-Dayya, "Bandwidth efficient QPSK in cochannel interference and fading," *IEEE Transactions on Communications*, vol. 43, no. 9, pp. 2464–2474, Sept. 1995.

[10] P. H. J. Chong and C. Leung, "NCFSK bit-error rate with unsynchronized slowly fading interferers," *IEEE Transactions on Communications*, vol. 49, no. 2, pp. 272–281, Feb. 2001.

[11] G. Caire, G. Taricco, J. Ventura-Traveset, and E. Biglieri, "A multiuser approach to narrowband cellular communications," *IEEE Transactions on Information Theory*, vol. 43, no. 5, pp. 1503–1517, Sept. 1997.

[12] W.-K. Ma and P. Ching, "Asymptotic minimum bit error rate property of maximum-likelihood multiuser detection," *IEEE Communications Letters*, vol. 7, pp. 425–427, Sept. 2003.

[13] M. J. Wilmut and L. L. Campbell, "Signal detection in the presence of cochannel interference and noise," *IEEE Transactions on Communications*, vol. 20, no. 6, pp. 1153–1158, Dec. 1972.

[14] N. C. Beaulieu and C. Leung, "Optimal detection of hard-limited date signals in different noise environments," *IEEE Transactions on Communications*, vol. COM-34, no. 6, pp. 619–622, June 1986.

[15] N. C. Beaulieu, "Penalties of sample-and-sum and weighted partial decision detectors in Gaussian noise," *IEEE Transactions on Communications*, vol. COM-35, no. 8, pp. 777–785, Aug. 1987.

[16] T. F. Wong, Q. Zhang, and J. S. Lehnert, "Decision-feedback MAP receiver for time-selective fading CDMA channels," *IEEE Transactions on Communications*, vol. 48, no. 5, pp. 829–840, May 2000.

[17] G. J. M. Janssen and S. B. Slimane, "Performance of a multiuser detector for M-PSK signals based on successive cancellation," in *Proc. IEEE International Conference on Communications, ICC 2001*, Helsinki, Finland, June 11–14 2001, vol. 1, pp. 31–35.

[18] N. Beaulieu, E. Biglieri, and M. Lai, "Sample rejection and importance sampling in the simulation of multidimensional signalling systems," *IEE Proceedings - I, Communications, Speech, and Vision*, vol. 140, no. 6, pp. 445–452, Dec. 1993.

[19] B. Hagerman, *Single-User Receivers for Partly Known Interference in Multi-User Environments*, Ph.D. thesis, Royal Institute of Technology, Stockholm, Sweden, Sept. 1995.

[20] J. G. Proakis, *Digital Communications*, 4th ed. New York: McGraw-Hill, 2000.

[21] J. M. Wozencraft and I. M. Jacobs, *Principles of Communication Engineering*. New York: John Wiley and Sons, 1965.

[22] B. Hagerman, "On optimum BPSK-detection with partly known co-channel interference and Gaussian noise," in *Proc. of The Nordic Radio Symposium*, Aalborg, Denmark, June 1992.

[23] T. V. Poon and N. C. Beaulieu, "Jointly and individually optimum receivers for BPSK signals in cochannel interference plus noise," in *Proc. IEEE Pacific Rim Conference on Communications, Computers, and Signal Processing, PACRIM 2003*, Victoria, British Columbia, Canada, Aug. 28–30 2003, vol. 2, pp. 530–532.

[24] R. Kwan and C. Leung, "Optimal detection of a BPSK signal with unsynchronized co-channel interferers," in *Proc. IEEE International Conference on Communications, ICC 1999*, Vancouver, British Columbia, Canada, 1999, pp. 73–77.

[25] G. J. M. Janssen, "Receiver structure for simultaneous reception of two BPSK modulate cochannel signals," *Electronics Letters*, vol. 29, no. 12, pp. 1095–1097, June 1993.

[26] M. K. Simon, S. M. Hinedi, and W. C. Lindsey, *Digital Communication Techniques: Signal Design and Detection*. Englewood Cliffs, NJ: Prentice Hall, 1994.

[27] S. Verdú, "Minimum probability of error for asynchronous Gaussian multiple-access channels," *IEEE Transactions on Information Theory*, vol. IT-32, no. 1, pp. 85–96, Jan. 1986.

[28] S. Verdú, "Maximum likelihood sequence detection for intersymbol interference channels: A new upper bound on error probability," *IEEE Transactions on Information Theory*, vol. IT-33, no. 1, pp. 62–68, Jan. 1987.

[29] G. D. Forney, Jr, "Lower bounds on error probability in the presence of large intersymbol interference," *IEEE Transactions on Communications*, vol. COM-20, no. 1, pp. 76–77, Feb. 1972.

[30] G. D. Forney, Jr, "Maximum likelihood sequence estimation of digital sequences in the presence of intersymbol interference," *IEEE Transactions on Information Theory*, vol. IT-18, pp. 363–378, May 1972.

[31] A. Leon-Garcia, *Probability and Random Processes for Electrical Engineering*, 2nd ed. Reading, Massachusetts, USA: Addison Wesley, 1994.

[32] T. V. Poon and N. C. Beaulieu, "Error performance analysis of a jointly optimal single cochannel interferer BPSK receiver," *IEEE Transactions on Communications*, to be published.

[33] T. V. Poon and N. C. Beaulieu, "Performance analysis of a jointly optimal BPSK receiver in cochannel interference," in *Proc. IEEE Global Telecommunications Conference GLOBECOM '03*, San Francisco, USA, Dec. 1–5 2003, vol. 3, pp. 1721–1725.

[34] M. C. Jeruchim, "Techniques for estimating the bit error rate in the simulation of digital communication systems," *IEEE Journal on Selected Areas in Communications*, vol. SAC-2, no. 1, pp. 153–170, Jan. 1984.

[35] M. C. Jeruchim, P. M. Hahn, K. P. Smyntek, and R. T. Ray, "An experimental investigation of conventional and efficient importance sampling," *IEEE Transactions on Communications*, vol. 37, no. 6, pp. 578–587, June 1989.

[36] K. Shanmugam and P. Balaban, "A modified Monte Carlo simulation technique for the evaluation of error rate in digital communications systems," *IEEE Transactions on Communications*, vol. COM-28, pp. 1916–1924, Nov. 1980.

[37] M. C. Jeruchim, "On the application of importance sampling to the simulation of digital satellite and multihop links," *IEEE Transactions on Communications*, vol. COM-32, no. 10, pp. 1088–1092, Oct. 1984.

[38] Q. Wang and V. K. Bhargava, "On the application of importance sampling to BER estimation in the simulation of digital communication systems," *IEEE Transactions on Communications*, vol. COM-35, no. 11, pp. 1231–1233, Nov. 1987.

[39] N. C. Beaulieu, "A composite importance sampling simulation technique for digital communication system simulation," *IEEE Transactions on Communications*, vol. 38, no. 4, pp. 393–396, Apr. 1990.

[40] D. Lu and K. Yao, "Improved importance sampling technique for efficient simulation of digital communication systems," *IEEE Journal on Selected Areas in Communications*, vol. 6, no. 1, pp. 67–75, Jan. 1988.

[41] B. R. Davis, "An improved importance sampling method for digital communication system simulations," *IEEE Transactions on Communications*, vol. COM-34, no. 7, pp. 715–719, July 1986.

[42] P. M. Hahn and M. C. Jeruchim, "Developments in the theory and application of importance sampling," *IEEE Transactions on Communications*, vol. COM-35, no. 7, pp. 706–714, July 1987.

[43] M. C. Jeruchim, P. Balaban, and K. S. Shanmugan, *Simulation of Communication Systems: Modeling, Methodology, and Techniques*, 2nd ed. New York: Kluwer Academic/Plenum Publishers, 2000.

[44] M. M.-F. Lai, "Importance sampling techniques for the estimation of block and bit error rates of block codes," M.Sc. thesis, Queen's University, Kingston, Ontario, 1990.

[45] P. Balaban, "Statistical evaluation of the error rate of the fiber guide repeater using importance sampling," *Bell System Technical Journal*, vol. 55, pp. 745–766, July 1976.

[46] R. V. Hogg and A. T. Craig, *Introduction to Mathematical Statistics*, 5th ed. Upper Saddle River, NJ: Prentice-Hall, 1995.

[47] S. M. Ross, *Simulation*, 3rd ed. San Diego, CA: Academic Press, 2002.

[48] P. Adams, "Biased Gaussian noise source for digital transmission system simulations," *Electronics Letters*, vol. 19, pp. 549–550, July 1983.

[49] G. Box and M. E. Muller, "A note on the generation of random normal deviates," *The Annals of Mathematical Statistics*, vol. 29, no. 2, pp. 610–611, June 1958.

[50] E. C. Posner, "The application of extreme-value theory to error-free communciations," *Technometrics*, vol. 7, no. 4, pp. 517–529, Nov. 1965.

[51] M. Abramowitz and I. A. Stegun, Eds., *Handbook of Mathematical Functions*, 10th ed. New York: Dover Publications, 1972.

[52] R. Kwan and C. Leung, "Optimal detection of BPSK signal in presence of two interferers," *Electronics Letters*, vol. 38, no. 20, pp. 1217–1219, Sept. 2002.

[53] R. Y. C. Kwan, "Single bit optimal detection of a BPSK signal in the presence of co-channel interferers," M. A. Sc. thesis, University of British Columbia, Vancouver, B.C., Canada, Aug. 1998.

[54] H. V. Poor and S. Verdú, "Single-user detectors for multiuser channels," *IEEE Transactions on Communications*, vol. 36, no. 1, pp. 50–60, Jan. 1988.

[55] Y.-C. Jenq, "Does a larger intersymbol interference result in a higher probability of error?," *IEEE Transactions on Communications*, vol. COM-28, no. 9, pp. 1771–1773, Sept. 1980.

[56] N. C. Beaulieu and J. Cheng, "Precise error-rate analysis of bandwidth-efficient BPSK in Nakagami fading and cochannel interference," *IEEE Transactions on Communications*, vol. 52, no. 1, pp. 149–158, Jan. 2004.